8-31-2020 10:30 AM

# Multiphase Equilibrium in A Novel Batch Dynamic VL-Cell Unit with High Mixing: Apparatus Design and Process Simulation

Jeonghoon Kong, *The University of Western Ontario*

Supervisor: de Lasa, Hugo, *The University of Western Ontario*
Co-Supervisor: Escobedo, Salvador, *The University of Western Ontario*
Co-Supervisor: Bhattacharya, Sujit, *Syncrude Canada Ltd*
A thesis submitted in partial fulfillment of the requirements for the Master of Engineering Science degree in Chemical and Biochemical Engineering

# Abstract

The availability of vapor pressure data is essential to validate thermodynamic models and enhance the thermodynamic correlations. Despite its importance, there is limited vapor pressure data of the multicomponent mixtures in open literature. This is the case for hydrocarbon/water blends as they are found in the naphtha recovery unit in the oil sand process.

This thesis uses a CREC-VL-Cell, a batch apparatus to measure the vapor pressures of n-octane/water, synthetic naphtha (SN)/water and solids/n-octane/water. The CREC-VL-Cell operates at thermal equilibrium with less than 1.6 % error using a 1080 rpm impeller speed and various optimized operational factors. This apparatus saves at least 8 hours of the degassing procedures using an air contained correction.

Aspen Hysys process simulator with the Peng Robinson Equation of State package is valuable to emulate CREC-VL-Cell dynamic data of the air-contained hydrocarbon/water by adjusting the volumetric flow of all the phases exiting a continuous separator unit. On this basis, vapor pressure data from the CREC-VL-Cell and Aspen Hysys-Peng Robinson Equation of State simulations are shown to compare well for both n-octane/water and synthetic naphtha (SN)/water blends.

On the other hand, mass balances derived CREC-VL-Cell data allows one to establish liquid and vapor molar fractions boundaries for n-octane/water blends. With these boundaries, additional discrimination of thermodynamic models is allowed. For instance, this shows significant discrepancies of the derived Aspen Hysys-Peng Robinson Equation of State molar fractions, with the anticipated molar fractions boundaries calculated via mass balances in the CREC-VL-Cell.



# Keywords

CREC-VL-Cell, Batch Dynamics, Multiphase equilibrium, Mixing, Process Simulation, VLE, Aspen Hysys, water, n-octane, Synthetic Naphtha, solids

## Summary for Lay Audience

Even though Canada's Oil industry has a significant role as the world's third-largest oil reservoir, the oil sand industry is facing challenges to minimize process contaminated water effluents. Naphtha Recovery Unit (NRU) is the last process step to recover residual naphtha which is used to dilute bitumen. Therefore, the NRU process must be optimized to increase the economic benefits and minimize the environmental footprint.

Vapor pressure data is crucial to investigate the extent of phase equilibrium in the NRU. Moreover, thermodynamic models and their enhanced correlations can be validated by using experimentally measured vapor pressures. However, restricted vapor pressure data of a multicomponent system limits the optimization of the NRU with feed streams composed of water, solids, bitumen and naphtha.

This MESc thesis considers an apparatus able to measure vapor pressures of complex mixtures. This apparatus designated as the CREC-VL-Cell, provides a batch dynamic measurements of vapor pressure in the 30℃ to 120 ℃ range. This method includes optimized design parameters such as mixing speed and unit shape factors.

N-octane/water, synthetic naphtha/water and solids/n-octane/water mixtures are used to measure the vapor pressure and the analysis of this data is reported in this thesis. Also, n-octane/water mixtures are further investigated to establish n-octane molar fractions limits.

This MESc thesis also uses a process simulator, Aspen Hysys with a Peng-Robinson Equation of State package, to investigate the behavior of complex mixtures. The continuous process model is modified to describe the experimental condition in the CREC-VL-Cell. The simulation results are compared to the experimental data validating in this way, the simulation results obtained.

As a result, this MESc project is developed to facilitate vapor pressure measurements, proposing a simulation method which validated with experimental data. This experimental study can also contribute to help setting a valuable research methodology for other hydrocarbon-water process separation applications.

*Dedication*

This thesis is dedicated to:

My beloved wife (Maria Paula Tovar)

and

My admired father (Jaewook Kong)

They have taught me how to love and how to work.

사랑하는 내 와이프 (마리아 파울라 토바)

그리고,

존경하는 아버지 (공재욱)에게

이 논문을 바칩니다.

# Acknowledgments

I would like to attribute this thesis to God, who helped me to be consistent in this academic journey.

I sincerely appreciate my supervisor, Dr. Hugo de Lasa, who gave me the most significant support to complete this project. His novelty, consistency and diligence will be the eternal model for me to pursue the engineering career. His soft leadership encouraged me to overcome the difficult tasks during this project. I will never forget his warmth and generosity.

Syncrude Canada Ltd. and Natural Sciences and Engineering Research (NSERC) made it possible for me to research this inestimable project at Western University.

Dr. Salvador Escobedo, my project's co-advisor and great friend, who always gave me priceless advice throughout the entire project. With his academic insight and mentorship, I was effectively able to troubleshoot all problems. His door was always open to listen to my concerns and to share his wisdom with me

I thank Dr. Sujit Bhattacharya for his invaluable feedback from the industrial point of view. He constantly discussed this project and suggested the creative method so that I could gradually improve the experimental approach in this thesis.

Dr. Sandra Lopez Zamora, who was a member of this project, continuously advised me in conceptual problems such as mathematics and thermodynamics based on her strong theoretical knowledge. For me, she was like a sister who supported me inside and outside of campus

Jose Muñoz, who provided effective technical support and helped me to find a novel approach in the experimental design.

Cesar Medina-Pedraza and Nicolas Torres Brauer who consistently shared their academic knowledge and wise advice. They were like my brothers and excellent friends who listened to my concerns.

Maureen Cordoba Perez and Bianca Rusinque who advised me to conduct my experiments smoothly and made me feel at home at the university. Thanks to them, the laboratory was my favourite place to be while at school.

Dr. Imtiaz Ahmed and Dr. Samira Rostom who supported me in finding the right path of the research scope with their wisdom. They helped me to navigate a way in the chemical engineering field.

Dr. Angel Lanza and Samantha Novoa made it possible for me to start my MESc studies. I would not have been able to further my knowledge and researched this engineering project without their support.

My Colombian in-law family, Carlos, Mariluz, Santiago, Eduardo, Margarita and Pablo, who sincerely cheered for me so that I could finish my studies.

Furthermore, my family in Korea, who supported me from 10,600km away, deserve great gratitude from me. My mom (Young-ui Kim) who lives in my heart as love, my dad (Jae-wook Kong) who is my model of diligence, my two sisters (Sun-gyeong, Im-gyeong) who are like mothers to me, my two brothers-in-law (Jae-hwan, Ji-hoon) who gave me unlimited support, my nieces (Yu-ju, Yu-na, Ian) and nephew (Yun-woo) who always made me smile.

Finally, my wife (Maria Paula Tovar), my companion and best friend, who always told me that I am the best and the smartest person to her. Her encouragement made me not give up even during the difficult times. She helped me to revise the draft of this thesis from start to finish. Moreover, I am very grateful to her for giving me the best gift, our baby.

Every portion of this thesis was possible due to the contribution of the people above.

# Table of Contents

**Abstract** ii

**Summary for Lay Audience** iii

**Acknowledgments** v

**List of Tables** x

**List of Figures** xiv

**Nomenclature** xxiii

**Chapter 1: Introduction** 1

**Chapter 2: Bibliographic Review** 4

2.1 Hydrocarbon – Water Mixture 4
*2.1.1 Alkane – Water* 5
*2.1.2 Naphtha – Water* 7
*2.1.3 Bitumen – water* 7

2.2 VLE Measuring Equipment 9
*2.2.1 Batch Method* 10
*2.2.2 Flow Method* 13

2.3 Thermodynamic Principles 14
*2.3.1 Activity Coefficient Model* 16
*2.3.2 Equation of State Model* 19

2.4 Multiphase Mixing 21
*2.4.1 Batch Stirred Tank* 21
*2.4.2 Impeller* 23
*2.4.3 Baffle* 25

2.5 Conclusions 27

**Chapter 3: Scope of the Research** 28

3.1 Particular Objectives 28

3.2 Accomplishments of Research 29

**Chapter 4: Dynamic System Design** 30

4.1 Heating System 30
*4.1.1 Temperature System* 30

*4.1.2 Pressure System* ..... *33*
*4.1.3 Thermo-fluid* ..... *34*
*4.1.4 CREC-VL-Cell Positioning* ..... *36*

4.2 Mixing System ..... 38
*4.2.1 Video Analysis* ..... *39*
*4.2.2 Sample Volume* ..... *40*
*4.2.3 Impeller* ..... *42*
*4.2.4 Baffle Design* ..... *46*
*4.2.5 Impeller Speed* ..... *49*

4.3 System Validation ..... 50
*4.3.1 Thermal Equilibrium Validation* ..... *50*
*4.3.2 Dynamic System Validation* ..... *52*

4.4 Conclusions ..... 56

**Chapter 5: Materials and Experimental Methods** ..... 57

5.1 Materials ..... 57
*5.1.1 Hydrocarbon Species* ..... *57*
*5.1.2 Synthetic Naphtha* ..... *59*

5.2 Experimental Methods ..... 62
*5.2.1 Preparation Steps* ..... *63*
*5.2.2 Sample Input to the CREC-VL-Cell* ..... *64*
*5.2.3 Temperature Controller Setup* ..... *65*
*5.2.4 Hot-plate with Stirring Capabilities* ..... *66*
*5.2.5 CREC-VL-Cell Mixing Setup* ..... *67*
*5.2.6 System Activation* ..... *68*
*5.2.7 Coil Cooling System* ..... *69*
*5.2.8 CREC-VL-Cell System Disassembly* ..... *70*

5.3 Conclusions ..... 71

**Chapter 6: Process Simulation Method** ..... 72

6.1 PFD Simulations ..... 72

6.2 Thermodynamic Model ..... 74

6.3 Conclusions ..... 79

**Chapter 7: Experimental Data Results and Discussion** ..... 80

7.1 Air Contained Fraction Correction ..... 80

7.2 VLE for Pure Chemical Species ..... 84

*7.2.1 VLE for Pure Alkane* ..... *85*
*7.2.2 VLE for Pure water* ..... *92*

7.3 VLE in n-octane/water Blends ..... 94
*7.3.1 P-T data* ..... *95*

7.4 VLE in water/synthetic naphtha (SN) Blends ..... 103
*7.4.1 P-T data on different synthetic naphtha concentration* ..... *103*
*7.4.2 P-T data at Different Impeller Speeds* ..... *106*

7.5 VLE in water -solids- n-octane Blends ..... 109

7.6 Conclusions ..... 119

**Chapter 8: Bounding Equilibrium Molar Fraction in the CREC-VL-Cell** ..... 120

8.1 Conservation Molar Fractions Based Model in the CREC-VL-Cell. ..... 120

8.2 Conclusions ..... 126

**Chapter 9: Conclusions and Recommendations** ..... 127

9.1 Conclusions ..... 127

9.2 Recommendations ..... 128

**Bibliography** ..... 129

**Appendices** ..... 143

Appendix A: Uncertainty ..... 143

Appendix B: Risk Analysis ..... 145

Appendix C. Aromatic Synthetic Naphtha ..... 151

Appendix D. CREC-VL-Cell Photos ..... 155

Appendix E. Copyright Permission ..... 156

**Curriculum Vitae** ..... 157

# List of Tables

Table 1. Classification of an Emulsion using as the basis the Droplet Size ..... 5

Table 2. Bitumen composition by Elements and SARA analysis [52] ..... 8

Table 3. Physical Properties of Possible Thermo-fluid candidates..... 34

Table 4. Liquid temperature, Gas temperature and Relative error data on dynamic measurement condition. Notes: (a) Relative error (red solid line) indicates a discrepancy between liquid and gas temperatures, (b) 2 wt% n-octane + 98 wt% water mixture is used on the test. ..... 51

Table 5. Properties of Alkanes..... 58

Table 6. Properties of Oil Sand Solids..... 59

Table 7. Typical naphtha composition [152] ..... 60

Table 8. Synthetic Naphtha Composition ..... 61

Table 9. Data comparison between theoretical air factor and experimental air factor. Notes: (a) SD indicates Standard deviation, (b) SE indicates Standard Error, (c) LB and UB indicate Lower bound and Upper bound respectively in 95 % Confidence Interval (CI) ..... 83

Table 10. Pmix comparison for n-octane between Literature data and CREC-VL-Cell experimental data ..... 86

Table 11. n-octane Experimental and Statistical data. Notes: (a) SD = Standard Deviation, (b) SE = Standard Error, (c) CI = Confidence Interval, (d) LB = Lower bound, (e) UB = Upper bound..... 86

Table 12. Pmix comparison for n-hexane between Literature data and CREC-VL-Cell experimental data ..... 87

Table 13. n-hexane Experimental and Statistical data. Notes: (a) SD = Standard Deviation, (b) SE = Standard Error, (c) CI = Confidence Interval, (d) LB = Lower bound, (e) UB = Upper bound..... 88

Table 14. Pmix comparison for n-decane between Literature data and CREC-VL-Cell experimental data..... 89

Table 15. n-decane Experimental and Statistical data. Notes: (a) SD = Standard Deviation, (b) SE = Standard Error, (c) CI = Confidence Interval, (d) LB = Lower bound, (e) UB = Upper bound..... 90

Table 16. Pmix comparison for n-dodecane between Literature data and CREC-VL-Cell experimental data..... 91

Table 17. n-dodecane Experimental and Statistical data. Notes: (a) SD = Standard Deviation, (b) SE = Standard Error, (c) CI = Confidence Interval, (d) LB = Lower bound, (e) UB = Upper bound..... 92

Table 18. Pmixcomparison for water between Literature data and CREC-VL-Cell experimental data..... 93

Table 19. water Experimental and Statistical data. Notes: (a) SD = Standard Deviation, (b) SE = Standard Error, (c) CI = Confidence Interval, (d) LB = Lower bound, (e) UB = Upper bound..... 94

Table 20. n-octane 1.0 wt% + water 99.0 wt% Experimental and Statistical data..... 96

Table 21. n-octane 2.0 wt% +water 98.0 wt% Experimental and Statistical data..... 96

Table 22. n-octane 4.0 wt% +water 96.0 wt% Experimental and Statistical data..... 96

Table 23. n-octane 6.0 wt% +water 94.0 wt% Experimental and Statistical data..... 97

Table 24. n-octane 20.0 wt% +water 80.0 wt% Experimental and Statistical data..... 97

Table 25. n-octane 50.0 wt% +water 50.0 wt% Experimental and Statistical data..... 98

Table 26. n-octane 80.0 wt% +water 20.0 wt% Experimental and Statistical data ..... 98

Table 27. n-octane 98.0 wt% +water 2.0 wt% Experimental and Statistical data ..... 99

Table 28. n-octane 0.1 wt% +water 99.9 wt% Experimental and Statistical data ..... 100

Table 29. n-octane 0.25 wt% +water 99.75 wt% Experimental and Statistical data ..... 101

Table 30. n-octane 0.5 wt% +water 99.5 wt% Experimental and Statistical data ..... 101

Table 31. n-octane 99.75.0 wt% +water 0.25 wt% Experimental and Statistical data ..... 102

Table 32. synthetic naphtha 2.5 wt% + water 97.5% Experimental and Statistical data..... 105

Table 33. synthetic naphtha 4.0 wt% + water 96.0 wt% Experimental and Statistical data. 105

Table 34. synthetic naphtha 97.5 wt% + water 2.5 wt% Experimental and Statistical data. 106

Table 35. n-octane 1.0 wt% + solids 1.0 wt% + water 98.0 wt% Experimental and Statistical data ..... 110

Table 36. n-octane 1.0 wt% + solids 20.0 wt% + water 79.0 wt% Experimental and Statistical data ..... 111

Table 37. n-octane 2.0 wt% + solids 1.0 wt% + water 97.0 wt% Experimental and Statistical data ..... 112

Table 38. n-octane 2.0 wt% + solids 20.0 wt% + water 78.0 wt% Experimental and Statistical data ..... 113

Table 39. n-octane 4.0 wt% + solids 20.0 wt% + water 76.0 wt% Experimental and Statistical data ..... 114

Table 40. n-octane 6.0 wt% + solids 20.0 wt% + water 74.0 wt% Experimental and Statistical data ..... 115

Table 41. n-octane 0.25 wt% + solids 20.00 wt% + water 79.75 wt% Experimental and Statistical data ..... 117

Table 42. Preliminary Hazard Analysis for VL-Cell operation ..... 145

Table 43. Compositions of n-paraffin group and aromatic group for Synthetic Naphtha .... 151

Table 44. Synthetic Naphtha compositions ..... 152

# List of Figures

Figure 1. Typical Naphtha Recovery Unit process diagram as reported in literature [4] ..... 2

Figure 2. Crude oil distillation curve [8]. Note: The arrows indicate the change of diesel production yield in different volumetric flow condition..... 3

Figure 3. Classification of VLE measuring apparatuses [70] ..... 10

Figure 4. A Schematic depiction of the static analytical equipment [67] ..... 11

Figure 5. Batch-Static Method Device : (1) and (2) feed cylinders; (3) temperature meter; (4) pressure display; (5) temperature controller; (6) pressure transducer; (7) liquid nitrogen trap; (8) vacuum pump; (9) syringe pump; (10) equilibrium cell; (11) batch liquid mixer; (12) syringe pump; (13) thermostated water batch; (14) and (15)circular bath; (16), (17) and (18) temperature probe. [86]..... 13

Figure 6. Vapor-Liquid Equilibrium simulation by Non-Random Two Liquid equation [16]18

Figure 7. Experimental setup for Visualization of  Phase Dispersion [120] ..... 22

Figure 8. Experimental illustration for solid-liquid mixtures and plexiglass prism for PIV experiment [121]..... 23

Figure 9. Description of the Standard Rushton Turbine [129] ..... 24

Figure 10. Pitched Blade Turbine [132] ..... 24

Figure 11. Experimental setup and schematic image of the dual impeller [133] ..... 25

Figure 12. Standard full baffled stirred tank [136] ..... 26

Figure 13. CFD modeling image of Interface baffle [137]..... 26

Figure 14. Cross-Section of the CREC-VL-Cell heating system ..... 31

Figure 15. Temperature measurement points at T1, T2 and T3 for Pure n-octane..... 32

Figure 16. CREC-VL-Cell illustration. Notes: (a) Exterior view, (b) Transversal view with Pressure transducer, Thermocouples and Impeller type ..... 33

Figure 17. Temperature changes of Silicon Oil and Cooking Corn Oil at different times ..... 36

Figure 18. Illustration of Thermo-fluid Vessel size difference. Notes: (a) Small Vessel type (Left) covers 80 % of CREC-VL-Cell height, (b) Large Vessel type(right) covers CREC-VL-Cell completely. ..... 37

Figure 19. Liquid temperature and Gas temperature comparison during the CREC-VL-Cell running. Notes: (a) Thermal equilibrium is a reference where gas and liquid have the same temperature, (b) Low Thermo-fluid level is a condition of using the small vessel type, (c) High Thermo-fluid level is a condition of using the large Vessel type. ..... 38

Figure 20. Batch Stirred tank shape factors: (a) T = Tank diameter, (b) H = Liquid depth, (c) D = Impeller diameter, (d) C = Off-bottom clearance. ..... 40

Figure 21. CREC-VL-Cell Mixing Video analysis for 2 wt% n-octane + 98 wt% water on 100mL and 140mL volumes. Mixing speed: 1080 rpm..... 41

Figure 22. Pmix for 2 wt% n-octane + 98 wt% water in the 20 ℃ to 110 ℃ range. Notes: (a) Saturation pressure using the immiscible model (red dash line), (b) 100 mL volume sample (orange filled square mark), (c) 140 mL volume sample (blue filled triangle mark), (d) 1080 rpm mixing speed is used, (e) Vertical bars represent standard deviation for at least three experimental repeats. ..... 42

Figure 23. Description of Marine Type Impeller Used in the CREC-VL-Cell ..... 43

Figure 24. CREC-VL-Cell Mixing Video analysis for 2 wt% n-octane+ 98 wt% water depending on impeller position Notes: C represents impeller clearance from the bottom to the impeller tip ..... 44

Figure 25. Pmix comparison between 2.5 cm clearance impeller position (Orange filled square mark) and 7.0 cm clearance impeller position (Blue filled triangle mark) in the 20 ℃

to 110 ℃ range. Notes: (a) Summation of water and n-octane saturation pressure is used to represent a completely immiscible model (Red dash line), (b) 1080 rpm mixing speed is used, (c) Vertical bars represent standard deviation for at least three experimental repeats. ..... 45

Figure 26. CREC-VL-Cell Mixing Video analysis for 78 wt% water + 20 wt% Silica sand + 2 wt% naphtha mixture depending on impeller position Notes: C determines impeller clearance height from bottom to the impeller tip ..... 46

Figure 27. Description of Selected CREC-VL-Cell Baffle System ..... 47

Figure 28. CREC-VL-Cell Mixing Video Comparing Interface Baffle and Internal Baffles for 20 wt% n-octane + 80 wt% water sample. Notes: (a) 240 Frames Per Second high-speed camera, (b) n-octane contains 0.001 wt% bitumen dye. ..... 48

Figure 29. Pmix comparison between Interface baffle (Orange filled square mark) and Internal baffle (Blue filled triangle mark) in the 20 ℃ to 110 ℃ range. Notes: (a) Summation of water and n-octane saturation pressure is used to represent a completely immiscible model (Red dash line), (b) 1080 rpm mixing speed is used, (c) Vertical bars represent standard deviation for at least three (3) experimental repeats. ..... 49

Figure 30. CREC-VL-Cell mixing video analysis compared to mixing speed for 1080 rpm (Left) and 1500 rpm (Right). ..... 50

Figure 31. Liquid temperature (x mark) and Gas temperature (square mark) on dynamic measurement condition. Notes: (a) Relative error (red solid line) indicates a discrepancy between liquid and gas temperatures, (b) 2 wt% n-octane + 98 wt% water mixture is used on the test. ..... 51

Figure 32. Temperature (Purple filled circle mark) and Pressure (Red filled diamond mark) change for 2 wt% n-octane + 98 wt% water at various running times. Notes: (a) Heating ramp is paused at 40 min to valid static measurement condition, (b) Heating ramp is reactivated after the Static method is maintained for 38 mins, (c) 1080 rpm mixing speed is used ..... 53

Figure 33. Pmix comparison between static measurement condition (black filled square mark) and dynamic measurement condition (blue solid line) in the 30 ℃ to 90 ℃ range. Notes: (a) Static method is in the yellow highlighted region, (b) Relative error (red solid line) indicates a discrepancy between the static method test and dynamic method test, (c) 1080 rpm mixing speed is used. ..... 54

Figure 34. Pmixcomparison between static measurement condition (black filled square mark) and dynamic measurement condition (blue solid line) in the 66 ℃ to 75 ℃ range. Notes: (a) Static method is in the yellow highlighted region, (b) Relative error (red solid line) indicates a discrepancy between the static method test and dynamic method test, (c) 1080 rpm mixing speed is used. ..... 55

Figure 35. Typical naphtha distillation curve by using Aspen Hysys®. Notes: (a) Red solid line represents True Boiling Point(TBP) – ASTM D2892 method, (b) Green solid line represents ASTM D2887 method. ..... 61

Figure 36. Psatv for naphtha in the range of 30 ℃ to 110 ℃. Notes: a) Aspen Hysys® simulated typical naphtha (black solid line), (b) synthetic naphtha in the CREC-VL-Cell. Note: Vertical bars represent standard deviations for experimental repeats. ..... 62

Figure 37. Schematic Description of CREC-VL-Cell Experimental Method ..... 63

Figure 38. Air/n-octane/water Process Flow Diagram in Aspen Hysys ..... 73

Figure 39. Air/Synthetic Naphtha/Water Process Flow Diagram in Aspen Hysys ..... 74

Figure 40. The saturation vapor pressure estimation with different thermodynamic models in Aspen Hysys. NRTL and UNIQUAC give essentially the same prediction, thus blue and black lines cannot be distinguished. Note: The mixture of *2 wt% n-octane + 98 wt% water + air* is used for all thermodynamic models..... 75

Figure 41. The saturation vapor pressure estimation with PR-EoS thermodynamic models in Aspen Hysys. Note: The experimental data of *0.1 wt% n-octane + 99.9 wt% water + air* is used to compare with the simulation results ..... 76

Figure 42. The saturation vapor pressure estimation with PR-EoS thermodynamic models in Aspen Hysys. Note: The experimental data of *0.25 wt% n-octane + 97.5 wt% water + air* is used to compare with the simulation results ..... 76

Figure 43. The saturation vapor pressure estimation with PR-EoS thermodynamic models in Aspen Hysys. Note: The experimental data of *1.0 wt% n-octane + 99.0 wt% water + air* is used to compare with the simulation results ..... 77

Figure 44. The saturation vapor pressure estimation with PR-EoS thermodynamic models in Aspen Hysys. Note: The experimental data of *2.5 wt% synthetic naphtha + 97.5 wt% water + air* is used to compare with the simulation results ..... 77

Figure 45. The saturation vapor pressure estimation with PR-EoS thermodynamic models in Aspen Hysys. Note: The experimental data of *4.0 wt% synthetic naphtha + 96.0 wt% water + air* is used to compare with the simulation results ..... 78

Figure 46. Comparison of $\Delta$PAir Experimental (Blue filled circle) and theoretical (Red solid line) in the 30 ℃ to 120 ℃ range. Note: Vertical bars represent standard deviation for experimental repeats. ..... 83

Figure 47. Pmix for n-octane and references data in the range of 30 ℃ to 110 ℃. Note: Vertical bars represent standard deviation ..... 85

Figure 48. Pmix for n-hexane and references data in the range of 30 ℃ to 110 ℃. Note: Vertical bars represent standard deviation ..... 87

Figure 49. Pmix for n-decane and references data in the range of 30 ℃ to 110 ℃. Note: Vertical bars represent standard deviation ..... 89

Figure 50. Pmix for n-dodecane and references data in the range of 30 ℃ to 110 ℃. Note: Vertical bars represent standard deviation ..... 91

Figure 51. Pmix for single water (Blue filled circle mark), *Lide (2004)* (Red filled circle) and *Cliefford & Hunter (1933)* reference in the range of 30 ℃ to 110 ℃.Note: Vertical bars represent standard deviation. ..... 93

Figure 52. Pmix for VLLE of the n-octane/water mixtures in the range of 30 ℃ to 110 ℃. Notes: (a) Summation of water and n-octane saturation pressures represent a completely immiscible model (purple solid line), (b) 1080 rpm mixing speed is used, (c) Experiment data is the average data of three or more experimental repeats. ..... 95

Figure 53. Pmix for VLE of n-octane – water mixture in the range of 30 ℃ to 110 ℃ range. Notes: (a) Summation of water and n-octane saturation pressures represent a completely immiscible model (purple solid line), (b) 1080 rpm mixing speed is used, (c) Experiment data is the average data of three or more experimental repeats. ..... 100

Figure 54. Pmix for 99.75 wt% n-octane + 0.25 wt% water in the range of 30 ℃ to 110 ℃ range. Notes: (a) Summation of water and n-octane saturation pressures represent a completely immiscible model (purple solid line), (b) 1080 rpm mixing speed is used, (c) Experiment data is the average data of three or more experimental repeats. ..... 102

Figure 55. Pmix for water /synthetic naphtha mixtures in the range of 30 ℃ to 110 ℃. Notes: (a) Summation of water and synthetic naphtha saturation pressures represent a completely immiscible model (purple solid line), (b) 1080 rpm mixing speed is used, (c) Vertical bars indicate the standard deviation of three or more experimental repeats. ..... 104

Figure 56. Mixing-speed effect for 2.5 wt% synthetic naphtha – 97.5 wt% water mixture in the range of 30 ℃ to 110 ℃. Notes: (a) Summation of water and synthetic naphtha saturation pressures represent a completely immiscible model (purple solid line), (b) 1080 rpm mixing

speed is used, (c) Vertical bars indicate the standard deviation of three or more experimental repeats. ..... 107

Figure 57. Mixing-speed effect for 4.0 wt% SN - 96.0 wt% water mixture in the range of 30 ℃ to 110 ℃. Notes: (a) Summation of water and synthetic naphtha saturation pressures represent a completely immiscible model (purple solid line), (b) 1080 rpm mixing speed is used, (c) Vertical bars indicate the standard deviation of three or more experimental repeats. ..... 108

Figure 58. Mixing-speed effect for 97.5 wt% water – 2.5 wt% synthetic naphtha mixture in the range of 30 ℃ to 110 ℃. Notes: (a) Summation of water and synthetic naphtha saturation pressures represent a completely immiscible model (purple solid line), (b) 1080 rpm mixing speed is used, (c) Vertical bars indicate the standard deviation of three or more experimental repeats. ..... 109

Figure 59. Pmix for 1.0 wt% n-octane and various water-solid compositions in the 30 ℃ to 110 ℃ range. Notes: (a) Summation of water and octane saturation pressures represent a completely immiscible model (purple solid line), (b) 1080 rpm mixing speed is used, (c) Vertical bars indicate the standard deviation of three or more experimental repeats. ..... 110

Figure 60. Pmix for 2.0 wt% n-octane and various water-solids compositions in the 30 ℃ to 110 ℃ range. Notes: (a) Summation of water and octane saturation pressures represent a completely immiscible model (purple solid line), (b) 1080 rpm mixing speed is used, (c) Vertical bars indicate the standard deviation of three or more experimental repeats. ..... 112

Figure 61. Pmix for 4.0 wt% n-octane and various water-solid compositions in the 30 ℃ to 110 ℃ range. Notes: (a) Summation of water and octane saturation pressures represent a completely immiscible model (purple solid line), (b) 1080 rpm mixing speed is used, (c) Vertical bars indicate the standard deviation of three or more experimental repeats. ..... 114

Figure 62. Pmix for 6.0 wt% n-octane and various water-solid compositions in the 30 ℃ to 110 ℃ range. Notes: (a) Summation of water and octane saturation pressures represent a completely immiscible model (purple solid line), (b) 1080 rpm mixing speed is used, (c) Vertical bars indicate the standard deviation of three or more experimental repeats. ..... 115

Figure 63. Pmix for 0.25 wt% n-octane and various water-solid compositions in the 30 ℃ to 110 ℃ range. Notes: (a) Summation of water and octane saturation pressures represent a completely immiscible model (purple solid line), (b) 1080 rpm mixing speed is used, (c) Vertical bars indicate the standard deviation of three or more experimental repeats. ..... 117

Figure 64. Molar fraction upper boundaries in n-octane/water mixtures and estimated molar fractions by PR-EOS ..... 125

Figure 65. Fault Tree Analysis for Chemical inhale and contact event ..... 149

Figure 66. Fault Tree Analysis for Pressure leak ..... 150

Figure 67. TBP analysis of Typical Naphtha and Synthetic Naphtha by using Hysys PR-EOS. Figure 68 describes the pressure change using as a reference, the CREC SN_Aroma0 synthetic naphtha without aromatics. One can see that The CREC SN_Aroma15 has less than 1.37 % pressure difference compared to the pressure of the CREC SN_Aroma0. As well one can observe that The CREC SN_Aroma10 has less than 2.2 %. ..... 152

Figure 68. Pressure changes of synthetic aromatic naphtha while compared to the CREC SN_Aroma0. ..... 153

Figure 69. Pressure changes of 97.5 wt% water + 2.5 wt% synthetic aromatic naphtha compared to the CREC SN_Aroma0 ..... 154

Figure 70. Pressure changes of 96.0 wt% water + 4.0 wt% synthetic aromatic naphtha compared to the CREC SN_Aroma0 ..... 154

Figure 71. CREC-VL-Cell setup image ..... 155

Figure 72. 275mL Equilibrium cell image ..... 155

Figure 73. Water-cooled heat exchanger in CREC-VL-cell ..... 155

# Nomenclature

**Symbols**

| | | |
|---|---|---|
| $f$ | $\{Pa\}$ | Fugacity |
| $G$ | $\{J/mol\}$ | Gibbs energy |
| $G^E$ | $\{J/mol\}$ | Excess Gibbs energy |
| $i$ | dimensionless | Component identity |
| $m_{oct}$ | $\{g\}$ | Total octane mass |
| $m_w$ | $\{g\}$ | Total water mass |
| $m_{oct}^l$ | $\{g\}$ | Liquid mass of octane |
| $m_w^l$ | $\{g\}$ | Liquid mass of water |
| $m_{oct}^v$ | $\{g\}$ | Vapor mass of octane |
| $m_w^v$ | $\{g\}$ | Vapor mass of water |
| $MW^l$ | $\{g/mol\}$ | Average molecular weight of liquids |
| $MW_{oct}$ | $\{g/mol\}$ | Molecular weight of octane |
| $MW_w$ | $\{g/mol\}$ | Molecular weight of Water |
| $n$ | $\{mol\}$ | Total moles |
| $n_{Air}$ | $\{mol\}$ | Air moles in the CREC-VL-Cell |
| $n_{oct}$ | $\{mol\}$ | Total octane moles |
| $n^l$ | $\{mol\}$ | Total moles in liquid phase |
| $n_{oct}^l$ | $\{mol\}$ | Octane moles in the liquid phase |
| $n_{oct}^v$ | $\{mol\}$ | Octane moles in the vapor phase |
| $n_w$ | $\{mol\}$ | Total water moles |
| $n_w^l$ | $\{mol\}$ | Water moles in the liquid phase |
| $n^v$ | $\{mol\}$ | Total moles in vapor phase |
| $n_w^v$ | $\{mol\}$ | Water moles in the vapor phase |
| $p_c$ | $\{Pa\}$ | Critical pressure |
| $p_{oct}$ | $\{Pa\}$ | Octane partial pressure |
| $p_w$ | $\{Pa\}$ | Water partial pressure |
| $P$ | $\{Pa\}$ | Total pressure |
| $P_{Air}$ | $\{Pa\}$ | Air pressure |
| $P_{Air,measured}$ | $\{Pa\}$ | Corrected air pressure |

| | | |
|---|---|---|
| $P_{empty\ cell}$ | $\{Pa\}$ | Air pressure in the empty cell |
| $P_{London,ON}$ | $\{Pa\}$ | Atmospheric pressure in London, Ontario |
| $P_{mix}$ | $\{Pa\}$ | Total saturation pressure of the mixture |
| $P_{oct}^{v}$ | $\{Pa\}$ | Octane saturation vapor pressure |
| $P_{w}^{v}$ | $\{Pa\}$ | Water saturation vapor pressure |
| $R$ | $\{m^3 \cdot Pa/K \cdot mol\}$ | Gas constant |
| T | {℃} | Temperature |
| $T_c$ | {℃} | Critical temperature |
| $T_{exp}$ | {℃} | Measured temperature |
| $T_r$ | {℃} | Reduced temperature |
| $U_{ii}$ | $\{J\}$ | Energy of evaporation |
| $U_{ji}$ | $\{J\}$ | Energy between the molecular surface |
| $V_{Air}$ | $\{m^3\}$ | Volume of Air |
| $V_m$ | $\{m^3\}$ | Molar volume |
| $V_w$ | $\{m^3\}$ | Total water volume |
| $V^l$ | $\{m^3\}$ | Volume of total liquid |
| $V_w^l$ | $\{m^3\}$ | Volume of liquid water |
| $V_w^v$ | $\{m^3\}$ | Volume of vapor water |
| $V^v$ | $\{m^3\}$ | Volume in the vapor phase |
| $V$ | $\{m^3\}$ | Total CREC-VL-Cell volume |
| $x$ | dimensionless | Moar fraction |
| $x_{min}$ | dimensionless | Minimum molar fraction |
| $x_{oct}$ | dimensionless | Octane molar fraction in the liquid phase |
| $x_w$ | dimensionless | Water molar fraction in the liquid phase |
| $y_{oct}$ | dimensionless | Octane molar fraction in the vapor phase |
| $y_w$ | dimensionless | Water molar fraction in the vapor phase |

**Greek Symbols**

| | | |
|---|---|---|
| $\gamma$ | dimensionless | Activity coefficient |
| $\gamma_{oct}$ | dimensionless | Octane activity coefficient |
| $\gamma_w$ | dimensionless | Water activity coefficient |
| $\Delta$ | dimensionless | Difference |
| $\kappa$ | $\{Pa\}$ | Isothermal compressibility |
| $\rho^l$ | $\{g/m^3\}$ | The average density of liquid |
| $\rho_w$ | $\{g/m^3\}$ | Water density |
| $\tau$ | dimensionless | Interaction factor |
| $\phi$ | dimensionless | Fugacity coefficient |
| $\omega$ | dimensionless | Acentric factor |

**Acronyms**

| | |
|---|---|
| CI | Confidence Interval |
| CN | Carbon Number |
| EOS | Equation of State |
| FPS | Frames Per Second |
| GC | Gas Chromatography |
| LB | Lower bound |
| NRTL | Non Random Two Liquid equation |
| NRU | Naphtha Recovery Unit |
| PR-EoS | Peng Robinson Equation of State |
| RPM | Rotation per minute |
| SD | Standard Deviation |
| SE | Standard Error |
| SN | Synthetic Naphtha |
| UB | Upper bound |
| UNIQUAC | Universal Quasichemical |
| VLE | Vapor Liquid Equilibrium |
| VLLE | Vapor Liquid Liquid Equilibrium |

# Chapter 1: Introduction

Canada's Oil sand industry has a significant role as the world's third-largest oil reservoir [1]. The oil sand industry still faces, however, challenges due to the poor oil sand properties compared to conventional oil [2]. Main issues that oil-sand processing should overcome are: (a) improved recovery yield, (b) minimization of the environmental impact.

The Naphtha Recovery Unit (NRU) performs an essential process task. It is the last step to recover residual diluent naphtha before the tailings are sent to an engineered dam, named tailing pond. Alberta Energy and Utilities Board controls Naphtha losses, and NRU operation requires significant amounts of energy to be operated [2]. Thus, the NRU process must be optimized and this to achieve maximum naphtha recovery, with minimum environmental footprint.

Figure 1 describes a schematic of the NRU process flowsheet. NRU is an equilibrium stage column which has been modified to separate a multicomponent mixture. Heated steam sprays to the liquid pool to vaporize the mixture, and the unit is operated near 100 ℃ and 100 kPa [3]. A demister pad on the top of the unit separates suspended solids in the vapor phase. The condensed water from the unit constantly refluxes to the system. Regarding the liquid pool with minimized naphtha, content is sent to the adjacent tailing pond.

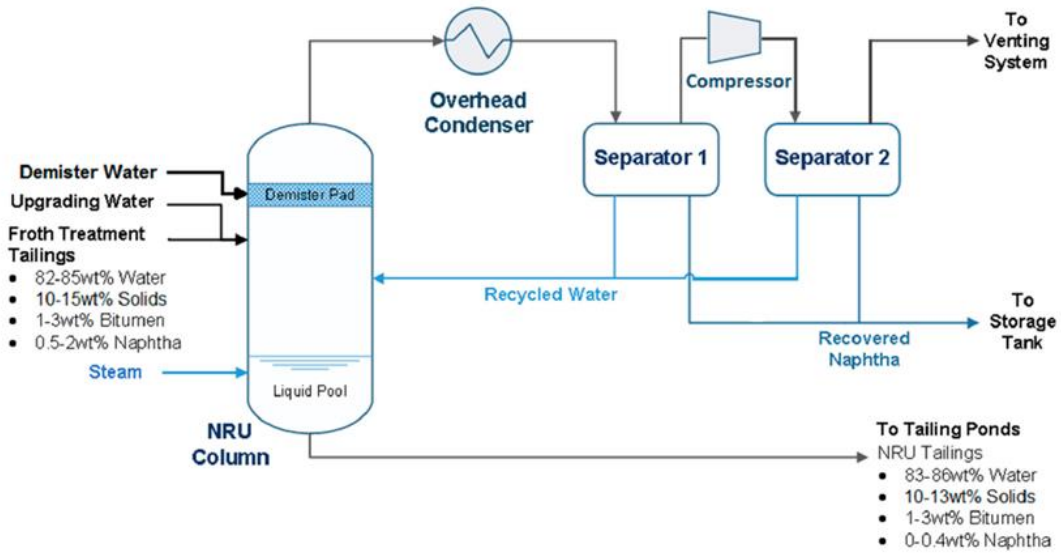


**Figure 1. Typical Naphtha Recovery Unit process diagram as reported in the literature** [4]

The NRU has been designed based on equilibrium phase principles. In principle, the closer to phase equilibrium the NRU operates, the higher the separation yield obtained. Therefore, phase equilibrium with mixing conditions is critical to reach the ideal operating condition in the NRU. In the NRU, the water-hydrocarbon thermodynamic phase equilibrium [5] is helped via mass transfer between interphases.

Given the above, vapor pressure data availability is of critical importance for the NRU. Vapour data is normally available in the technical literature together with thermodynamic correlations for enhancing phase compositions [6]. However, the availability of water-naphtha vapor pressure, as well as the related thermodynamics, is very limited in the open literature. Therefore, further information on these parameters in the 30-110 ℃ is critical for further improvements in the NRU [7].

Figure 2 reports a distillation curve of crude oils, as reported in the literature [8]. One can observe that naphtha displays a 65 ℃ to 230 ℃, the lowest distillation temperature from various hydrocarbon products. Given n-octane shows a 125.6 ℃ boiling point, close to the

average boiling point from typical light naphtha [9], n-octane can be considered to represent naphtha in the present study.

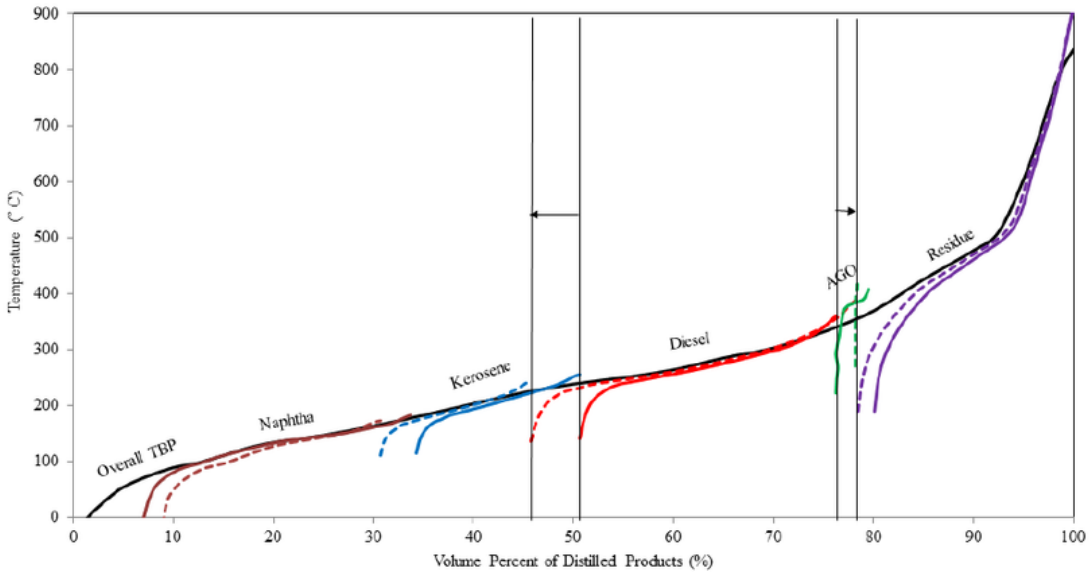


**Figure 2. Crude oil distillation curve** [8]**. Note: The arrows indicate the change of diesel production yield in different volumetric flow condition.**

Additionally, to improve thermodynamics predictions in the NRU, a Synthetic Naphtha (SN) blend can be prepared, including five (5) paraffinic compounds with n-octane being the main mixture component, as will be described later in 5.1.2. Furthermore, and to have a comprehensive analysis with multiphase blends simulating the ones fed in the NRU, kaolin clay and silica sand can also be added to n-octane-water blends.

Regarding studies relevant for the NRU, a CREC-VL-Cell apparatus was designed to measure the saturation vapor pressure of water-hydrocarbon multicomponent mixture. (Escobedo et al., 2020) The selected design was validated in the present thesis, by using high-speed video images and changes in the impeller mixing speed. On this basis, optimized mixing conditions were determined. As well, a "dynamic operation" was chosen measuring vapor pressures with the thermal level in the cell changing via a 1.22 °C/min ramp, gathering in every experiment a very significant amount of relevant thermodynamic data.

# Chapter 2: Bibliographic Review

The thermodynamics of multicomponent mixtures is a challenging research subject [10]. In this respect, multicomponent mixtures have to be considered from the perspective of molecular interaction [11]. Despite its issues, thermodynamics of multicomponent-multiphase systems is increasingly being considered in both academia and industry [12]. This literature review analyses the various possible approaches reported in previous studies.

Although the experimental determination is the most effective way to establish phase equilibrium for the entire temperature, pressure and concentration ranges of interest, it is too expensive [13]. Thus, thermodynamic models can be employed very effectively [14] to design and simulate process units [15], [16]. In this respect, one of the biggest concerns for engineers is to decide about an adequate thermodynamic model for the simulation. [17], [18].

## 2.1 Hydrocarbon – Water Mixture

Hydrocarbon-water mixtures are reviewed with the goal of understanding immiscibility liquid behavior. In this regard, the partially miscible liquid may form a two-phase liquid system [19].

While temperature, pressure, molecular size and mixing are factors influencing miscibility, the chemical species polarity is a leading effect [20]. Water forms high polar molecules with electrons being pulled towards the oxygen atom. Hydrocarbons, on the other hand, mainly contain hydrogen and carbon atoms. As hydrogen and carbon display low electronegativity between constitutive atoms, hydrocarbons have low polar characteristics [21]. Therefore, water and hydrocarbon show the main differences and, as a result, low miscibility.

Due to this water and hydrocarbon low miscible behavior, these species can be separated rather easily until hydrocarbons in water reach low concentrations [22]. Then hydrocarbon is enough to contaminate discharge water streams, with a resulting negative impact on the environment [23].

Hydrocarbons in water can be considered in the multiphase systems designated as emulsions. [24]. Emulsions can contain two or more liquid mixtures, with one being in a droplet form [25]. The physical properties of these emulsions determine light scattering and stability tests [26]. However, the droplet size is probably the main criterion to distinguish them. Table 1 reports the blend classification using as the basis of the droplet size of a particle in the solvent phase [27].

**Table 1. Classification of an Emulsion using as the basis the Droplet Size**

| Solution | Colloid | Suspension |
|---|---|---|
| ~ 1nm | 1 ~ 100nm | 100nm ~ |

### *2.1.1 Alkane – Water*

Alkanes (or paraffinic compounds) are acyclic saturated hydrocarbons, with the $C_nH_{2n+2}$ general formula [28]. Due to the fact that alkanes only contain hydrogen and carbon, they are bound to have extremely low polarity [29]. Therefore, the solubility in water is anticipated to be low, given the “like dissolves like” principle [30]. Alkanes are versatile substances in engineering applications, such as solvents, thermo-fluids, and fuels [31]. Due to the various usages, the alkane separation from water has been researched for decades [32].

The solubility of alkanes in water can be influenced by the number of carbons, with solubility decreasing for the larger carbon chain molecules [33]. Furthermore, this solubility declines even more rapidly if the carbon number is more significant than 11 [34]. This behavior can be explained as a reduced opportunity of a larger alkane carbon chain molecule to become in contact with water [34].

Furthermore, micelle formation can be a significant factor in determining the hydrocarbon solubility level [35]. In fact, the hydrocarbon micelle in water may increase the non-equilibrium solubility, decreasing the solubility rate [36].

Shaw (1989) derived an empirical equation representing the hydrocarbon molar fraction in water and the influence of the carbon numbers [37]. Thus, one can see that this equation anticipates a decreasing exponentially with the carbon number.

$$\ln x = -3.9069 - 1.51894\, CN \qquad \text{Equation 1}$$

Where,

$x =$ molar fraction of alkanes in water, CN = alkanes carbon number

Mączyński et al. (2004) derived a more advanced equation for alkane solubility in water via Equation 2. This equation, which also includes the temperature effect, was generated by using 32 binary mixtures. This equation has the special advantage of not requiring adjustable parameters to predict the solubility level. [38]

$$lnx = lnx_{min} + C_3 b\left[\frac{T_{min}}{T} + \ln\left(\frac{T}{T_{min}}\right) - 1\right] \qquad \text{Equation 2}$$

Where,

$x$ = molar fraction of alkanes in water, $x_{min}$ = minimum molar fraction of alkanes, $C_3$ = data variance, $b$ = coefficient in $lnx_{min}$, $T_{min}$ = temperature of minimum molar fraction, $T$ = temperature of the molar fraction.

One should note that the alkane low solubility level in water causes scattering in measurements. Thus, accuracy is limited [39]. This led to developing statistical approaches, such as the Statistical Associating Fluid Theory (PC-SAFT), which uses binary parameters and carbon numbers [40], [41].

### *2.1.2 Naphtha – Water*

Naphtha is a hydrocarbon blend (hydrocarbon cut) from petroleum processing [42]. Naphtha can be further classified in light naphtha and heavy naphtha. Light naphtha contains hydrocarbons with 5-6 carbons, while Heavy naphtha hydrocarbons with 6- 12 carbons [43].

More specifically, naphtha contains paraffinic, aromatic and naphthenic compounds [44]. Given the low polarity of hydrocarbons, solubility in water is relatively low for naphtha. However, aromatic compounds are somewhat of an exception dissolving more the water, as these substituents groups in the benzene ring can display polarity [45]. Thus, the overall solubility of naphtha in water is of importance given it can help to mitigate the environmental impact in the heavy oil process using naphtha as a solvent.

Naphtha-water has rarely been studied in open-literature. Phase equilibrium of naphtha in water has been investigated in the context of aromatic compounds extraction only [46]. The scarcity data about this subject may be due to the following:

(1) Naphtha is challenging to be characterized composition-wise

(2) Adequate phase equilibrium cells are hard to design

(3) The existing thermodynamic models lack good agreement for the naphtha in highly diluted water systems.

### *2.1.3 Bitumen – water*

Bitumen is a semi-solid petroleum compound with high viscosity and adhesive properties [47]. Compared to conventional oil, bitumen contains mainly carbon and impurities, such as nitrogen, sulphur and heavy metals [48]. Bitumen is a distilled product from conventional oil. However, bitumen can be obtained naturally in Canada [49]. Despite its low grade and high impurities, the oil sand process can be significantly upgraded with the product of upgrading being later refined [50].

Bitumen contains 300 ~ 2000 chemical compounds [51]. Due to the huge number of chemical species, it can be characterized based on elemental composition. Furthermore,

SARA (Saturates, Aromatics, Resins and Asphaltenes) analysis can also be used to understand the value of bitumen into fractions. Bitumen can display variable solubility with this depending on the solvent of choice. [52]. Table 2 reports the bitumen characteristic, including elemental composition and SARA analysis.

**Table 2. Bitumen composition by Elements and SARA analysis** [52]

| Elements | wt% | SARA analysis | wt% |
|---|---|---|---|
| Carbon | 83.2 ± 0.9 | Saturates | 16.1 ± 2.1 |
| Hydrogen | 9.7 ± 0.4 | Aromatrics | 48.5 ± 2.3 |
| Nitrogen | 0.4 ± 0.2 | Resins | 16.8 ± 1.2 |
| Sulphur | 5.3 ± 0.2 | Asphaltene | 18.6 ± 1.8 |
| Oxygen | 1.7 ± 0.3 | | |

There is limited technical literature on bitumen-water phase behavior [53], [54], with the main goal of these publications being operating conditions for in-situ extraction and refining processes in the oil sand industry.

Amani et al. (2013) analyzed bitumen – water phase behavior at a high temperature and pressure. X-ray transmission tomography was used to show coexisting phases in the 9.2 ~ 96.6 wt% bitumen in the water range [55]. The experimental conditions were validated by well-known mixtures such as 1-methylnaphthalene in water and toluene in water. Literature data were used to compare with the experimental data. Since the research targeted to find adequate operating conditions for bitumen extraction, the critical point of water was studied in three-phase equilibrium conditions (vapor –liquid-liquid). [55]

Regarding naphtha-bitumen-water blends studies, they are valuable, given naphtha is a typically used diluent to meet pipeline transportation specifications by reducing the bitumen viscosity [56]. Yang and Czarnecki (2002) studied the influence of naphtha-bitumen ratios in hydrocarbon-water blends. It was observed that the solubility of water in bitumen was highly dependent on naphtha/bitumen ratio in the bitumen, while bitumen in water was highly immiscible, with this being a function of the molecules polarity differences [57]. One should note that the stability of the formed emulsion collapsed when the naphtha/ bitumen ratio (N/B) was in the 0.5 to 1.5 range [57].

Regarding bitumen-water emulsions stability, it is of significance to mention phase behavior [58], [25]. In this respect, a third agent, namely an emulsifier frequently designated surfactant, can influence species immiscibility [59]. This is the case of naphthenic acids and porphyrins [60]. Therefore, bitumen-water blends can form stable emulsions, which are problematic to deal with, in the oil sand processes [61].

## 2.2 VLE Measuring Equipment

Vapor Liquid Equilibrium (VLE) experimental data is of critical importance for hydrocarbon-water separation processes [62] such as distillation, extraction and separation [63]. Experiment data is also essential to validate thermodynamic phase equilibrium models [64], [65]. Hence, the decision on the VLE measurement apparatus selection is a significant matter in both academic and industrial settings.

VLE data has to be obtained under “dynamic” phase equilibrium, with the rates of condensation and evaporation being the same [66], [63]. Therefore, the assessment of this “dynamic” phase equilibrium is required in the apparatus that maximizes the data points [67], using automated units [64].

Despite the growing demands for the VLE databases, there is limited data in the open-literature, with this data being also restricted to a limited number of chemical species blends [68]. Thus, VLE measurement apparatus are needed for addressing the following [69]: (a) Easy access, (b) Enhanced Accuracy, (c) Low Cost, (d) Short Measurement Times.

Figure 3 reports a classification of the existing VLE measurement devices [70]. The developed phase equilibrium measurements are divided into: a) “Batch” methods and b) “Flow” methods [71]. Batch and Flow devices differentiate each other, in the way they approach equilibrium. The flow method develops measurements while the species blend circulated through the equipment, whereas the batch method measures phase equilibrium in a close cell of a set volume [72]. Both devices measure: a) phase compositions withdrawing a sample, b) total pressure via a digital pressure gauge [73].

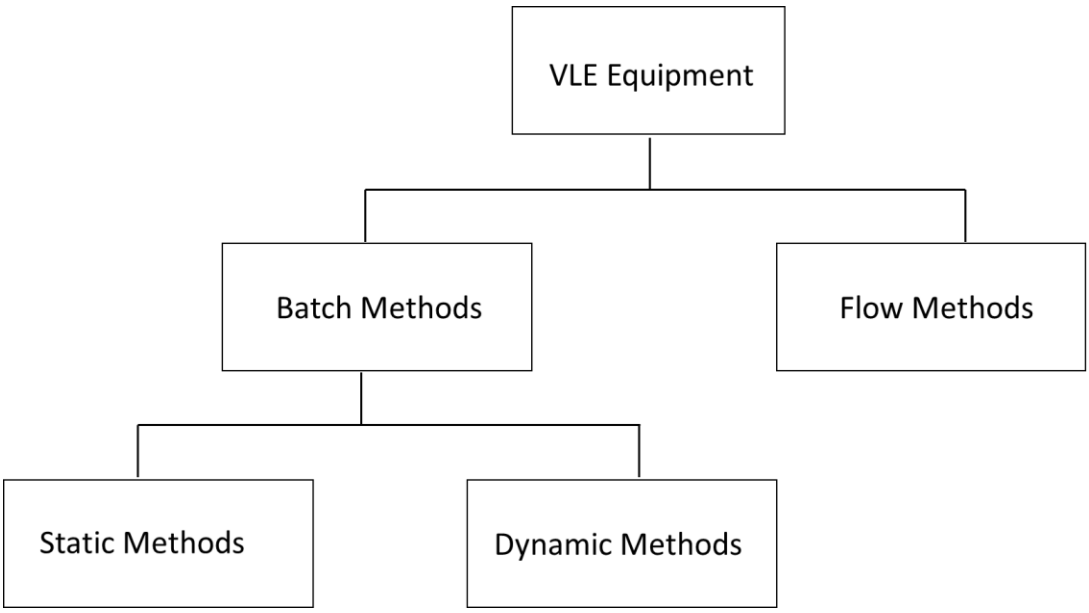


**Figure 3. Classification of VLE measuring apparatuses** [70]

### *2.2.1 Batch Method*

The batch method keeps phase equilibrium and measures the physical properties of a sample in a closed system [74]. In the "batch-static" mode, the cell is vacuumed prior to the run, with injectors used to feed the sample once the low pressure condition is attained [75]. During the experiment, the loaded sample has to be mixed well, so that the sample reaches the phase equilibrium condition rapidly [76]. Batch-static methods are the most widely used for phase equilibrium research because of their simplicity. Furthermore, both a small amount and a diversity of samples can be studied [77]. However, the cell requires special designs to be able to afford high temperature and pressure conditions, without leaks and pressure vacuum being lost [78].

Figure 4 describes a schematic of a "Batch-Static" analytical equipment. One should notice that the sampling is directed towards analytical equipment, e.g. Gas Chromatography and Mass Spectrometry to measure the sample composition [67].

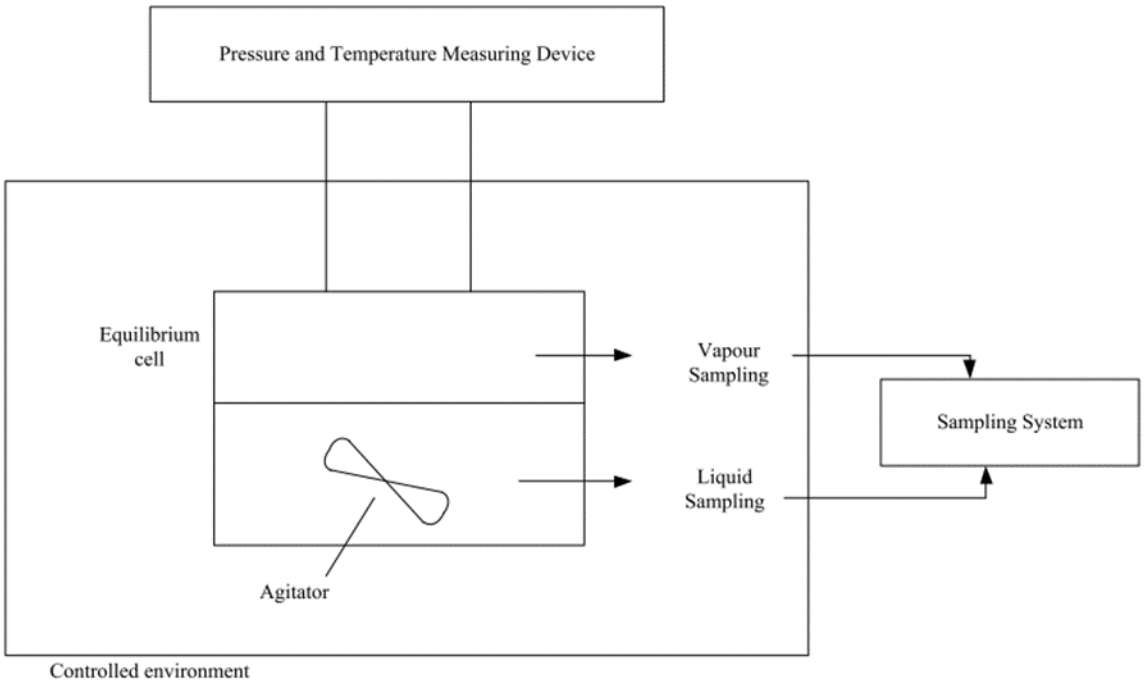


**Figure 4. A Schematic depiction of the static analytical equipment** [67]

This method offers however challenges: a) the samples taken for analysis must be much smaller than the one contained in the cell and this without disturbing pressure or mixing conditions [78], b) one has to ascertain that the sample taken is a representative from either the liquid or the gas phases, with this being even more challenging in multiphase systems, with two liquid phases.

Furthermore, the following are additional disadvantages of the "Batch-Static Method" with concentration measurements method [79]:

(1) Calibrating analysis is difficult.

(2) Degassing must be proceeded to get rid of impurities.

(3) The aqueous-based sample is difficult to be analyzed using conventional columns and detectors.

On the other hand, the “Batch-Static” method with both total pressure and temperature measurement is another option [80]. Using this approach, the compositions of both vapor and liquid are calculated, knowing the experimental measured temperature and pressure values [81].

The “Batch-Static” Method with pressure and temperature measurements is simple to implement, involving a much lower cost [82],[83],[75]. This method reduces experimental uncertainties from sampling, sample preparation and sample analysis [76]. Furthermore, the Batch-Static” Method with pressure and temperature measurement can be applied for a broader range of chemical species blends [84].

The Batch-Static” Method with pressure and temperature measurements offers the following challenges [76]:

(1) There is no information obtained from phase compositions.

(2) Thermodynamic consistency is given by the summation of molar fractions being one cannot be directly checked.

(3) Degassing must proceed with the run given impurities or dissolved gas affecting the obtained data.

Figure 5 reports a typical design of a “Batch-Static” Method, as given by Uusi-Kyyny et al. (2012). The apparatus measures the total pressure and analyzes the phase behavior of the mixture by numerical calculation. Degassing and injecting methods are successfully conducted, measuring 21 equilibrium conditions [85]. This method was found adequate to measure the phase equilibrium of two miscible liquids mixture considering the known temperature, pressure and volume information. Water as a thermo-fluid given run is used in the 50 ℃ and 90 ℃ range.

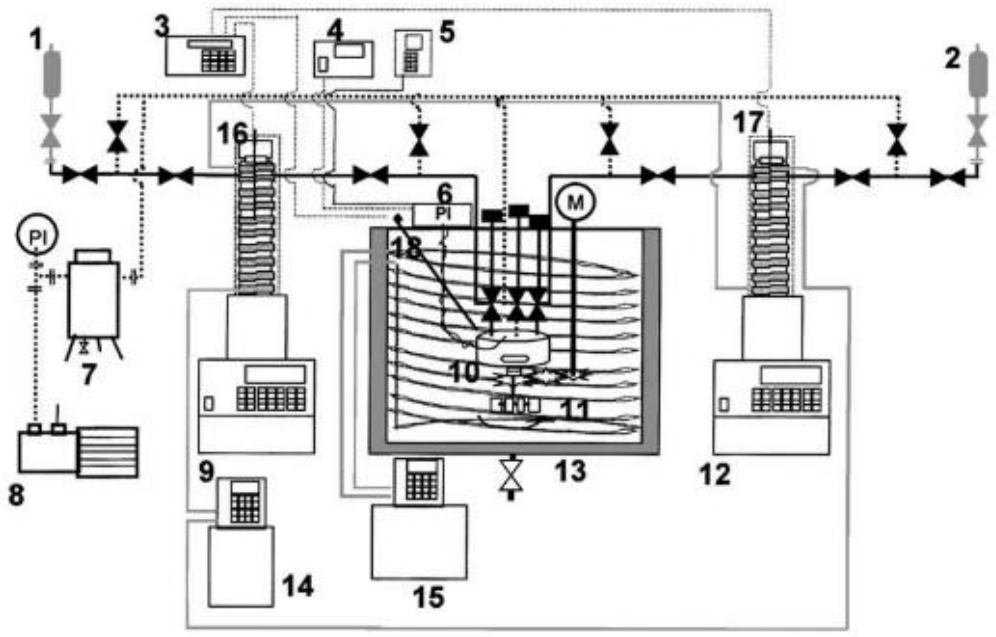


**Figure 5. Batch-Static Method Device : (1) and (2) feed cylinders; (3) temperature meter; (4) pressure display; (5) temperature controller; (6) pressure transducer; (7) liquid nitrogen trap; (8) vacuum pump; (9) syringe pump; (10) equilibrium cell; (11) batch liquid mixer; (12) syringe pump; (13) thermostated water batch; (14) and (15)circular bath; (16), (17) and (18) temperature probe.** [86]

### *2.2.2 Flow Method*

The flow method involves a cell with a flow of chemical species continuously circulated to reach equilibrium at all times [67]. In the flow method, the cell pressure is controlled, so the vapor and liquid phases reach a steady-state after a given period [69], [80]. The flow method does not have a high cost though it involves a higher complexity than the batch [76]. The apparatus is relatively easy to assemble and can be optimized for specific phase equilibrium studies [87].

The flow method can as well divided into three: (1) Single Vapor Pass, (2) Single Vapor and Liquid Pass, (3) Phase Recirculation.

The Single Vapor Pass Flow method involves a vapor phase flowing in the cell only, with the liquid phase being stagnant [67]. This method is recommended for using with a vapor

phase occupying most of the cell volume [81]. This method allows researchers to investigate the thermodynamics of mixtures rather quickly [87], being restricted to pure compounds, given its otherwise unstable equilibrium [69], [67].

The Single Vapor and Liquid Pass Flow method involve a high-pressure pump feeding both gas and the liquid phases into the measuring cell [76]. This apparatus provides a stable equilibrium condition for wide range of boiling point samples [88]. [84]. However, the experimental protocol method of this technique is complicated, with a flow rate and liquid level difficult to control [87], [81].

The Phase Recirculation Flow method involves two flows [67], with phases recirculated until they reach equilibrium [89]. Therefore, two pumps are required. This method provides, in principle, enhanced phases helping to reach the rapid phase equilibrium [87]. However, because of the active movement of the flow, [76] close control of the operation of two pumps is needed with the data quality varying on the system operator [76].

## 2.3 Thermodynamic Principles

Fugacity is a "theoretical based parameter" involved in phase equilibria[90]. Thus, VLE condition can be expressed by using the fugacity in the liquid phase and gas phase as follows [91], [92], [93]:

For pure liquids,

$$f_i^L(T,P) = \phi_i^{sat}(T,P_i^{sat})P_i^{sat} \exp\left[V_i^L\left(\frac{P-P_i^{sat}}{RT}\right)\right] \qquad \text{Equation 3}$$

Where,

$f$ = fugacity, $\phi$ = fugacity coefficient, T = temperature, P = Pressure, V = Volume, sat = saturation state pure component quantity, i = component identity, R = gas constant

For the liquid solution, an activity coefficient model can be introduced using the fugacity equation.

$$\hat{f}_i^L = \gamma_i x_i f_i^L \qquad \text{Equation 4}$$

where,

$\gamma$ = activity coefficient, $x$ = Liquid phase molar fraction, ^ = partial molar property

Applying pure liquid fugacity to the solution, a general expression for liquid fugacity can be derived,

$$\hat{f}_i^L = \gamma_i x_i \phi_i^{sat} P_i^{sat} \exp\left[V_i^L \left(\frac{P - P_i^{sat}}{RT}\right)\right] \qquad \text{Equation 5}$$

Meanwhile, the activity coefficient, $\gamma_i$, can be measured in experiments and fitted to the excess Gibbs energy.

$$ln\gamma_i = \frac{\bar{G}_i^E}{RT} = \frac{1}{RT}\left[\frac{\partial(nG^E)}{\partial n_i}\right]_{T,P,n} \qquad \text{Equation 6}$$

where,

$G^E$ = excess Gibbs energy

For pure vapor,

$$f_i^v(T,P) = \phi_i(T,P)P \qquad \text{Equation 7}$$

As well, one can note that the fugacity coefficient can be measured by the deviation from the ideal gas behavior using the $\phi_i(T,P)$ activity coefficient.

Regarding a vapor phase in a multicomponent mixture, an equation analogous to Equation 8 can be considered with the fugacity coefficient calculated by using an equation of State (EOS). Thus, a general equation for fugacity in a gas mixture is the following,

$$\hat{f}_i^v(T,P) = \hat{\phi}_i(T,P)y_i P \qquad \text{Equation 8}$$

Where,

$y_i P$ = Partial pressure

At vapor-liquid phase equilibrium with the Gibbs free energies being the same in the two phases, and consequently the fugacity being as well the same, the VLE conditions can be expressed:

$$\hat{f}_i^L(T, P, x_i) = \hat{f}_i^v(T, P, y_i) \qquad \text{Equation 9}$$

Hence, Equation 5 and Equation 8 can be used to represent the liquid phase fugacity and gas phase fugacity as follows,

$$\gamma_i x_i \phi_i^{sat} P_i^{sat} \exp\left[V_i^L \left(\frac{P - P_i^{sat}}{RT}\right)\right] = \hat{\phi}_i(T, P) y_i P \qquad \text{Equation 10}$$

### *2.3.1 Activity Coefficient Model*

The activity coefficient describes the deviation of the mixture behavior from ideality [94] as the ratio of actual fugacity over the standard fugacity. [95] [96] [97].

Regarding liquid fugacity, its prediction involves an activity coefficient [92] [98]. The main feature of the activity coefficient is to treat liquid different from vapor [99] as a deviation from an ideal solution and ideal-gas behavior.

The Non-Random Two Liquid (NRTL) model is reported as one most commonly used to calculate activity coefficients (Renon and Pranusnitz,1968). The NRTL equation is also known as the Local-Composition method from the Wilson equation, which correlates well VLE data [92]. NRTL equation provides a good representation of non-ideal mixtures, polar compounds and partially immiscible systems [100].

Reid et al. (1988) explained the NRTL equation for a binary mixture as follows [101],

$$ln\gamma_1 = x_2^2 \left[\tau_{21}\left(\frac{G_{21}}{x_1 + x_2 G_{21}}\right)^2 + \frac{\tau_{12} G_{12}}{(x_2 + x_1 G_{12})^2}\right] \qquad \text{Equation 11}$$

$$ln\gamma_2 = x_1^2\left[\tau_{12}\left(\frac{G_{12}}{x_2 + x_1 G_{12}}\right)^2 + \frac{\tau_{21}G_{21}}{(x_1 + x_2 G_{21})^2}\right] \quad \text{Equation 12}$$

where

$$lnG_{12} = -\alpha\tau_{12} \quad \text{Equation 13}$$

$$lnG_{21} = -\alpha\tau_{21} \quad \text{Equation 14}$$

where $\tau_{12}, \tau_{21}$ are the dimensionless interaction factor, related to the energy parameter as follows:

$$\tau_{12} = \frac{\Delta b_{12}}{RT} = \frac{U_{12} - U_{22}}{RT} \quad \text{Equation 15}$$

$$\tau_{21} = \frac{\Delta g_{21}}{RT} = \frac{U_{21} - U_{11}}{RT} \quad \text{Equation 16}$$

Where,

$U_{ji}$ = energy between the molecular surface, $U_{ii}$ = energy of evaporation, $\alpha, b_{12}, b_{21}$ =specific parameters to given species, depending on the composition and temperature.

If the NRTL model is adapted to determine the liquid phase properties, a single parameter equation can be derived, called the Margules activity coefficient model.

The activity coefficient at infinite dilution can be calculated from Equation 13 to Equation 16 as follows:

$$ln\gamma_1^{\infty} = [\tau_{21} + \tau_{12}\exp(-\alpha_{12}\tau_{12})] \quad \text{Equation 17}$$

$$ln\gamma_2^{\infty} = [\tau_{12} + \tau_{21}\exp(-\alpha_{12}\tau_{12})] \qquad \text{Equation 18}$$

The above NRTL equation describes the local composition in the liquid-solution where non-random molecular orientations are led by molecular forces in the liquid solution [92].

The NRTL equation shows excellent performance for liquid-liquid and vapor-liquid equilibrium conditions [102] as follows: a) for non-ideal mixtures good simulation of experimental data [92], b) for partially miscible systems and polar compounds accurate data representation [103].

Zygula (2001) used the NRTL model and compared equilibrium data by using three commercial simulators in an ethylbenzene separation column, as shown in Figure 6. The three (3) simulators showed good agreement with the experimentally studies non-ideal mixture [16].

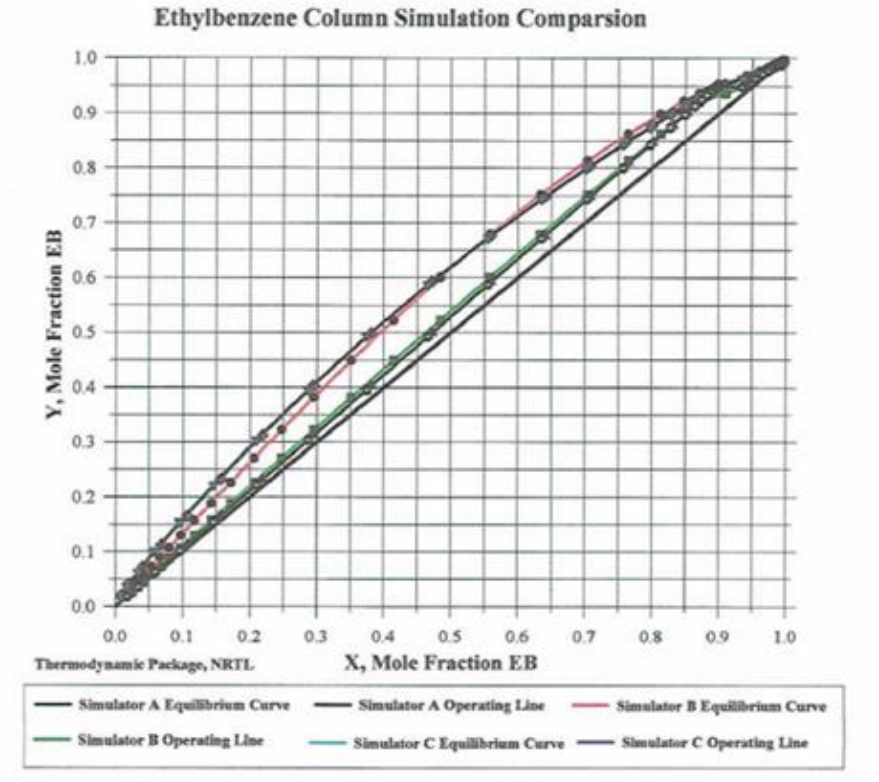


**Figure 6. Vapor-Liquid Equilibrium simulation by Non-Random Two Liquid equation** [16]

### 2.3.2 Equation of State Model

An equation of state (EOS) is the mathematical relationship between pressure, temperature, volume and composition [92]. EOS is appropriate for specific applications [104].

Peng Robinson equation of state (PR EOS) is the most widely used EOS model developed by Peng and Robinson(1976) for the ideal hydrocarbon system. The equation can be summarized by the following:

$$p = \frac{RT}{V_m - b} - \frac{a\alpha}{V_m^2 + 2bV_m - b^2} \quad \text{Equation 19}$$

With

$$a = \frac{0.45724R^2T_c^2}{p_c} \quad \text{Equation 20}$$

$$b = \frac{0.7780RT_c}{p_c} \quad \text{Equation 21}$$

$$\alpha = \left(1 + \kappa\left(1 - T_r^{\frac{1}{2}}\right)\right)^2 \quad \text{Equation 22}$$

$$\kappa = 0.37464 + 1.54226\omega - 0.26992\omega^2 \quad \text{Equation 23}$$

$$T_r = \frac{T}{T_c} \quad \text{Equation 24}$$

Where

$T_c$ = Critical temperature, $p_c$ = Critical pressure, $\kappa$ = isothermal compressibility, $T_r$ = reduced temperature, $V_m$ = molar volume, $\omega$ = the acentric factor.

The PR-EOS model is typically adequate for natural gas processes [105]. For instance, the PR-EOS can provide high accuracy for gas condensate given the ease of compressibility factor and liquid density calculations [106].

Although the PR-EOS shows good performance for hydrocarbon mixtures under the described conditions, this model may not be adequate near the critical region [106]. A possible reason for this being the density fluctuation affecting thermodynamic properties under these conditions [104]. One should note that density variations are ignored in PR-EOS, given it is difficult to incorporate them in the EOS [107].

Due to the limitation of PR-EOS, some advanced thermodynamic models were developed by adjusting the original PR-EOS. Stryjek and Vera (1986) published significant modifications as PRSV1 and PRSV2 equations. PRSV1 improves the compressibility and acentric factor by adding the additional parameters in the equation, as shown in Equation 25 and Equation 26. [108]

$$\kappa = \kappa_0 + \kappa_1 \left(1 + T_r^{\frac{1}{2}}\right)(0.7 - T_r) \qquad \text{Equation 25}$$

$$\kappa_0 = 0.378893 + 1.4897153\omega - 0.17131848\omega^2 + 0.0196554\omega^3 \qquad \text{Equation 26}$$

Despite PRSV1 improvements, this model was not accurate enough for phase equilibrium calculations with temperature changes [108]. Thus, a PRSV2 model was introduced to enhance VLE calculations by two additional temperature depending terms applied over ninety pure compounds. [108].

$$\kappa = \kappa_0 + \left[\kappa_1 + \kappa_2(\kappa_3 - T_r)\left(1 - T_r^{\frac{1}{2}}\right)\right]\left(1 + T_r^{\frac{1}{2}}\right)(0.7 - T_r) \qquad \text{Equation 27}$$

$$\kappa_0 = 0.378893 + 1.4897153\omega - 0.17131848\omega^2 + 0.0196554\omega^3 \qquad \text{Equation 28}$$

Since PRSV equations have also shown weaknesses in the temperature range below the critical temperature, many researchers have proposed alternative formulation to enhance the accuracy range [106]. Twu et al. (1998) pointed out the importance of hydrogen bonding and proposed a model in the non-ideal system [109]. Nader and Behzad (2007) connected the Peng-Robinson equation of state model and van der Waals mixing rule to predict stable non-ideal mixtures [13].

## 2.4 Multiphase Mixing

Multiphase flow refers to the simultaneous flow of two or more phases [110]. Most chemical process units are operated under multiphase flow conditions. Thus, the investigation of multiphase behavior is significant to enhance the industrial process [111]. In this chapter, various shape factors are reviewed to determine the condition of multiphase mixing for the apparatus design.

This section discusses technical literature on mixing as relevant to the Naphtha Recovery Unit (NRU). The NRU unit is a typical multiphase flow system, which is composed of 83-86 wt% water, 10-13 wt% Solids, 1-3 wt% Bitumen and 0-0.4 wt% naphtha [112]. In this separation column, the complex liquid multiphase flow is also combined with steam injection [113]. Column pressure, feed pre-heat conditions and NRU design are the main factors affecting performance [114].

Since various operating conditions may affect mixing and phase dispersion behavior, these issues in conjunction with phase equilibria, have to be analyzed [115].

### *2.4.1 Batch Stirred Tank*

Batch stirred tanks are mainly used to study multiphase flow, given the great advantage of its flexible size [116]. Furthermore, researchers can select various agitators in the system. Geometric parameters, such as impeller and vessel type, can also be easily modified to investigate shape factors [117].

Phase dispersion is an essential fluid dynamic condition to allow accurate measurements in a batch stirred unit [118]. Although phase dispersion behavior can be studied with various means, the interfacial area per unit column can be effective to understand phase dispersion [119]. Figure 7 reports the schematic experimental setup used to study phase distribution.

In this respect, Abu-Farah et al. (2014) developed a non-baffled stirred reactor to visualize the cyclohexane and water immiscible binary system. A video camera and red tracer were used in that study. The radial and axial volume tracer compositions were measured by using the sample withdrawal method. On this basis, the minimum impeller speed to achieve the

uniform distribution was determined. Both video analysis and sample withdrawal methods were compared to validate the results. Volume fraction, radial position, axial position, and mixing speed were chosen to establish complete dispersion of the largely immiscible phases. [120]

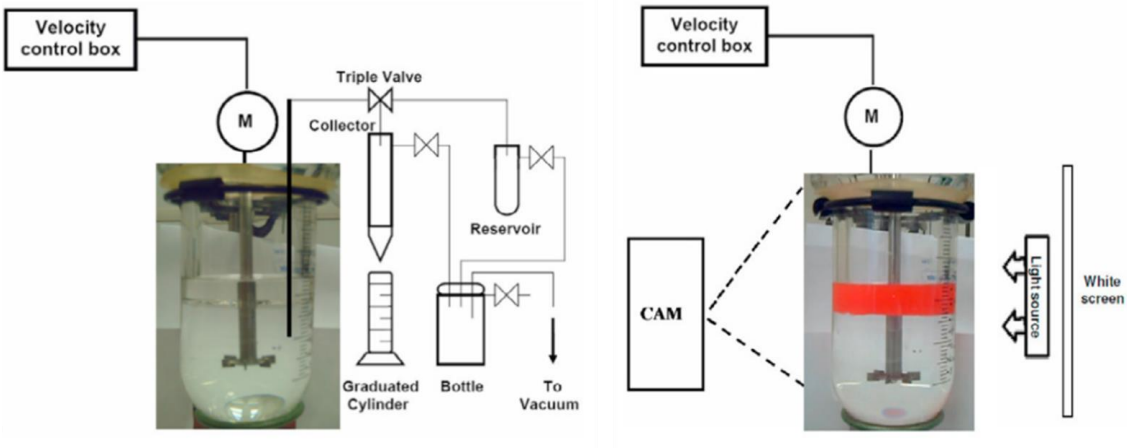


**Figure 7. Experimental setup for Visualization of Phase Dispersion** [120]

Gradov et al. (2017) reported an example of a solid-liquid mixing study in a batch stirred tank unit. Various carboxymethyl cellulose (CMC) solutions were measured taking as the basis the volumetric mass transfer.

Figure 8 provides a schematic description of the unit as well as the optical apparatus for flow visualization using Solid Partial Image Velocimetry. Images capture velocity and flow movement using the particle tracing. The generated laser sheet produced two-dimensional images of the solid-liquid mixture. [121]

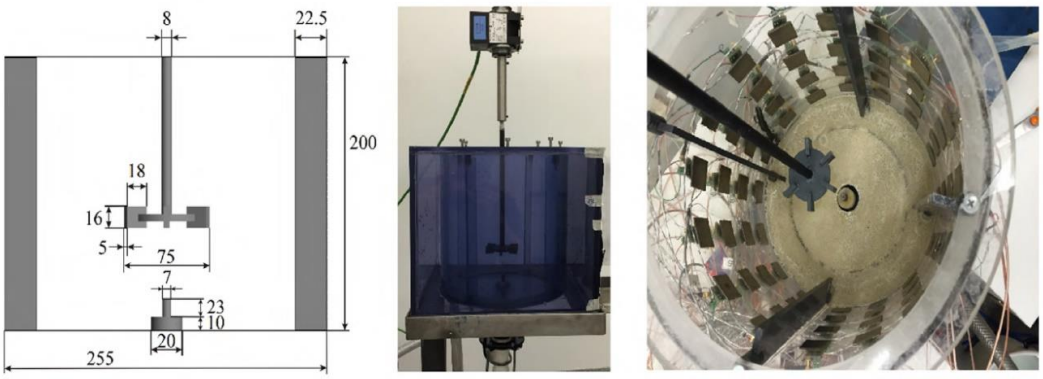


**Figure 8. Experimental illustration for solid-liquid mixtures and plexiglass prism for PIV experiment** [121]

### *2.4.2 Impeller*

The impeller is an agitation component moving fluid from one point to another by mechanical action [116]. The impeller is a critical component in a batch given its strong influence on mixing [122]. Impellers are typically placed on a shaft located in the central batch position. [123]. Furthermore, the impeller design determines hydraulic performance, with different chemical species blends displaying variable transport capacity with the same impeller [124]. Therefore, both the position and design of the impeller have to be carefully decided for a particular mixture.

When one decides to apply an impeller in a stirred tank reactor, two issues should be considered; (1) radial flow, (2) axial flow. Radial flow impellers are used to provide shear stress [125]. Immiscible fluid and high viscosity mixture normally require this shear stress promoting impellers to have homogenous mixing. On the other hand, axial flow impellers are applied to provide high-speed mixing [126]. Thus, suspended solids or high-density materials can be adequately agitated with axial flow impellers [116].

Figure 9 reports the standard Rushton Turbine, which is widely used as a radial flow agitator. The Rushton turbines are designed with six (6) flat vertical blades. The Rushton turbine is used for gas mixture mixing due to its radial positioned flat blade [127]. However, the Rushton turbine application is limited to its use to low-impeller speeds conditions because the impeller power decreases with impeller speeds [128].

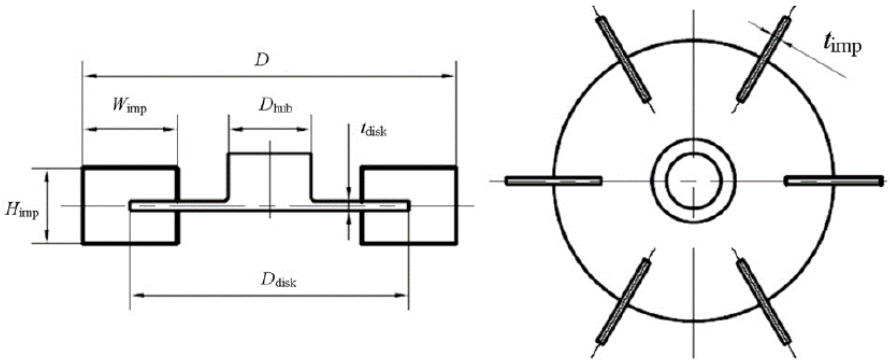


**Figure 9. Description of the Standard Rushton Turbine** [129]

Figure 10 describes the pitched blade turbine, which can be considered in the category of the axial impeller. The pitched blade turbine promotes a significant fluid up-flow and down-flow [130]. Axial impellers can provide high power at high-mixing speed conditions [131]. Regarding the pitched blades, the up-flow pitched blades typically deliver a better mixing performance than downflow mixing [116]

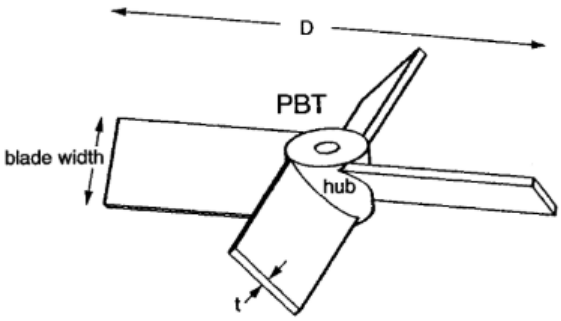


**Figure 10. Pitched Blade Turbine** [132]

Trad et al. (2017) compared nine unbaffled dual-impeller designs that impose both radial mixing and axial mixing in the system. Figure 11 shows the specific geometric design of a dual impeller system. This dual-impeller was designed considering position, rotational speed and liquid injection placing and this to provide good mixing in a liquid-solid waste mixture. Application of this impeller was focused on low 50 to 150 rpm speeds and this to

sustain the biomass production. Results obtained showed that dual-impeller configuration was appropriate to avoid solid deposition and enhanced liquid to gas mass transfer. [133]

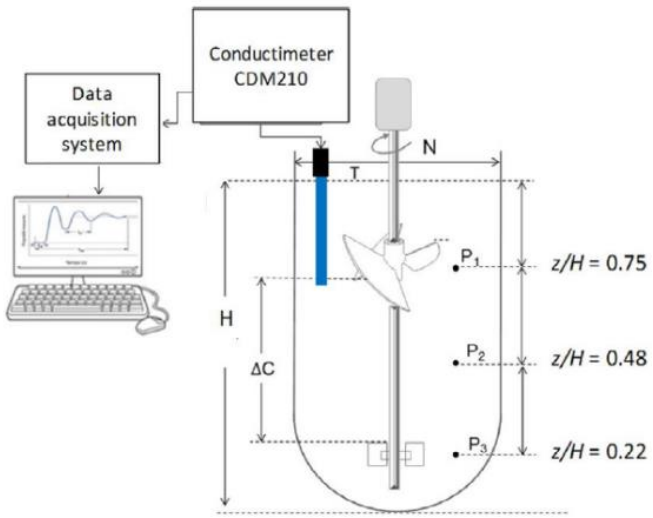


**Figure 11. Experimental setup and schematic image of the dual impeller** [133]

### *2.4.3 Baffle*

Baffles are an obstacle to the fluid flow tangential motion [116]. When the impeller movement forms a vortex, the gas phase achieves a significant interface area fraction [134]. However, vortex formation may not be as effective, given the high speeds of agitation in the circumferential direction [135]. Therefore, baffles are designed to act as vortex breakers supporting efficient mixing.

Figure 6 reports the standard full baffled stirred tank, designed to prevent stagnant flow.

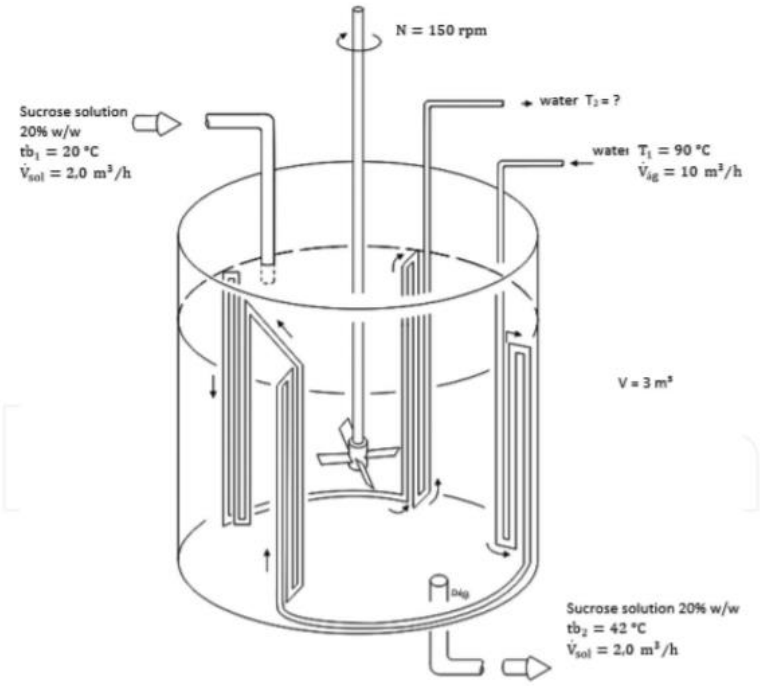


**Figure 12. Standard full baffled stirred tank** [136]

Pukkella et al. (2019) studied 'Interface baffle' with baffles placed at the interface region. The CFD simulation of 'interface baffles' is described in Figure 13. The interface baffle was used with a solid-liquid mixture with the Lagrangian particle tracking to predict the mixing patterns. [137]

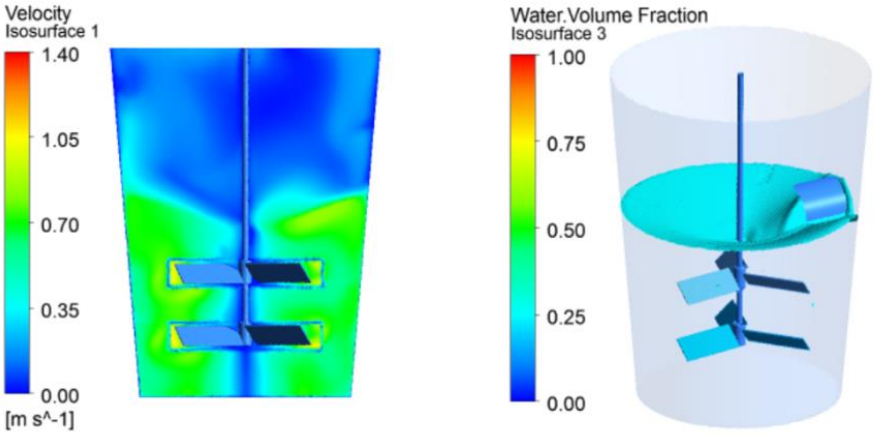


**Figure 13. CFD modeling image of Interface baffle** [137]

## 2.5 Conclusions

The thermodynamics of multicomponent-multiphase systems is of significant importance for both academia and the industry. To understand the multicomponent-multiphase systems, this chapter reviews the technical literature as follows: (1) Hydrocarbon-water blends, (2) VLE equipment, (3) Mixing, (4) Thermodynamic models

Based on the discussion of the technical literature, the following conclusions can be advanced:

(1) Water-hydrocarbon blends are typical multiphase-multicomponent mixtures. They can cause significant environmental effects by forming a partially miscible liquid in water process discharges. Among the group of hydrocarbons involved, naphtha and bitumen are most challenging to characterize composition-wise. Despite their significance, water-hydrocarbon blends have scarcely been studied and they should be as in the present study, subject of important research.

(2) VLE measurement devices can be classified as batch methods and flow methods. Batch-static methods are the most widely used because they require small samples, and the procedures are relatively simple. However, "Batch-static" cells are significantly restricted to the amount of data obtained from every run, and improved "Batch-dynamics" methods as in the present study are advisable.

(3) Intense multiphase mixing is a critical condition to be achieved in a VLE cell. The size of the batch stirred tank, the type of impeller, and the baffle positioning are all contributing factors. It is with this view that mixing conditions and their impact on thermodynamics in a new CREC-VL cell are analyzed in the present thesis.

(4) VLE phase equilibrium can be determined using an EoS (Equation of State) for the vapour phase and activity coefficient for the liquid phase. Alternatively, both EoS models can be considered for the vapor and liquid phases, as is the PR-EoS (Peng Robinson Equation of State) widely used for hydrocarbon system. However, in water-hydrocarbon mixtures, the PR-EoS may be inaccurate, and new enhanced thermodynamic models are needed.

# Chapter 3: Scope of the Research

The intent of this research is to provide enhanced understanding of multiphase/multicomponent species in the context of a wastewater plant in the oil sand industry. The proposed approach considers the study of vapor pressures of multicomponent mixtures, such as n-octane/water, naphtha/water and solids/naphtha/water using a batch operated CREC-VL Cell. Process flow simulations, such as Aspen Hysys, are considered to emulate the CREC-VL batch Cell data. The valuable experimental data results obtained suggest the value of the CREC-VL-Cell to evaluate thermodynamic models.

## 3.1 Particular Objectives

Based on these objectives, the following is proposed for this present study.

a) To develop a batch dynamic equilibrium apparatus, called the CREC-VL-Cell. To establish the experimental methodology to measure the vapor pressures of the solid-liquid-liquid-gas mixtures.

b) To measure phase equilibrium starting from 20 ℃ up to 110 ℃, using a. 1.22 ℃/min heating ramp.

c) To optimize the thermal equilibrium condition, with different thermo-fluid types and CREC-VL-Cell positions.

d) To optimize the mixing of the multicomponent/multiphase mixing using various operational parameters such as sample volume, impeller position, baffle type, impeller speed and transparent plexiglass unit replica.

e) To develop a synthetic naphtha, able to emulate the distillation curve of industrial naphtha.

f) To establish an air contained correction fraction, allowing run development in the CREC-VL Cell, without need of sample degassing using vacuum.

g) To develop an Aspen Hysys continuous process simulation that emulates the batch dynamic experiment methodology.

h) To analyze the saturation vapor pressures of n-octane/water mixtures.

i) To analyze the saturation vapor pressures of Synthetic Naphtha/water mixtures.

j) To analyze the saturation vapor pressures of Solids/n-octane/water mixtures.

k) To establish a mass balance method able to assess with CREC-VL-Cell data, the applicability of thermodynamic models.

## 3.2 Accomplishments of Research

a) A full manuscript (Manuscript 1) entitled "Understanding Synthetic Naphtha Recovery from Water Streams: Vapor-Liquid-Liquid Equilibrium (VLLE) Studies in a New VL-Cell Unit with High Intensity Mixing" submitted to the reputable chemical engineering journal ***Chemical Engineering and Processing - Process Intensification*****.** Chapter 4, 5 and 7 of this thesis essential components of that manuscript.

**b)** Conference Abstract (Abstract 1) entitled "Thermodynamics of Hydrocarbon/Water Systems: Challenges and a Binary Interaction Parameter (BIP) Based Modelling Approach Using Experimental Data". This Abstract was submitted in ***Canadian Chemical Engineering Conference 2020.*** Chapter 6 and 7 report the experimental results in this abstract

# Chapter 4: Dynamic System Design

In this chapter, we introduce the CREC-VL-Cell apparatus allowing “dynamic” measurements. The CREC-VL-Cell can measure both pressure and temperature continuously throughout the run. Three (3) design aspects are reviewed in this chapter to ensure the adequacy of the dynamic runs: (1) Heating of the cell, (2) Mixing in the cell and (3) Measurements Validation.

While various phase equilibrium set-ups are proposed in the open literature, there is limited availability of units adequate to investigate multicomponent mixtures. The CREC-VL-Cell offers dynamic measurements to analyze phase equilibria in solid-liquid-liquid-gas in multicomponent mixtures. It is anticipated that the proposed CREC-VL-Cell design will become a valuable tool for experimental based thermodynamic phase equilibrium research.

## 4.1 Heating System

In the CREC-VL-Cell, heat is provided to secure a linear temperature with run time (linear ramp). During “dynamic” measurements, both the total pressure and cell temperature are simultaneously monitored. One should notice that for the designed CREC-VL-Cell, it was observed that a selected 1.22 ℃/min heating ramp was viable for good “dynamic” measurements.

Thus, the CREC-VL-Cell system was designed for heating both the heat transfer fluid surrounding the cell and the CREC-VL-Cell itself to facilitate the “dynamic” method implementation.

### *4.1.1 Temperature System*

Figure 14 reports the cross-section image of the CREC-VL-Cell heating system designed in Solidworks®. The CREC-VL-Cell heating system included three (3) main functions: (1) it supplies a temperature ramp to the sample being studies, (2) it measures temperature and pressure in real-time and (3) it allows quick sampling once the run completed.

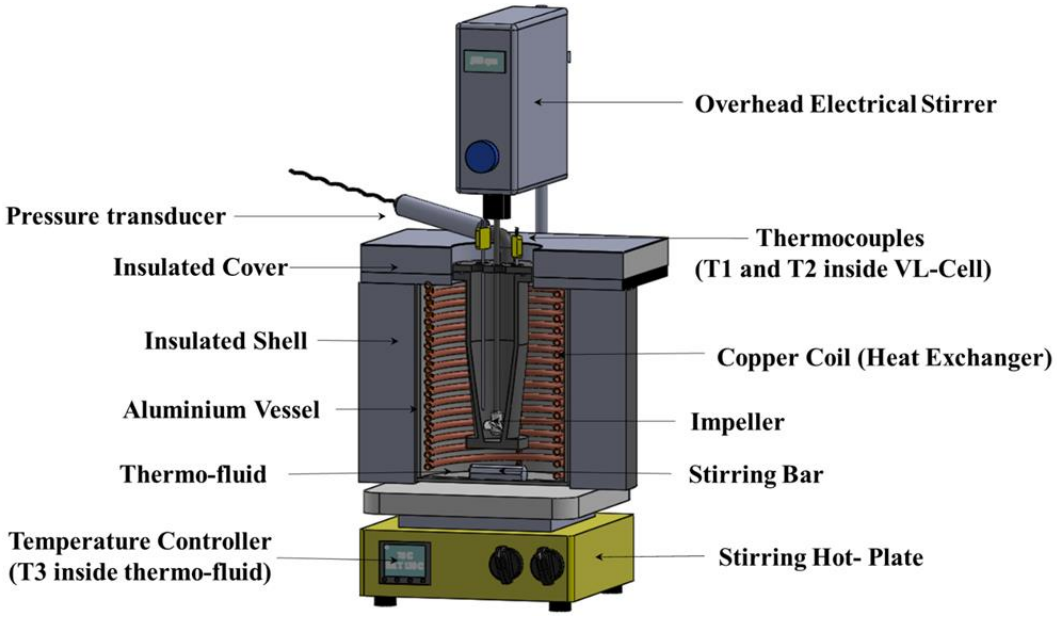


**Figure 14. Cross-Section of the CREC-VL-Cell heating system**

An electrically heated plate provides heat to the thermo-fluid filling an external aluminum vessel. A magnetic stirrer mixes the thermo-fluid at 350 rpm. The agitated thermo-fluid provides the forced convection required in the external thermofluid bath of the CREC-VL-Cell.

A temperature controller is connected to the stirred heated plate to provide feedback control. The temperature controller of the CREC-VL-Cell provides a linear temperature increase, with the temperature controller adjusting the electric power provide to the stirred heated plate.

The linear temperature increase elevates the system pressure progressively in the closed CREC-VL-Cell, with the selected 1.22 ℃/min ramp being adequate for the selected dynamic runs. Temperature and pressure data are collected continuously by a data acquisition system. The acquired physical properties can be analyzed with various methods, such as isothermal and isobaric conditions. Consequently, consecutive VLE data up to 120 ℃ can be achieved in 90 min.

Chilled water can flow through a copper coiled heat exchanger. The heat exchanger facilitates the readiness for the next experiment, reducing the sample temperature rapidly. In terms of safety, the heat exchanger was implemented for reducing hazardous while handling the warm heating oil.

Figure 15 reports a typical temperature measurement during the experiment. T1 and T2 are temperature readings of the liquid sample, while T3 is the temperature of the thermo-fluid.

Typical, 100 mL of pure n-octane is used in every run in the CREC-VL-Cell. A data acquisition module connects T1, T2 and T3 K-type thermocouples through a USB desktop. This allows confirming that the temperature difference between the two locations in the CREC-VL-Cell does not surpass 0.5 ℃ throughout the entire experiment, with differences with the thermo-fluid temperature being limited to 10 ℃.

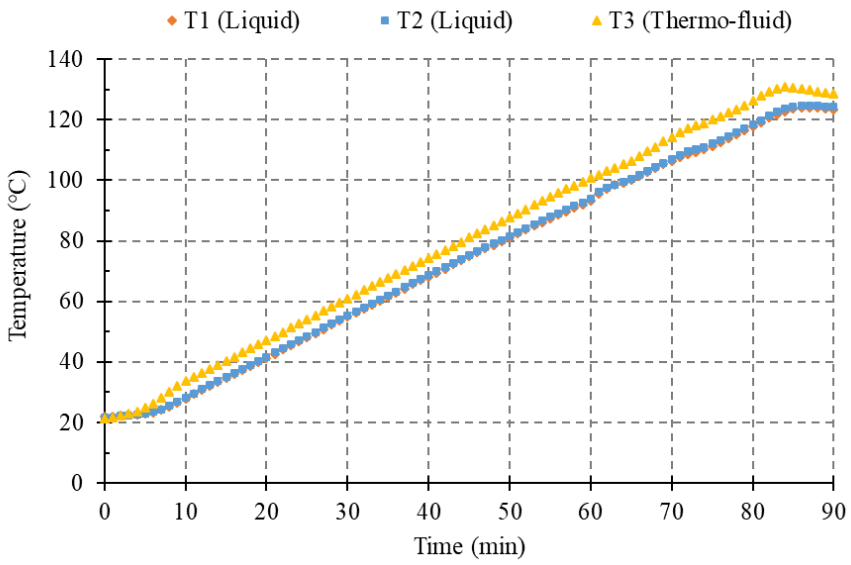


**Figure 15. Temperature measurement points at T1, T2 and T3 for Pure n-octane**

Figure 16 reports the CREC-VL-Cell as designed using Solidworks®. One can see the positioning of the strategically located thermocouples to measure the liquid temperature. Data from these two thermocouples are monitored to examine the local temperature variations inside the CREC-VL-Cell. The average readings from these two thermocouples allow establishing the average sample liquid temperature.

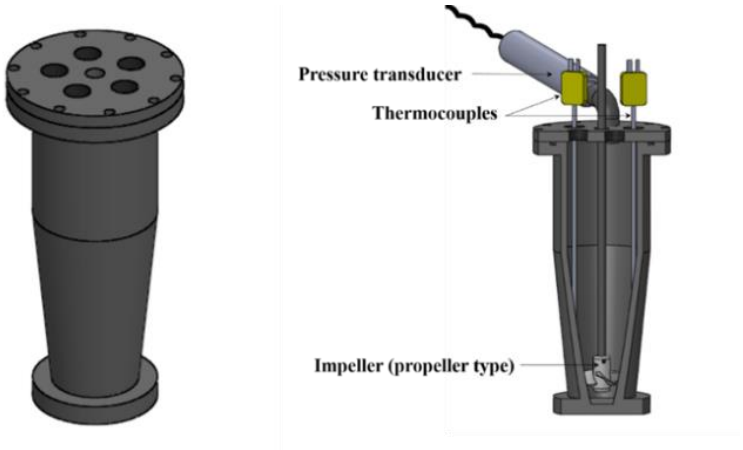


**Figure 16. CREC-VL-Cell illustration. Notes: (a) Exterior view, (b) Transversal view with Pressure transducer, Thermocouples and Impeller type**

One should note that the dynamic temperature method proposed in the present study, can be implemented thanks to the high mixing provided by the CREC-VL-Cell impeller. This high mixing is promoted by the fluid forced convection in the cell, making thermal gradients small. This mixing effect will be discussed further in Chapter 4.2

### *4.1.2 Pressure System*

The total pressure is measured in the CREC-VL-Cell using a pressure transducer connected to a desktop USB, which converts the pressure data into an electric signal. The data acquisition program records the continuous vapor phase during every experiment. The pressure data is acquired in real-time, together with the temperature data. This enabled the establishment of the sample physical properties needed for thermodynamic vapor-liquid model validation.

While the CREC-VL-Cell involves a simple digitalized pressure measuring system, pressure misreadings due to the leakage are a challenging issue. This is particularly the case, considering the CREC-VL-Cell must be operated at 1080 rpm impeller speed and up to 3.5 atm pressure.

### *4.1.3 Thermo-fluid*

The thermo-fluid is a liquid material with a thermal conductivity allowing good heat transfer to the CREC-VL-cell. Silicon oil is a widely used thermo-fluid given its inertness [138]. However, due to the high viscosity of the silicone oil with limited forced convection in the CREC-VL-Cell, it is considered inadequate for dynamic measurements. Thus, several fluid candidates can be considered as a thermo-fluid alternative given their physical properties as reported in Table 3

**Table 3. Physical Properties of Possible Thermo-fluid candidates.**

| **Properties** | **Water** | **Silicone oil** | **Engine oil** | **Corn oil** |
|---|---|---|---|---|
| **Viscosity (cp) at 40℃** | 0.6 | 55.0 | 30.0 | 31.0 |
| **Boiling point (℃)** | 100 | 374 | 300 | 300 |
| **Flash point (℃)** | - | 160 | 215 | 320 |
| **Smoke point (℃)** | - | - | - | 230 |
| **Thermal Conductivity (W/(m*K) at 20℃** | 0.59 | 0.12 | 0.15 | 0.17 |
| **Economic factor** | 0.01 | 1.00 | 0.50 | 0.05 |

Notes: (a) Viscosity governs the required forced convection, (b) Boiling point, Flashpoint and Smoke point determine the material usage temperature limit, (c) Thermal conductivity governs the heat transfer, (d) Economic factor determines the price based on Silicone oil commercial cost as a reference.

Viscosity is a significant property which determines the required forced convection in the CREC-VL-Cell. Since the magnetic stirrer agitates the thermo-fluid, high viscosity negatively affects fluid mixing. One should note that limited forced convection yields irregular heat transfer in the CREC-VL-Cell, with the lower cell sections gaining comparatively more heat than the top cell section. Therefore, a low viscosity thermo-fluid is advisable to promote good heat transfer.

Regarding the thermofluid boiling point range, the present study offers choices. In this respect, the thermo-fluid for the present study must have a higher boiling point than 150 ℃ to investigate naphtha recovery.

The thermal conductivity is as well, a parameter defining how much heat can be transferred through the material. In our case, heat must flow from a heated plate to an aluminum vessel and then to a thermo-fluid before it moves to the sample being studied. Table 3 reports that corn oil has a $0.165\ \frac{W}{m \cdot K}$ thermal conductivity, which shows that corn oil transfer heat more rapidly than silicon oil or engine oil

The flashpoint and the smoke point are two other properties to be considered in terms of health and safety. The oil flashpoint is given by the ignition oil temperature having a heat source nearby. Corn oil has a 320 ℃ flashpoint, with this flashpoint being higher than silicon oil and engine oil-which. The smoke point is given by the temperature level when a cooking oil starts burning the fatty acid fraction, fuming to the vapor phase. In this regard. Corn oil should be used below 230°C smoke point in all applications, preventing the emission of hazardous gases and reduction of utilization time.

The economic factor addresses a cost comparison based on the price of silicon oil. In this respect, one can notice that corn oil does not only have adequate physical properties in CREC-VL-Cell but is merely 5 % of silicon oil cost.

Figure 17 compares the temperature ramp of the present study, using silicon oil and corn oil. The temperature controller sets the linear ramp at 1.22 ℃/min for both thermo-fluids. One can observe that corn oil provides a much more stable heating rate than silicone oil. This linearly increasing temperature with corn oil is due to the combination of lower viscosity and heat conductivity.

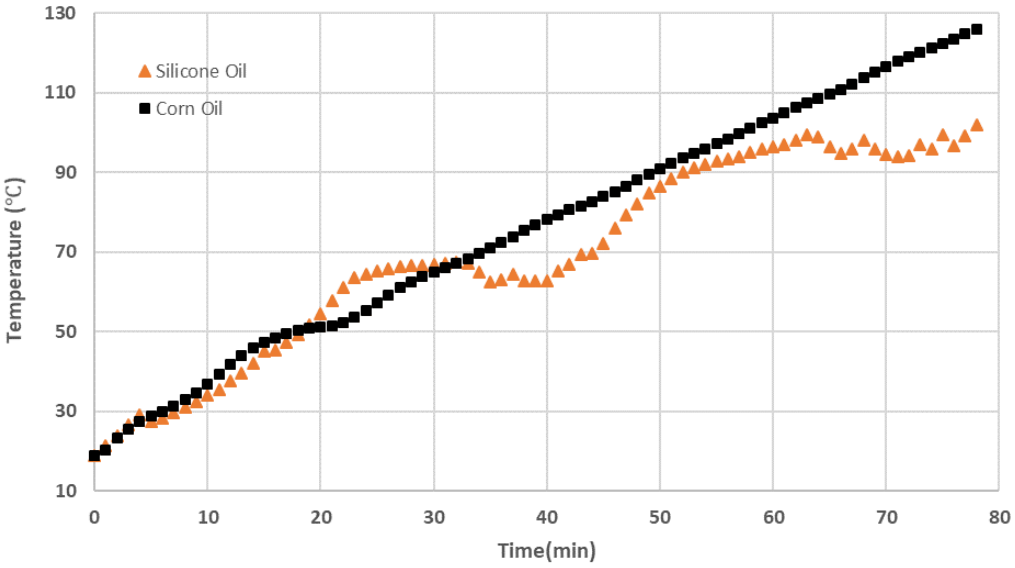


**Figure 17. Temperature changes of Silicon Oil and Cooking Corn Oil at different times**

### *4.1.4 CREC-VL-Cell Positioning*

The vessel containing the thermo-fluid was sized to allow a consistent and repeatable temperature ramp in the CREC-VL-Cell sample. Elevated temperature from thermo-fluid should provide an equal thermal level to the vapor and liquid phases. Therefore, the thermo-fluid must contact the entire CREC-VL-Cell.

Figure 18 compares the Thermo-fluid vessel size difference designed in Solidworks®. The large vessel type can cover the entire CREC-VL-Cell height, while the small vessel covers only 80 % of CREC-VL-Cell height. The small vessel type was initially designed to reduce Thermo-fluid consumption and energy waste.

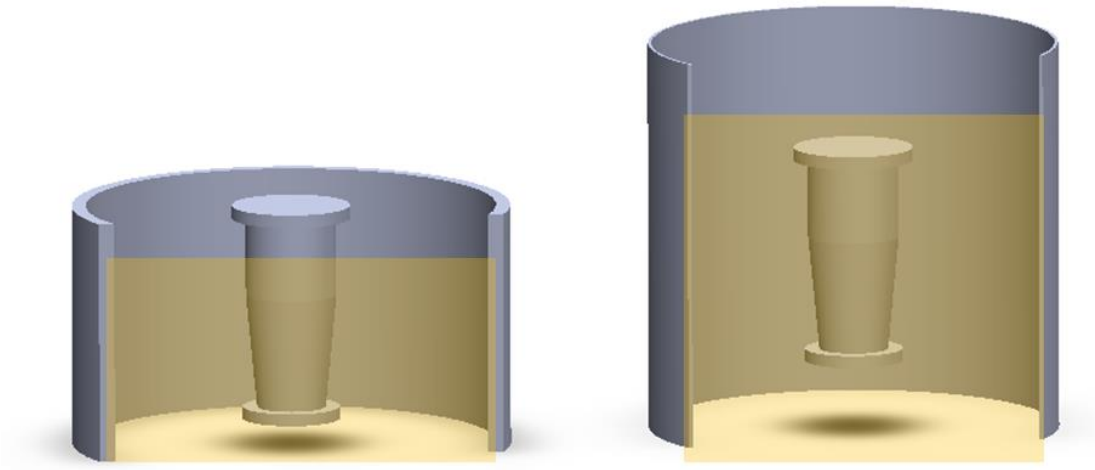

**Figure 18. Illustration of Thermo-fluid Vessel size difference. Notes: (a) Small Vessel type (Left) covers 80 % of CREC-VL-Cell height, (b) Large Vessel type(right) covers CREC-VL-Cell completely.**

Figure 19 describes how the thermo-fluid vessel size affects the thermal equilibrium for 2 wt% n-octane + 98 wt% water mixture. One should note that a close difference between liquid temperature and gas temperature, desired condition for thermal equilibrium, was only achieved with the high thermal level as described in Figure 19.

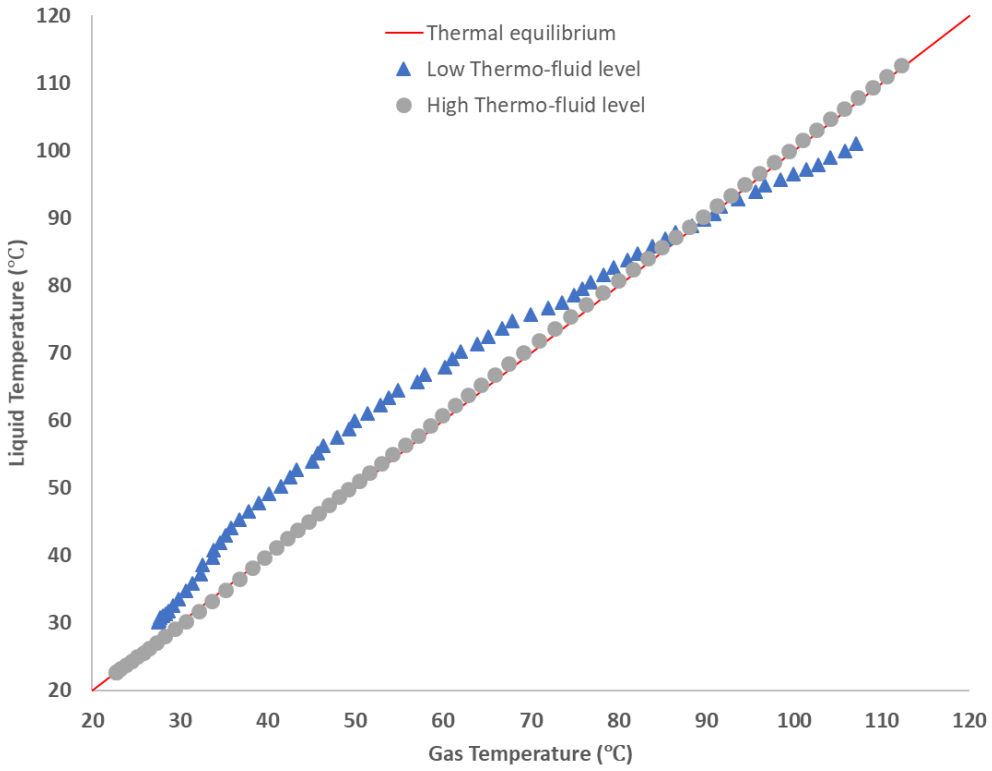


**Figure 19. Liquid temperature and Gas temperature comparison during the CREC-VL-Cell running. Notes: (a) Thermal equilibrium is a reference where gas and liquid have the same temperature, (b) Low Thermo-fluid level is a condition of using the small vessel type, (c) High Thermo-fluid level is a condition of using the large Vessel type.**

As well, it was observed that 350 rpm impeller speed in the thermofluid vessel was also required to minimize the thermal gradients, between the top and bottom regions of the CREC-VL-Cell.

## 4.2 Mixing System

Mixing affects the dynamic thermodynamic equilibrium measurements. The CREC-VL-Cell is equipped with an impeller allowing good mixing of the hydrocarbon-water samples.

Mixing in a multicomponent system may accelerate mass transfer between the continuous phase and dispersed phases [139]. A concentration gradient is a main driving force to transfer the mass between different phases and components. Thus, mixing helps to move

fluid elements from a high concentration region to a low concentration region. Furthermore, good mixing is critical in solid-liquid multiphase systems because aggregates may disturb the phase equilibrium. In this respect, a high mixing may help to redistribute the droplets and reduce the aggregate sizes.

Also, heat transfer is enhanced by improving mixing. Temperature difference drives heat fluxes between phases. Mixing can force fluid motion and heat transport, with convection and conduction being the dominant heat transfer mechanisms [140].

In this chapter, phase mixing is studied for n-octane/water and solid/n-octane/water multicomponent blends. A high-speed camera is also used to analyze mixing. As well, the operation of an electrically driven stirrer is monitored using a delivered torque-speed relation. Based on these observations, the influence of various cell geometrical factors is established.

### *4.2.1 Video Analysis*

Fluid dynamic visualization allows one to determine homogenous mixing and relate it to the associated cell geometrical factors. A high-speed camera with 240 frames per second (FPS) was used to analyze mixing patterns. The video sequences recorded with the high-speed camera show fluid motion at ten (10) times slower speed than the 24 FPS of a regular video. To proceed with the visualization experiments, a Plexiglass transparent unit, with the same dimensions as the CREC-VL-Cell, was built.

A 2 wt % n-octane + 98 wt% water blend was selected to represent a liquid blend for the video analysis. For the 2 wt % n-octane + 98 wt% water blend, a dye is required to analyze mixing, given blend components are colorless. To address this, 0.0001 wt% black bitumen was chosen to dye the n-octane phase, given its non-polar character.

Figure 20 reports the typical batch stirred tank dimensions. One should note that determining dimensionless numbers in the CREC-VL-Cell is a difficult task, given the complex cell geometry. Despite this, fluid flow visualization was considered using a close CREC-VL-Cell geometry.

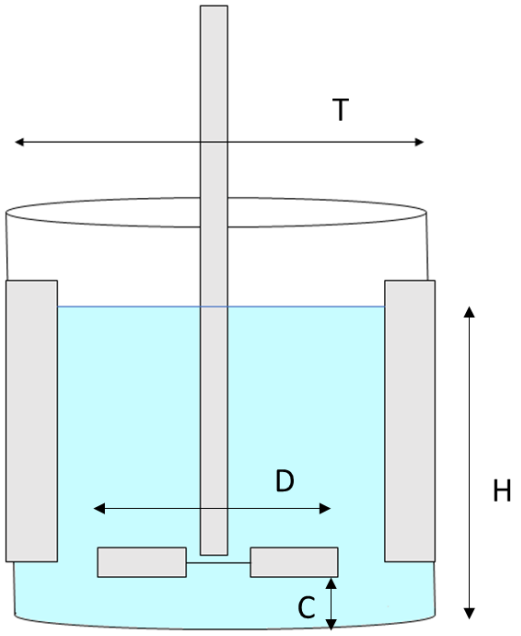


**Figure 20. Batch Stirred tank shape factors: (a) T = Tank diameter, (b) H = Liquid depth, (c) D = Impeller diameter, (d) C = Off-bottom clearance.**

### *4.2.2 Sample Volume*

Figure 21 compares the influence of the sample volume for 2 wt% n-octane + 98 wt% water mixture. Both 100 mL and 140mL sample volumes are studied. One can observe that for the 140mL sample, the impeller speed at 1080 rpm appears to be inadequate. Reduced dispersion causes bigger n-octane droplets, with n-octane aggregation in the impeller and shaft regions.

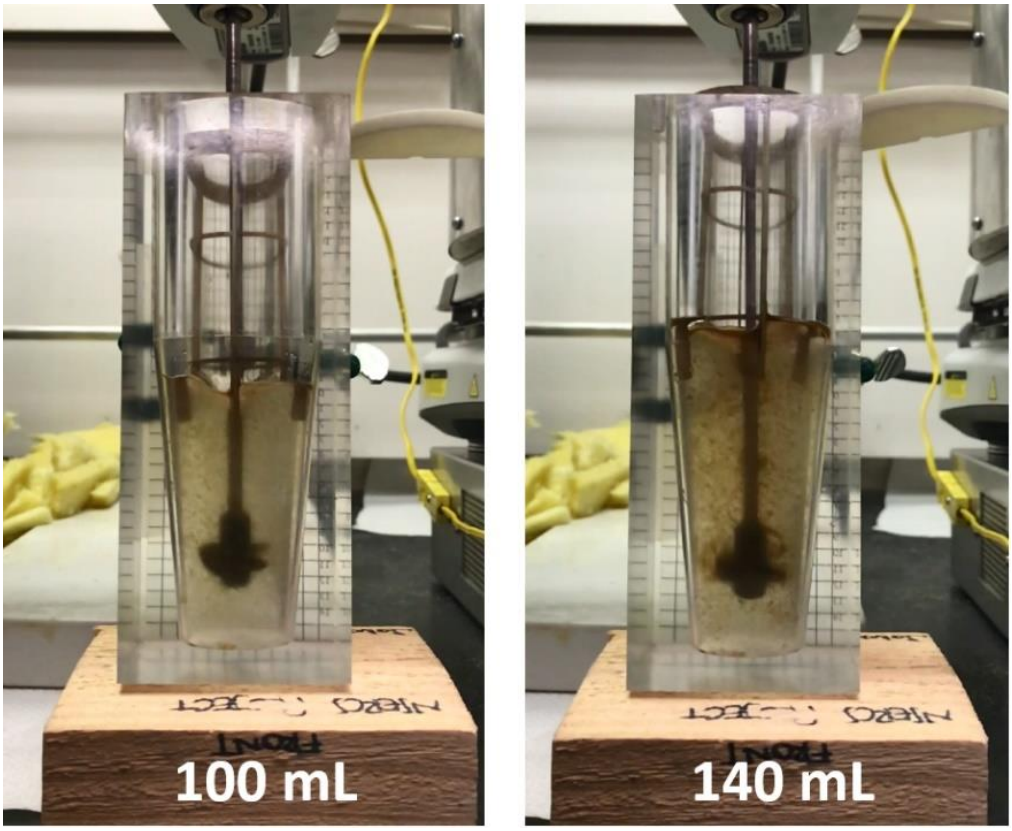


**Figure 21. CREC-VL-Cell Mixing Video analysis for 2 wt% n-octane + 98 wt% water on 100mL and 140mL volumes. Mixing speed: 1080 rpm**

Furthermore, Figure 22 reports vapor pressure for 100mL and 140 mL samples. One can notice that for the 140mL volume sample, there is insufficient dispersion, leading to reduced vapor pressure. This difference is, however, minimized considerably at 110 ℃. Thus, dynamic measurements in the 30-110°C have thus to be restricted to sample volumes not exceeding 100mL.

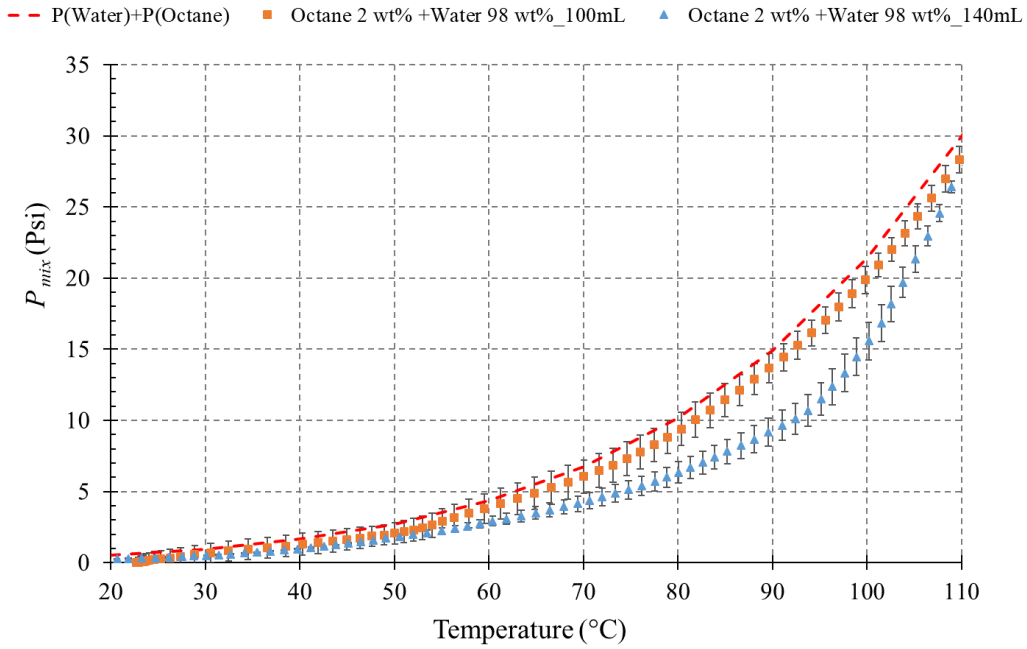


**Figure 22. $P_{mix}$ for 2 wt% n-octane + 98 wt% water in the 20 ℃ to 110 ℃ range. Notes: (a) Saturation pressure using the immiscible model (red dash line), (b) 100 mL volume sample (orange filled square mark), (c) 140 mL volume sample (blue filled triangle mark), (d) 1080 rpm mixing speed is used, (e) Vertical bars represent standard deviation for at least three experimental repeats.**

### *4.2.3 Impeller*

Homogenous multiphase dispersion is required in multicomponent systems. Density differences combined with limited solubility may cause phase separation. Increasing the mixing speed does not entirely solve this problem. Hence, adequate mixing patterns must be induced as well, via the selection of a suitable impeller type.

Figure 23 illustrates the marine type impeller used in CREC-VL-Cell. The marine type impeller provides a flow pattern with a significant fluid axial velocity component so that various phases are mixed without phase stratification. Furthermore, marine type impeller may contribute to forced heat convection as well. Since the CREC-VL-Cell bottom region

is close to heated-plate, the axial forced convection helps maintaining a close thermal level in all regions of the cell.

**Figure 23. Description of Marine Type Impeller Used in the CREC-VL-Cell**

In addition to the lower section marine impeller, a marine impeller is also placed in the upper cell gas phase section. Thus, and altogether, the CREC-VL-Cell is equipped with two marine impellers: one at the bottom liquid section and a second one at the gas upper section. One should mention that the gas impeller also contributes to the gas mixing in the upper cell so that both liquid and gas phases are kept under turbulent flow conditions.

Figure 24 describes the different marine type impeller positions to disperse the immiscible mixture. One can see that 7.0 cm impeller height position provides insufficient multiphase dispersion. Therefore, a smaller impeller height position of 2.5 cm or below is required to provide a good multiphase dispersion.

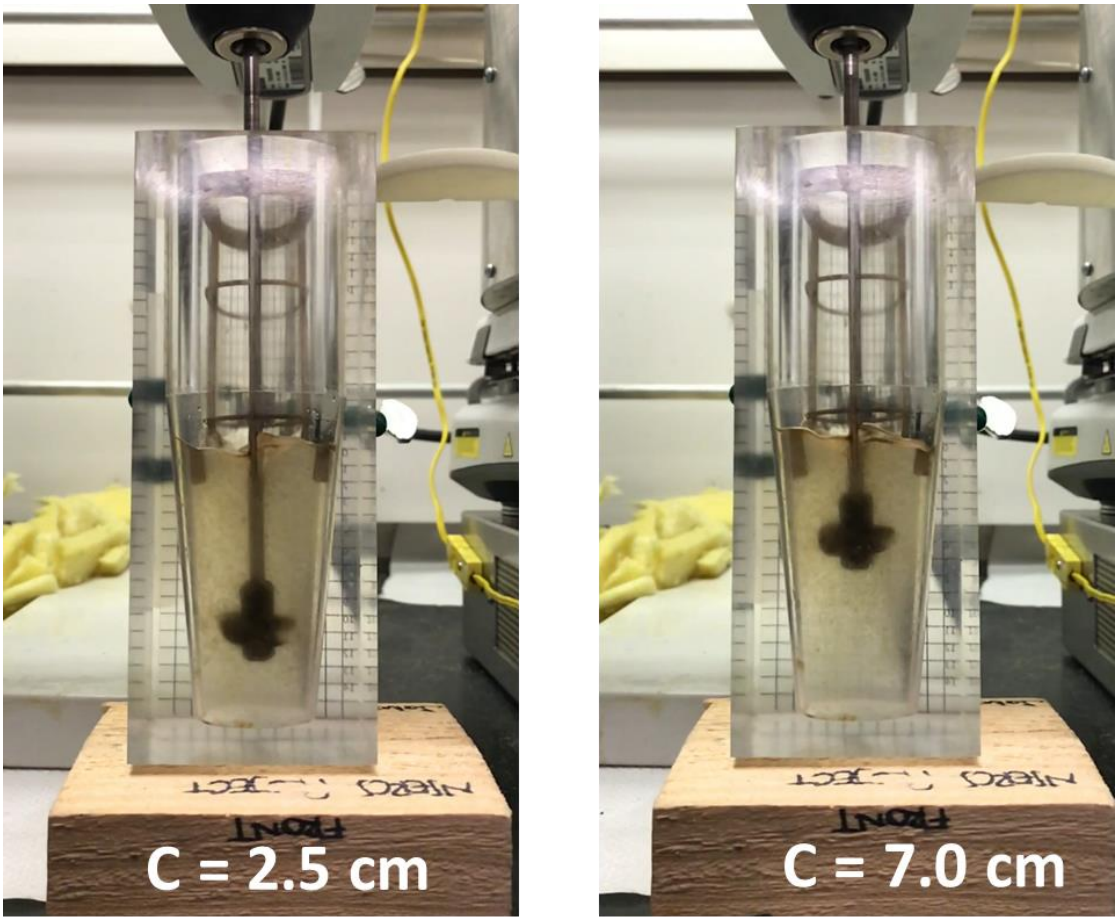


**Figure 24. CREC-VL-Cell Mixing Video analysis for 2 wt% n-octane+ 98 wt% water depending on impeller position Notes: C represents impeller clearance from the bottom to the impeller tip**

Figure 25 compares the thermodynamic data obtained with variable impeller clearance height. For 7.0 cm impeller clearance height shows a deviation in the 90-110 °C range. Therefore, one can observe that the unstable mixing patterns led to incorrect lower mixing saturation pressure.

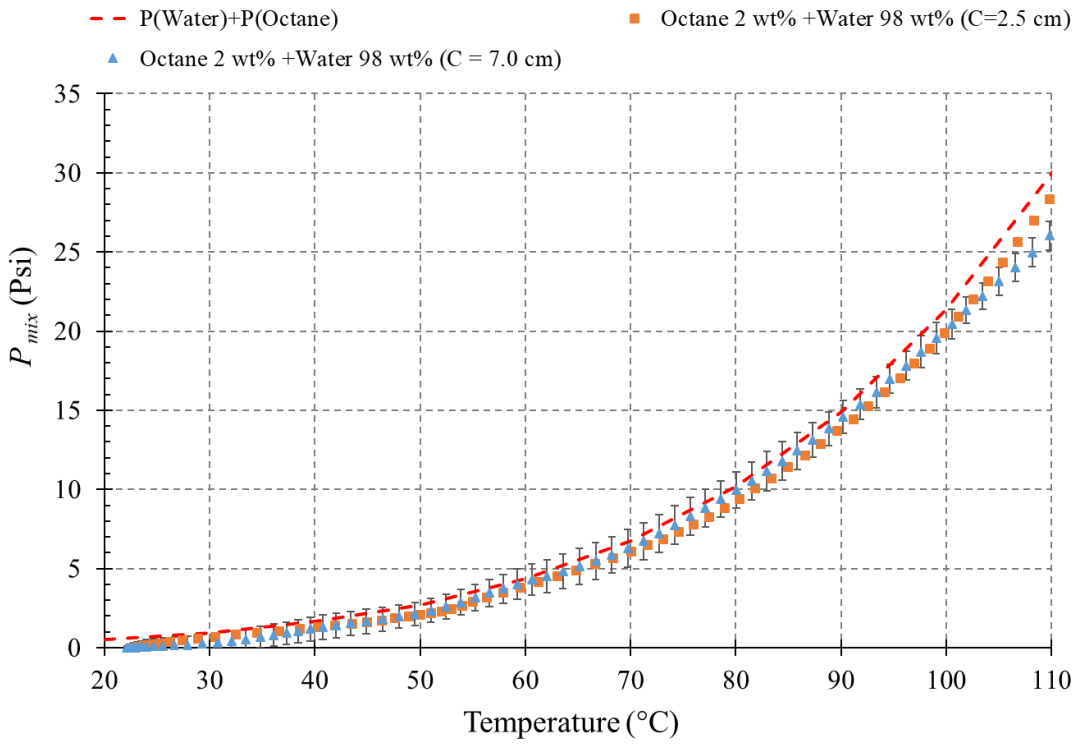


**Figure 25. $P_{mix}$ comparison between 2.5 cm clearance impeller position (Orange filled square mark) and 7.0 cm clearance impeller position (Blue filled triangle mark) in the 20 ℃ to 110 ℃ range. Notes: (a) Summation of water and n-octane saturation pressure is used to represent a completely immiscible model (Red dash line), (b) 1080 rpm mixing speed is used, (c) Vertical bars represent standard deviation for at least three experimental repeats.**

Another issue of importance, as reported in Figure 26, is the axial impeller position while using a silica sand/naphtha/water mixture. In this respect, the effect of impeller axial positions was tested again. One can notice that silica sand tends to segregate in the lower section while using the 7.0 cm axially positioned impeller. However, when selecting the 1.5 cm axially positioned impeller, well-dispersed solid/hydrocarbon/water dispersion is obtained. Hence, one can conclude that the 1.5 cm axially placed impeller position is adequate in the CREC-VL-Cell for achieving good multicomponent mixing.

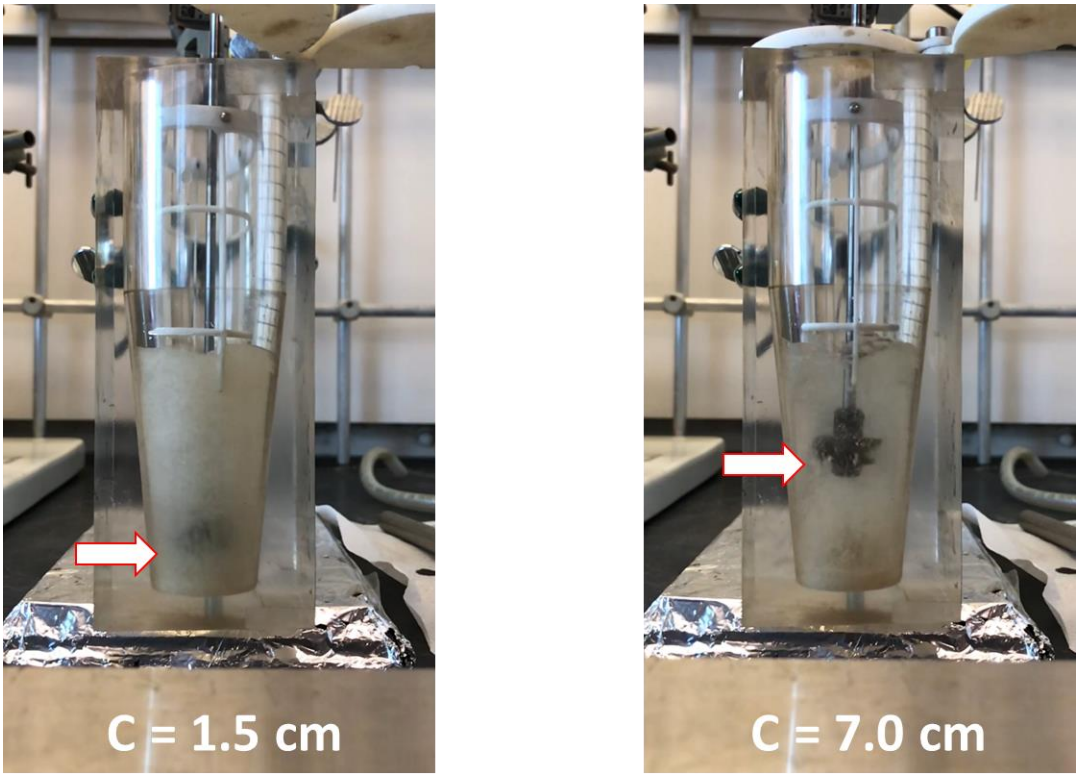


**Figure 26. CREC-VL-Cell Mixing Video analysis for 78 wt% water + 20 wt% Silica sand + 2 wt% naphtha mixture depending on impeller position Notes: C determines impeller clearance height from bottom to the impeller tip**

### *4.2.4 Baffle Design*

Regarding the selected marine impeller for the CREC-VL cell, it can present several issues such as: (a) limited radial mixing, (b) vortex formation. Vertical baffles can reduce these issues, inducing tangential liquid motion [116]. Figure 27 describes the vertical baffle used in CREC-VL-Cell. One can see that with the selected baffle design, the vertical baffle section immersed in the liquid phase can be adjusted. So, the influence of the vertical baffle length positioning on mixing can be established.

**Figure 27. Description of Selected CREC-VL-Cell Baffle System**

Figure 28 reports the mixing as a function of the baffle axial position. One can observe that vertical baffles placed close to the interface [137] are good on breaking the liquid vortex. However, vertical baffles immersed in the liquid phase are not so effective, creating a less well-mixed top liquid section.

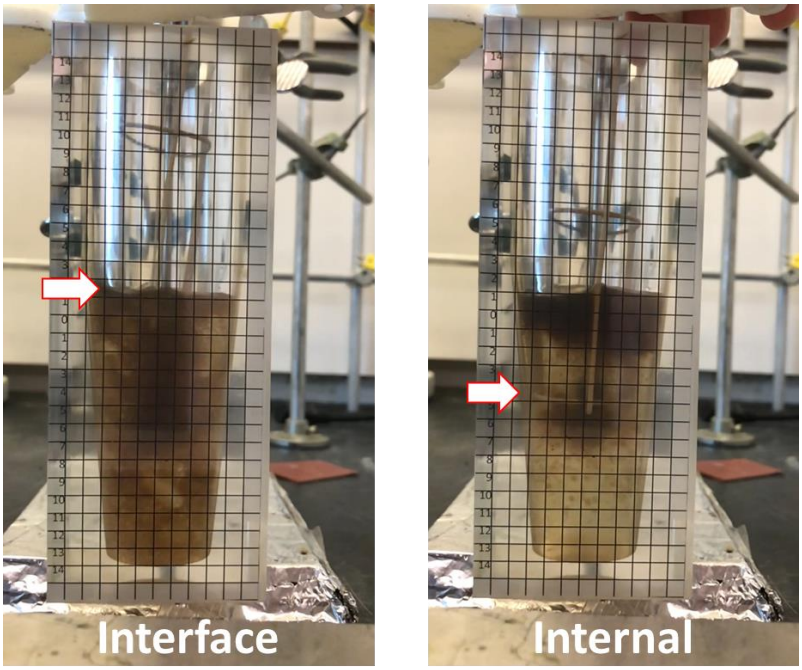


**Figure 28. CREC-VL-Cell Mixing Video Comparing Interface Baffle and Internal Baffles for 20 wt% n-octane + 80 wt% water sample. Notes: (a) 240 Frames Per Second high-speed camera, (b) n-octane contains 0.001 wt% bitumen dye.**

Figure 29 reports a comparison of vapor pressure measurements using vertical baffles placed in the gas-liquid near interface or alternatively partially immersed baffles in the liquid. One can notice that internally placed vertical baffles, shows lower vapor pressure than the ones obtained with interface positioned vertical baffles. This reduced vapor pressure for vertical baffles immersed in the liquid phase, is assigned to the insufficient phase dispersion in the CREC-VL-Cell, with vertical baffles near the interface being a preferred position. Thus, vertical baffles strategically placed in the near gas-liquid interface are recommended, as is implemented in the various CREC-VL-Cell runs of the present study.

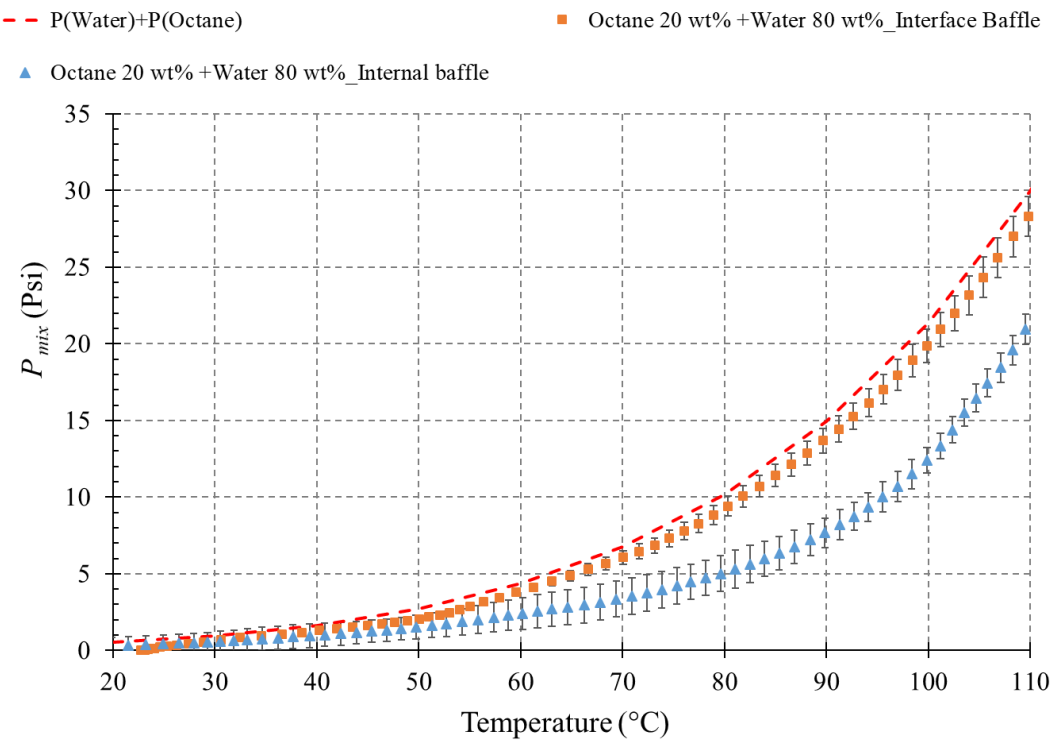


**Figure 29. $P_{mix}$ comparison between Interface baffle (Orange filled square mark) and Internal baffle (Blue filled triangle mark) in the 20 ℃ to 110 ℃ range. Notes: (a) Summation of water and n-octane saturation pressure is used to represent a completely immiscible model (Red dash line), (b) 1080 rpm mixing speed is used, (c) Vertical bars represent standard deviation for at least three (3) experimental repeats.**

### *4.2.5 Impeller Speed*

Regarding impeller speeds, insufficient mixing speed causes stagnant regions in the CREC-VL-Cell. Poor mixing deteriorates the quality of thermodynamic equilibrium measurements, with this being assigned to limited mass transfer via a phase layer separation. Therefore, high-speed mixing is required for adequate "dynamic" runs. However, excessive mixing speed can bring out operational problems.

Figure 30 shows pure water mixing with this being a function of the impeller mixing speed. At 1500 rpm mixing speed shows cavitation. Cavitation may lead to a bubble formed in the liquid due to the rapid pressure change [141]. This bubble formation and bubbles

collapse could damage the impeller as a result of the material fracture. Furthermore, excessive friction is a disadvantage of over-mixing. High friction could damage both the shaft and the packing cones. Damage of packing cones can lead to pressure leak, with significant errors in vapor pressure measurements.

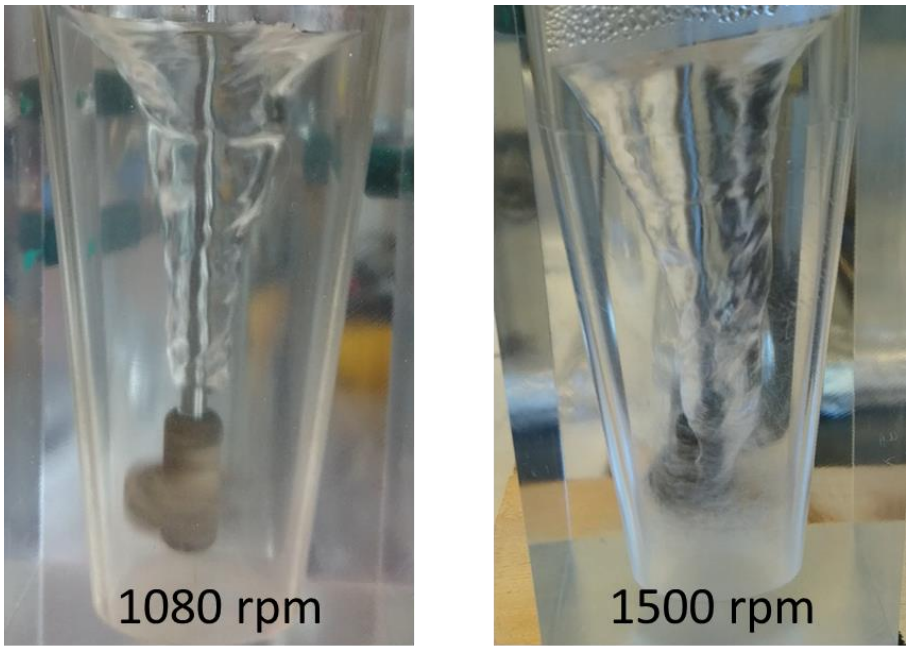


**Figure 30. CREC-VL-Cell mixing video analysis compared to mixing speed for 1080 rpm (Left) and 1500 rpm (Right).**

As a result, it was found that a good compromise for having good mixing with no influence of cavitation is to operate the impeller in the 1080-1200 rpm range. The impeller velocity range was the one used, in various vapour-liquid equilibrium measurements in the present study.

## 4.3 System Validation

### *4.3.1 Thermal Equilibrium Validation*

Thermal equilibrium in a fluid is reached when all fluid elements either gas or liquid have the same temperature [142]. In order to check that close to thermal equilibrium was achieved in the CREC-VL-Cell, two thermocouples were placed in the liquid phase and one thermocouple in the gas phase. With this end, the two temperature readings in the

liquid phase of the CREC-VL-Cell, were averaged and compared with the temperature readings in the gas phase.

Figure 31 compares the temperature between the liquid phase and the gas phase for 2 wt% n-octane + 98 wt% water mixture, using a 1080 rpm impeller speed. Table 4 also reports the temperatures recorded during a "dynamic" run. One can see that the liquid temperature and gas temperature are very close at all times, with the relative error between them being always smaller than 1.6 %. One can notice that this error is being even smaller in the 60 - 100 °C range. Therefore, one can conclude that the CREC-VL-Cell operated at 1080 rpm provides stable thermal equilibrium at all conditions examined in the 30 - 100 °C range.

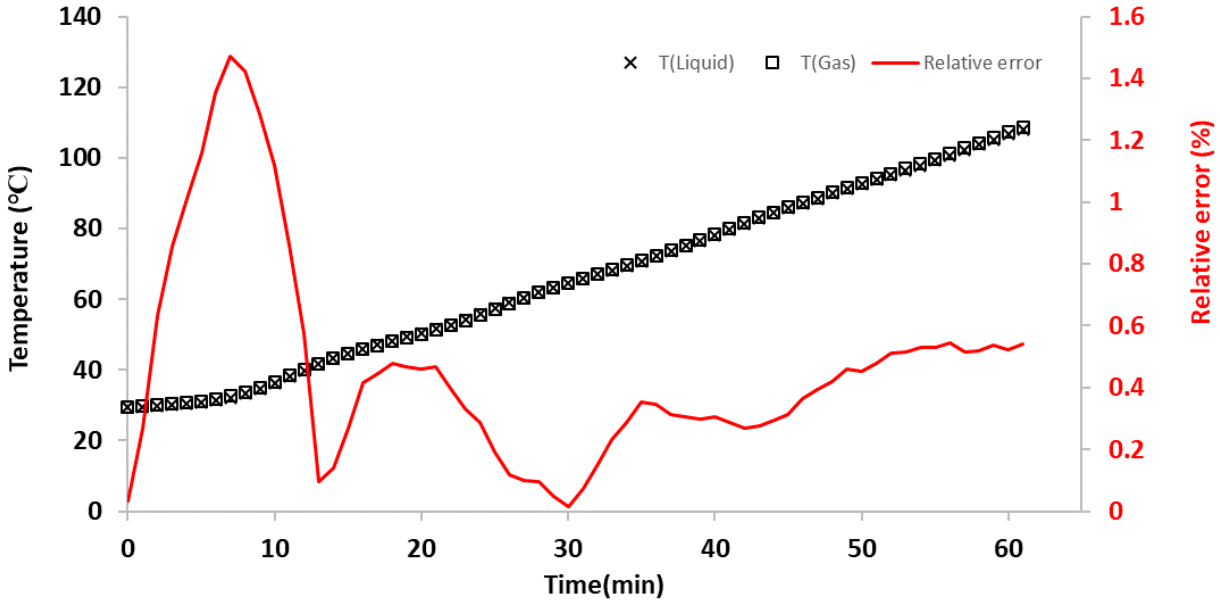


**Figure 31. Liquid temperature (x mark) and Gas temperature (square mark) on dynamic measurement condition. Notes: (a) Relative error (red solid line) indicates a discrepancy between liquid and gas temperatures, (b) 2 wt% n-octane + 98 wt% water mixture is used on the test.**

**Table 4. Liquid temperature, Gas temperature and Relative error data on dynamic measurement condition. Notes: (a) Relative error (red solid line) indicates a**

**discrepancy between liquid and gas temperatures, (b) 2 wt% n-octane + 98 wt% water mixture is used on the test.**

| Liquid Temperature (°C) | Gas Temperature (°C) | Relative Error (%) |
|---|---|---|
| 30.04 | 29.85 | 0.63 |
| 40.12 | 39.89 | 0.57 |
| 50.15 | 50.38 | 0.45 |
| 60.43 | 60.49 | 0.09 |
| 71.01 | 70.76 | 0.35 |
| 80.00 | 79.77 | 0.28 |
| 90.20 | 89.82 | 0.42 |
| 101.25 | 100.7 | 0.54 |
| 110.71 | 110.12 | 0.54 |

### *4.3.2 Dynamic System Validation*

The CREC-VL-Cell measures both pressure and temperature while using a 1.22 ℃/min heating rate ramp, in the 30 ℃ to 120 ℃ range. In order to validate the "dynamic" measurements, results were compared with those of a designated "static" method. In the static method, the cell temperature is kept constant at a preset value during an extended time period.

Figure 32 reports the "static" method temperatures and compared them with the ones from dynamic runs. During the "static method" the following steps are adopted: a) the heating ramp is paused at 40 minutes, b) a pre-set temperature is kept at the target level for 38 minutes, c) concluded this, the heating ramp is restored employing a 1.22 ℃/min ramp.

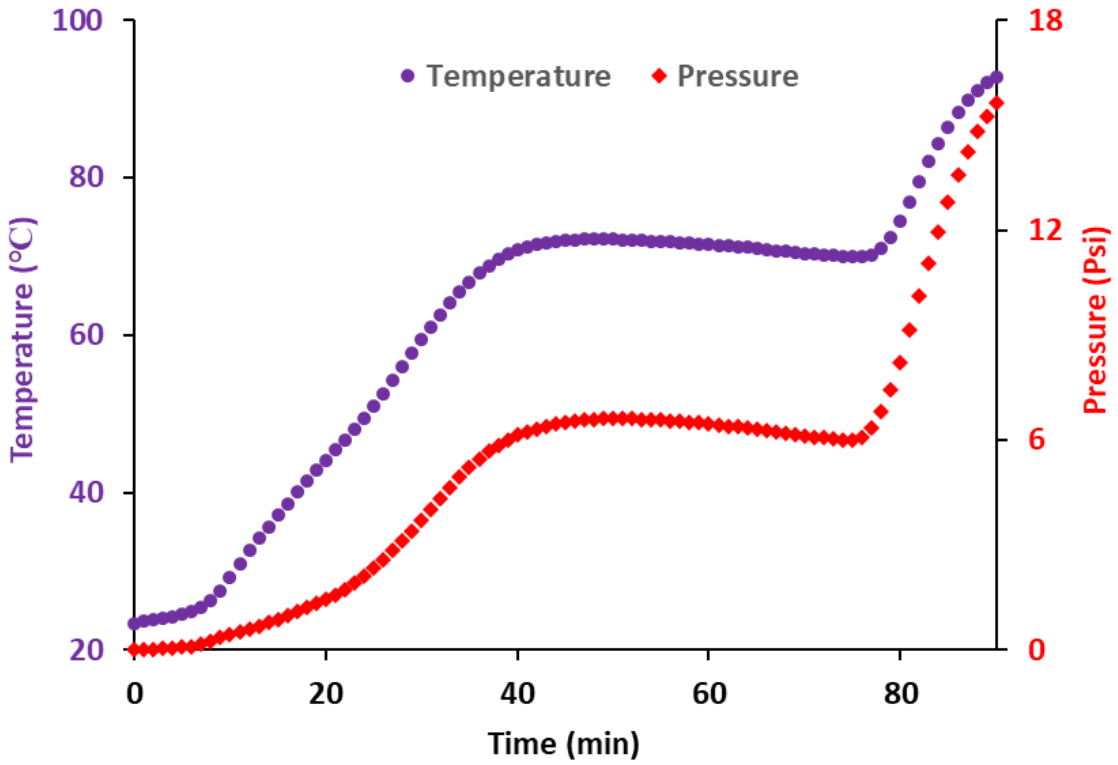


**Figure 32. Temperature (Purple filled circle mark) and Pressure (Red filled diamond mark) change for 2 wt% n-octane + 98 wt% water at various running times. Notes: (a) Heating ramp is paused at 40 min to valid static measurement condition, (b) Heating ramp is reactivated after the Static method is maintained for 38 mins, (c) 1080 rpm mixing speed is used**

Figure 33 compares the vapor pressure-temperature using "static" and "dynamic" measurements in the CREC-VL-Cell. The yellow highlighted box reports the region where the "static" and "dynamic" measurements are compared. Thus, one can see that temperature and pressure from both methods are essentially identical, which validates the applicability of the dynamic measurement technique.

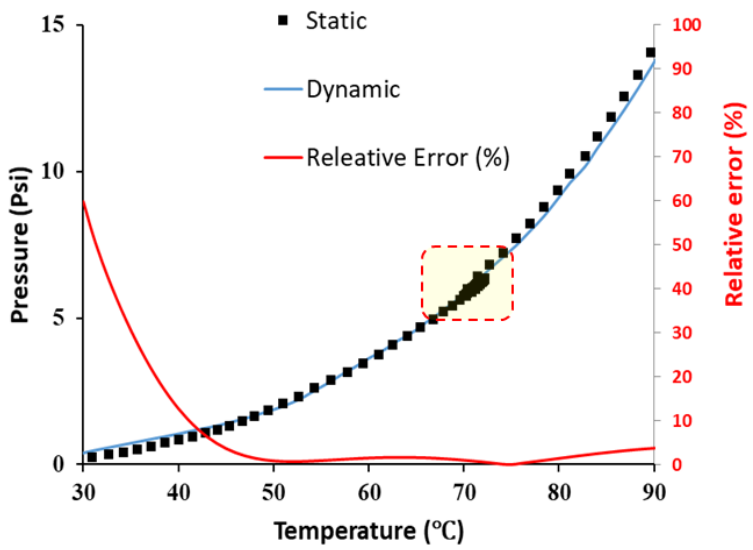


**Figure 33. $P_{mix}$ comparison between static measurement condition (black filled square mark) and dynamic measurement condition (blue solid line) in the 30 ℃ to 90 ℃ range. Notes: (a) Static method is in the yellow highlighted region, (b) Relative error (red solid line) indicates a discrepancy between the static method test and dynamic method test, (c) 1080 rpm mixing speed is used.**

For better visualization of agreement, Figure 34 reports an expanded in the 66 ℃ to 75 ℃ range. One can see that the "static" method shows a good agreement with the "dynamic" method with less than 1 % relative error deviation.

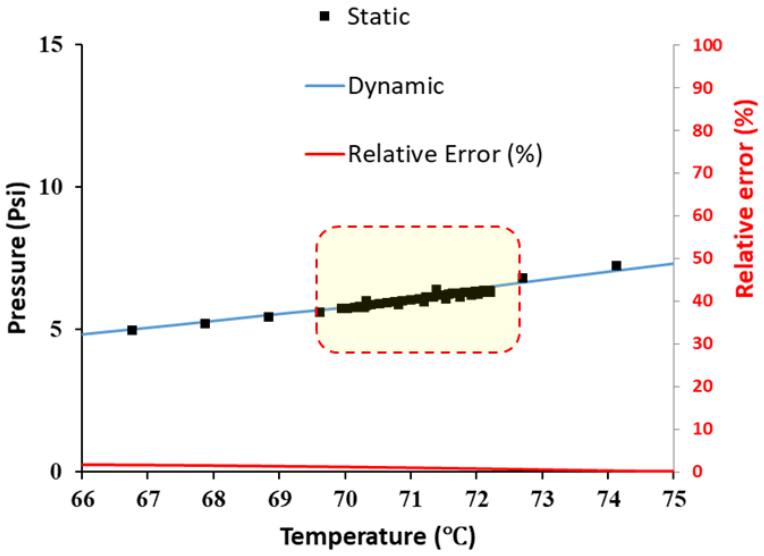


**Figure 34. $P_{mix}$ comparison between static measurement condition (black filled square mark) and dynamic measurement condition (blue solid line) in the 66 °C to 75 °C range. Notes: (a) Static method is in the yellow highlighted region, (b) Relative error (red solid line) indicates a discrepancy between the static method test and dynamic method test, (c) 1080 rpm mixing speed is used.**

As a result, one can conclude that "dynamic" runs in the CREC-VL-Cell were validated using the "static" method, a typical approach in conventional VLE apparatus. One should note that the static method is time-consuming and tedious [143]. On the other hand, using the "dynamic" method in the CREC-VL-Cell many temperature-pressure conditions are evaluated in a single run, which provides significant strength to the thermodynamic equilibrium studies developed.

## 4.4 Conclusions

(1) The CREC-VL-Cell operated at dynamic conditions (1.22 ℃/min heating ramp) successfully measures temperatures and pressures at phase equilibrium. The dynamic operation is validated by comparing it with a conventional static method. The relative errors between dynamic and static methods are less than 1.0 %.

(2) The CREC-VL-Cell bath operated with low viscosity and high thermal conductivity cooking corn oil, as the thermo-fluid is adequate to provide the needed impeller driven forced convection.

(3) The CREC-VL-Cell position in the thermo-fluid bath is successfully optimized with minimum temperature differences between the gas phase and the liquid phase. The relative error between phases is less than 1.6 % in the entire experiment.

(4) The CREC-VL-Cell mixing is positively established using a 240 FPS high-speed camera and a Plexiglass unit replica. Bitumen traces in the n-octane phase are employed to follow the n-octane droplets in these videos.

# Chapter 5: Materials and Experimental Methods

This chapter describes the properties of various component mixtures, such as hydrocarbons, water and solids, used in the present study. Regarding hydrocarbon mixtures employed, they emulate the typical naphtha. In this respect, the adequacy of the composition of the selected naphtha, is validated using the experimental and simulated vapor pressures in the CREC-VL-Cell and using Aspen Hysys®.

Following this, this chapter describes the experimental methodology. First, the CREC- VL-Cell equipment and data acquisition software are reviewed, showing the consistency with ASTM D5191-13 methodology advised for vapor pressure measurements.

## 5.1 Materials

### *5.1.1 Hydrocarbon Species*

The multicomponent system of the present study involved water, n-hexane, n-heptane, n-octane, n-decane and n-dodecane as hydrocarbon chemical species.

Regarding water, deionized water was used in all the experimental studies. Concerning the alkanes, they were obtained from Sigma-Aldrich. Table 5 reports their main properties including purity, water content and with these properties established using gas chromatography and Karl Fisher titration, respectively.

Alkanes are non-polar compounds, which are partially miscible liquids in water. Thus, in the wastewater system, this represents a challenge given the fact that it undermines the water and hydrocarbon separation process performance [144]. Despite this slight hydrocarbon solubility in water, the potential negative impact on the environment may be significant.

Table 5. Properties[1] of Alkanes

| Properties | n-hexane | n-heptane | n-octane | n-decane | n-dodecane |
|---|---|---|---|---|---|
| Formula | $C_6H_{14}$ | $C_7H_{16}$ | $C_8H_{18}$ | $C_{10}H_{22}$ | $C_{10}H_{22}$ |
| Molar weight (g/mol) | 86.18 | 100.20 | 114.23 | 142.28 | 170.33 |
| Purity (%) | >97.0 | >96.0 | >99.0 | >99.0 | >99.0 |
| Water content (%) | 0.01 | 0.02 | 0.00 | 0.01 | 0.00 |

Silica sand and clay [145] are two solid materials that are involved in the multicomponent blend from heavy oil sand mining. Therefore, their physicochemical behavior in the partially miscible hydrocarbon-water mixture is relevant. In addition, the research on the effects of using silica sand in these multiphase derived mixtures from oil sand processes is also relevant [146].

Table 6 reports the properties of silica sand and clay. Silica sand and kaolin clay were obtained from the *Lane Mountain Company* and *Edgar Minerals*, respectively. Silica Sand involves a 99.9 % crystalline silica phase, while Kaolin Clay contains a 99.9 % Kaolinite. Both solids are insoluble in water. However, the particle size, solid surface area and solid dissolution may influence the effectiveness of the hydrocarbon-water separation processes [147].

[1] For more properties information refer to Mateiral Safety Data sheets from Sigma-Aldrich

Table 6. Properties of Oil Sand Solids

| Properties | Silica Sand[2] | Kaolin Clay[3] |
|---|---|---|
| Formula | $SiO_2$ | $Al_2Si_2O_5(OH)_4$ |
| Specific Gravity | 2.65 | 2.65 |
| Median Particle size ($\mu m$) | 554.79 | 1.36 |
| Solubility | Insoluble | Insoluble |
| BET Surface Area ($m^2/g$) | 0.83 [148] | 30.62 |

Silica sand and kaolin clay may also be involved in the Naphtha Recovery Unit with different particle sizes: kaolin clay contributes with fine particles (1.36 microns average), while silica sand with relatively large particle (553 microns average). Although solids compositions may vary, a good average can be simulated using 70 wt% Silica sand and 30 wt% kaolin clay [149].

### *5.1.2 Synthetic Naphtha*

Naphtha can be defined as a liquid hydrocarbon mixture refined from crude oil [150]. In the oil sand industry, naphtha is used as a diluent to reduce the viscosity of bitumen allowing it to flow through the pipelines [145]. Also, the naphtha reduces density and viscosity of the bitumen so that water and solids can be easily separated in gravity settlers and centrifuges.

NRU is a separation unit column to treat wastewater stream from Froth Treatment Unit with naphtha losses being a significant issue. Therefore, the thermodynamic behavior of the diluted naphtha-water mixture is essential to increase the naphtha recovery.

Naphtha fractions can be divided into light naphtha and heavy naphtha components, with this being a function of its boiling point. Light naphtha contains hydrocarbons with 5 to 6

[2] For more properties information refer to EPK clay Safety Data Sheet from Edgar Minearal

[3] For more properties information refer to Silica sand Safety Data Sheet from Lane Mountain Company

carbon numbers, while heavy naphtha includes chemical species with 7 to 12 carbon numbers [151].

Table 3 reports typical naphtha composition from the open literature sources [152]. Even if naphtha is a complex hydrocarbon blend, its composition can be described using twenty-seven (27) hydrocarbon species.

Table 7. Typical naphtha composition [152]

| Component | wt% | Component | wt% | Component | wt% |
|---|---|---|---|---|---|
| n-Butane | 1.5 | n-Octane | 5.4 | n-Hexane | 8.6 |
| 1,3-Dimecyclohexane | 7.0 | 2-Mheptane | 2.4 | 2-Mpentane | 6.0 |
| n-Decane | 7.0 | Toluene | 3.0 | 3-Mpentane | 4.0 |
| n-Nonane | 2.6 | m-cyclohexane | 4.8 | 23-Mbutane | 0.8 |
| o-Xylene | 1.0 | n-Heptane | 4.4 | Cyclopentane | 1.5 |
| 3-Moctane | 2.7 | 3-Mhexane | 3.8 | n-Pentane | 10.3 |
| p-Xylene | 1.9 | 2-Mhexane | 2.8 | i-Pentane | 4.2 |
| e-Benzene | 2.0 | Cyclohexane | 2.8 | | |
| 26-Mheptane | 1.9 | Benzene | 1.8 | | |
| Ecyclohexane | 2.0 | Mcyclopentan | 4.1 | Total | 100.3 |

Given the above, it was decided to represent in the present study, a typical naphtha using a limited number of paraffinic components, designated as “synthetic naphtha” (SN).

Aspen Hysys® can be used to generate distillation curves for typical naphtha and report them as temperature boiling points versus hydrocarbon mixture volume or mass fractions, as in Figure 1 [153].

This can be accomplished using Aspen Hysys® with Oil Manager and specific naphtha assay data which involve bulk properties, light ends and heavy ends, paraffinic, aromatic and naphthenic fractions. Figure 35 describes the distillation curve for typical naphtha using Aspen Hysys®. In this figure, the True Boiling Point (TBP) and ASTM D2887 distillation are compared, showing close agreement [154], [155].

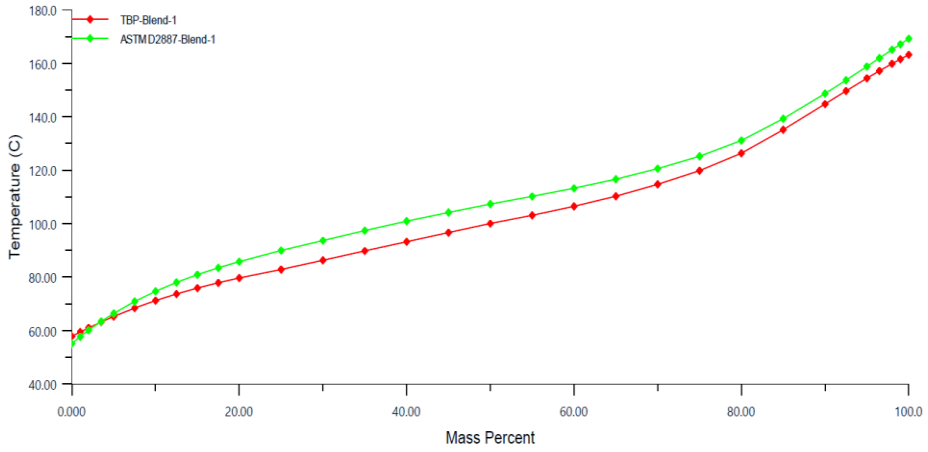


Figure 35. Typical naphtha distillation curve by using Aspen Hysys®. Notes: (a) Red solid line represents True Boiling Point(TBP) – ASTM D2892 method, (b) Green solid line represents ASTM D2887 method.

Regarding TBPs for synthetic naphtha, it can be described using close-cut fractions from the distillation curve [156]. Pure components can be used to model these close-cut fractions [157]. In the research, alkanes in the 6 to 12 carbon range were selected for the synthetic naphtha, including n-hexane, n-heptane, n-octane, n-decane, n-dodecane to cover the entire naphtha boiling point.

Table 8 reports the simulated naphtha composition using: a) 60 wt% of n-octane, b) 22 wt% n-heptane and 10 wt% n-hexane to account for the light ends and c) 6 wt% n-decane and 2 wt% n-dodecane for representing the heavy ends.

**Table 8. Synthetic Naphtha Composition**

| n-hexane | n-heptane | n-octane | n-decane | n-dodecane |
|---|---|---|---|---|
| 10 wt% | 22 wt% | 60 wt% | 6 wt% | 2 wt% |

Figure 36 reports a comparison of vapor pressure for a typical Naphtha [152] using Aspen Hysys®, and the experimentally observed vapor pressure for synthetic naphtha as per Table 4. Peng-Robinson fluid package is used in the Aspen Hysys® for simulations. The experimentally observed saturation vapor pressure of synthetic naphtha was measured by using a CREC-VL-Cell. Note that a 1080 rpm impeller speed recommended for ensuring

adequate mixing of liquid phases. Figure 36 reports that synthetic naphtha and Aspen Hysys® typical simulated naphtha are in good agreement. As a result, the synthetic naphtha of the present study involving five (5) alkanes is validated as a proper choice to simulate a typical.

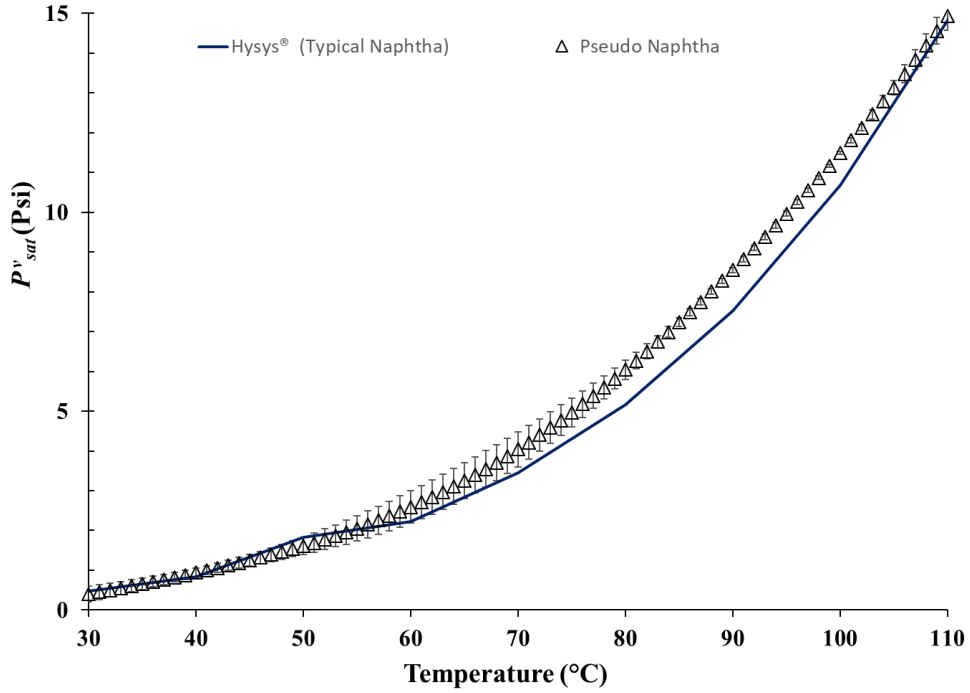


Figure 36. $\boldsymbol{P^v_{sat}}$ for naphtha in the range of 30 ℃ to 110 ℃. Notes: a) Aspen Hysys® simulated typical naphtha (black solid line), (b) synthetic naphtha in the CREC-VL-Cell. Note: Vertical bars represent standard deviations for experimental repeats.

On this basis, one can conclude that the results of Figure 36 show that synthetic naphtha can be used to emulate typical naphtha thermodynamics in the CREC-VL-Cell, to study the vapor pressure of different naphtha-water blends.

## 5.2 Experimental Methods

Figure 37 schematically describes the experimental CREC-VL-Cell assembly and its operation. The numbers in Figure 37 describe the various steps required for data acquisition during an experiment. On this basis, the data acquisition proceeds during a run are as follows:

(1) The temperature controller is set for delivering a 1.22 ℃/min rate heating ramp.

(2) The magnetic stirrer starts the agitation of the thermo-fluid, using a 350-rpm rotational speed to induce fluid forced convection.

(3) Following this, the sample is loaded in the CREC-VL-Cell, and cell-top lid is closed.

(4) The sample placed inside the CREC-VL-Cell, is mixed with the impeller speed at 1080 rpm.

(5) Both thermocouple and pressure transducer data are interfaced with the data acquisition system to record both temperature and pressure in real time.

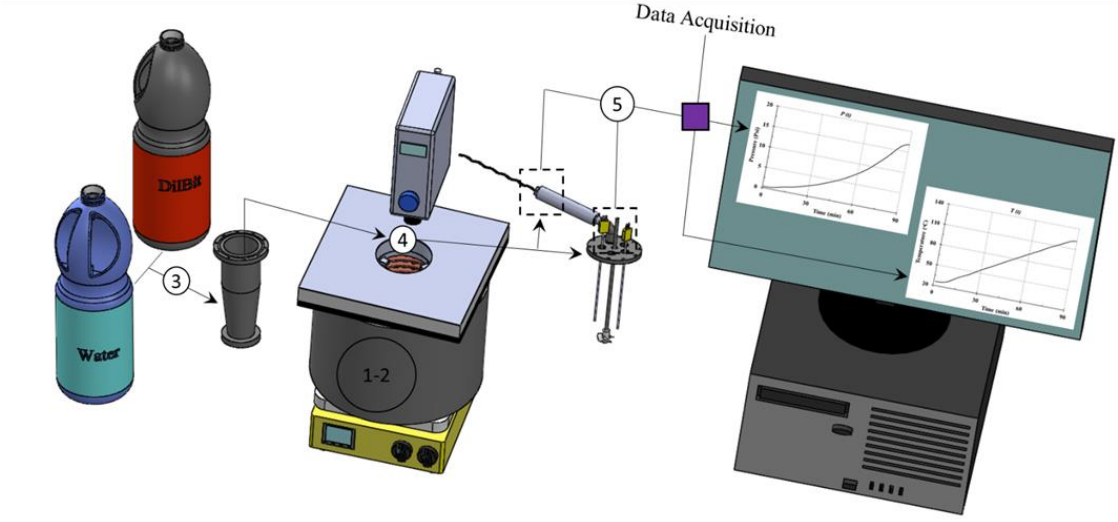


Figure 37. Schematic Description of CREC-VL-Cell Experimental Method

### *5.2.1 Preparation Steps*

Regarding the experiments developed, and prior to each of them, the CREC-VL-Cell was cleaned using a soft fabric before and after performing the VL equilibrium runs. To this end, the bottle sampler was cleaned thoroughly to remove any contaminants. CREC-VL-Cell accessories, such as temperature controller and pressure transducer, were also

disassembled to remove any condensed sample fraction and be ready for reliable measurements preventing contamination of fluid from previous runs.

Regarding the cleaning steps, the following was adopted:

(1) Wash CREC-VL-Cell and accessories by using 2-propanol

(2) Wipe the CREC-VL-Cell and accessories with paper-towels

(3) Blow the CREC-VL-Cell and accessories using compressed air

(4) Vacuum the CREC-VL-Cell and accessories with a nozzle.

(5) After drying the CREC-VL-Cell and accessories, retighten the various components well

(6) Cover the CREC-VL-Cell with the cell-top lid and check for pressure leaks using compressed air.

(7) Store the CREC-VL-Cell and accessories in the laboratory fume hood to minimize the contact with other laboratory contaminants.

(8) Collect the resulting chemical waste and dispose it via the university occupational safety and health (OHS) regulations.

### *5.2.2 Sample Input to the CREC-VL-Cell*

The sample for the experiment is fed to the CREC-VL-Cell sampler. One should note that the typical recommended sample amount is 100 mL±10 liquid. An excessive amount of liquid sample, typically over 110 mL, may be detrimental for good mixing and is not recommended. To this end, 10 mL Syringes and a Laboratory Balance Scale are used to feed the sample accurately to the CREC-VL-Cell.

Once the feeding of the sample is completed, the CREC-VL-Cell is covered with the cell-top lid. The CREC-VL-Cell top lid holds three thermocouples (one for the gas phase, two for the liquid phase), one pressure transducer, one impeller shaft and one septum. The

septum allows the injection of the additional sample during the experiment. The lid is secured with ten (10) bolts with an O-ring proving the cell sealing.

### *5.2.3 Temperature Controller[4] Setup*

An Omega™ i-series temperature controller and a thermocouple system helped delivering a 1.22 °C/min temperature ramp in the CREC-VL-Cell.

Before using the temperature controller, the system must be autotuned. The autotuning calculates the PID parameters of the CREC-VL-Cell. Process output variations are monitored to decide the proper control rate. Note that the autotuning setpoint must be at least 10 °C above the process value. Also, the Dumping factor has to be set to 0003 to respond to the output changes during the Autotune [158].

To accomplish this, the following procedures have to be implemented:

(1) Ensure that no water remains in the heat exchanger copper line. The water residue may cause high pressure to the copper line given that the CREC-VL-Cell is designed to operate over 100 °C. To accomplish this, it is recommended to open the ball valves of the CREC-VL-Cell and blow the compressed air through the heat exchanger line.

(2) Set the controller to STANDBY mode to prevent temperature increases during the setup period.

(3) Select the operational temperature in the SETPOINT 1 (SP1) mode.

(4) Go to the CONFIGURATION (CNFG) menu and choose the RAMP mode. Set the heating ramp rate by measurement time. Lastly, enable the RAMP setup. In this regard, one should note that if one tests the dynamic condition, SOAK menu can be applied to hold a temperature for the input time.

---

[4] For more information check the user's guide of the temperature and process controller i.series from Omega™

(5) Return to the main menu and release the STANDBY mode. When the system is ready to run, set the temperature controller specifications:

(a) Warm-up rated desired accuracy during 30 min

(b) Accuracy: ±0.5 °C temp; 0.03 % reading process

(c) Resolution: 10μV process

(d) Temperature Stability: TC at 25°C, 0.05°C/°C

### *5.2.4 Hot-plate[5] with Stirring Capabilities*

The hotplate of the present study is equipped with a rotating magnetic field that secures via a 60 mm magnetic stirring bar and a 350 rpm, good mixing in the 6.3 liters aluminum thermo-fluid bath container. One should note that it is important to continuously monitor thermo-fluid mixing, given viscosity of the fluids as in the thermo-fluid, may hinder mixing. Reduced mixing may cause an unstable temperature ramp.

The aluminum thermo-fluid vessel is equipped with two thermocouples. One thermocouple is connected to the temperature controller, while the other provides the temperature readings for the data acquisition module in real-time.

The Hotplate with magnetic rotating filed has the following specifications:

(a) Voltage: 120 V; Current Intensity: 8.9 A; Power: 1070 Watts

(b) Max. Temperature: 540°C

(c) Max. Recommended Flask Size: 4 L for this type of plate size (7”x7”)

---

[5] For more information refer to the Cimarec™ Stirring Hot Plates: Operation Manual and Part List from Thermo Scientific.

### 5.2.5 CREC-VL-Cell Mixing Setup

After CREC-VL-Cell is immersed in the thermo-fluid, the impeller shaft is connected to the electrical overhead starrier. While the impeller speed can cover the 0 to 1200 rpm range, the 1080 rpm is the optimum speed selected for the present study. In this respect, low-mixing speed causes an undesirable and unstable dynamic condition during experiments. On the other hand, the over mixing has to be avoided, given that this leads to cavitation.

Regarding the impeller shaft, it must be placed in a vertical position avoiding a tilt. A slightly inclined impeller shaft leads to severe vibration and noise in the CREC-VL-Cell, with vibration causing potential damage to the packing cones.

VELP Overhead Stirrer[6] has the following procedures:

(1) Turn the switch "ON" to have the digital display in the overhead stirrer. The display shows both the set impeller speed and actual impeller speed.

(2) Set the impeller speed and time are controlled by encoder knob.

(3) Press the encoder knob to activate the mixing timer and the stirring time

(4) Press the encoder knob for 3 seconds to check the torque trend value, with 10 ~ 15 minutes being required to obtain the exact torque trend.

Overhead Stirrer Specification:

(a) Admitted power supply: 110-230V, 50/60Hz (+/-10%)

(b) Max. input / output power: 120 W/180 W

(c) Weight: 2.5 Kg (5.5 lb); Dimensions (WxHxD): 80x215x196 mm (3.1x8.5x7.7 in)

[6] For more information refer to the instruction Manual from VELP Scientifica (DLS Overhead stirrer F201A0155).

(d) Speed range at nominal load: 50-2000 rpm

(e) Maximum torque stirrer shaft: 40 Ncm

(f) Maximum stirring H2O volume: 25 L

(g) Clamping chuck range: from 1 to 10 mm

### *5.2.6 System Activation*

Before the temperature controller is activated, 15 ~ 30 minutes must be allowed for the system to reach an equilibrium. Liquid and gas temperatures must reach a steady-state value where no further variation in the temperature occurs. When the system reaches equilibrium, one has to active the temperature controller and start recording both the temperature and pressure using the temperature acquisition software and pressure acquisition software, respectively.

Regarding the Omega™ Temperature acquisition[7] system, one has to comply with the following:

(1) Connect the multiple thermocouples to the data acquisition module. The module connects to the desktop USB to record the temperature continuously.

(2) Set both the measurement method and thermocouple channels on the NEW-SETTING menu.

(3) Create a NEW DATA menu file to save the data

(4) Press START RECORDING both time and temperature.

(5) View with the help from VIEW SPREADSHEET the time and temperature are recorded. These data can be plotted using the VIEW GRAPH menu.

---

[7] For more information refer to the Omega™ TC-08 user's guide and for more details to the electronic manual.

Concerning the Omega™ Pressure acquisition[8] system one has to proceed as follows:

(1) Connect the pressure transducer cable to the desktop USB.

(2) Set the experimental steps on the CONFIGURATION menu.

(3) Press the START button on the CHARTING menu to plot the real-time pressure data.

(4) Press the START button on the LOGGING menu to collect pressure data continuously.

(5) Save the measured time and pressure data as recorded by pressing the SAVE AS EXCEL button.

(6) Develop a final check, ensuring that both the reference readings of the gauge placed on the CREC-VL-Cell lid and the data recorded by the pressure are the same.

### *5.2.7 Coil Cooling System*

Regarding the cooling system, a heat exchanger coil was placed inside the thermo-fluid bath. When required, normally following every experiment, cooling water was circulating in the heat exchanger coil to reduce the temperature rapidly. This heat exchanger coil can ensure operator safety reducing hazardous handling of hot thermo-fluid.

In order to use the heat exchanger coil, the following procedure was used:

(1) Disable the RAMP system and reduce the set temperature to 0 °C in the temperature controller.

(2) Open the ball valves to allow the flow of cooling water through the coil heat exchanges. Leave the ball valves open until the system temperature goes down to 20 °C or below.

---

[8] For more information visit https://www.omega.ca/en/sensors-and-sensing-equipment/pressure-and-strain/pressure-transducers/p/PX409-VAC

(3) Close the ball valves near the water chiller.

(4) Blow compressed air into the heat exchanger coil line to remove the remaining water.

(5) Close all the ball valves to be ready for the next experiment.

### *5.2.8 CREC-VL-Cell System Disassembly*

Once the cooling step is completed, the CREC-VL-Cell can be disassembled to get it ready for a new experiment. To accomplish this, the following are the recommended steps:

(1) Unplug the various thermocouple from the CREC-VL-Cell,

(2) Loosen the overhead stirrer and disassembly the impeller shaft,

(3) Pull out the CREC-VL-Cell from the thermo-fluid and remove hexagonal bolts from the CREC-VL-Cell lid,

(4) Remove the liquid sample from the CREC-VL-Cell by using a separation funnel. Dispose of the waste in the designated bottle,

(5) Repeat the cleaning procedure as described in 5.2.1 Section.

One should note that the CREC-VL-Cell experimental method complies with the ASTM D5191-13, Standard Test Method for Vapor Pressure of Petroleum Products (Mini Method). The ASTM D5191-13 is a standard procedure for measuring vapor pressure of petroleum products using automated vapor pressure instruments [159].

## 5.3 Conclusions

(1) The CREC-VL-Cell experimental methods were developed carefully, accounting for both accuracy of measurements as well as minimization of hazardous operating conditions.

(2) Five Alkanes (n-hexane, n-heptane, n-octane, n-decane and n-dodecane) were selected to emulate the boiling point of typical naphtha, with the resulting alkane mixture designated as synthetic naphtha (SN). The resulting SN vapor pressures were comparable to those of typical naphthas, as simulated by using Aspen Hysys PR-EoS.

(3) A 30 wt% Silica sand and 70 wt% kaolin clay solid blend was chosen to emulate solids in the Naphtha Recovery Unit.

# Chapter 6: Process Simulation Method

Aspen Hysys is a commercial simulator that can be used for process design as well as process simulation. Furthermore, Aspen Hysys provides various fluid packages allowing the prediction of vapor-liquid thermodynamics in multicomponent mixtures. These thermodynamic models can be customized by changing the phase properties, such as species interaction parameters. Therefore, in order to simulate the condition of the phase equilibrium, both the fluid package and the modelling condition need to be carefully chosen.

## 6.1 PFD Simulations

Adequate Process Flow (PFD) simulations are essential to compare with experimental CREC-VL-Cell data. This successful PFD must rely on good thermodynamics.

Concerning the PFD, it must be as concise as possible with the minimum number of units. In this study, two (2) mixers, a flash drum (Separator), and Adjust function are considered. The “upstream” mixer (MIX-100) is selected to blend the water, hydrocarbons and air fed to the Flash Drum. The Flash Drum delivers at the exit, two phases (liquid and vapor) in equilibrium. These two Flash Drum phases are combined in a second “downstream” mixer (MIX-101) unit to form a single outcoming stream. An Adjust function modifies the Flash Drum total pressure until the total outcoming volumetric flow of the MIX-101 unit equals the total volumetric flow fed to the Flash Drum. Thus, under these conditions, the VL equilibrium data from the Aspen Hysys becomes equivalent to the data obtained in the constant volume of CREC-VL-Cell.

Figure 38 reports the air/n-octane/water blend fed to the Aspen Hysys PFD. To accomplish this, a 275 mL/h total steady volumetric flow is considered to perform an equivalent separation as in the 275 mL constant volume CREC-VL-Cell. One should note that n-octane, water and air feed compositions were selected to be identical as the initial compositions in the CREC-VL-Cell.

Regarding the Flash Drum temperature, the temperature was set at a given thermal level (e.g. 60 °C), where one would like to compare data with the one obtained in the CREC-VL-Cell. Then, the total pressure in the Flash Drum (2-phase Separator) is modified using an Adjust Function until the Flash Drum outlet combined volumetric flow becomes the same as the incoming volumetric flow. To accomplish this, a Secant numerical method is employed iterating the Flash drum total pressure until incoming and outcoming volumetric flows are the same with a given set 0.01 mL/h tolerance.

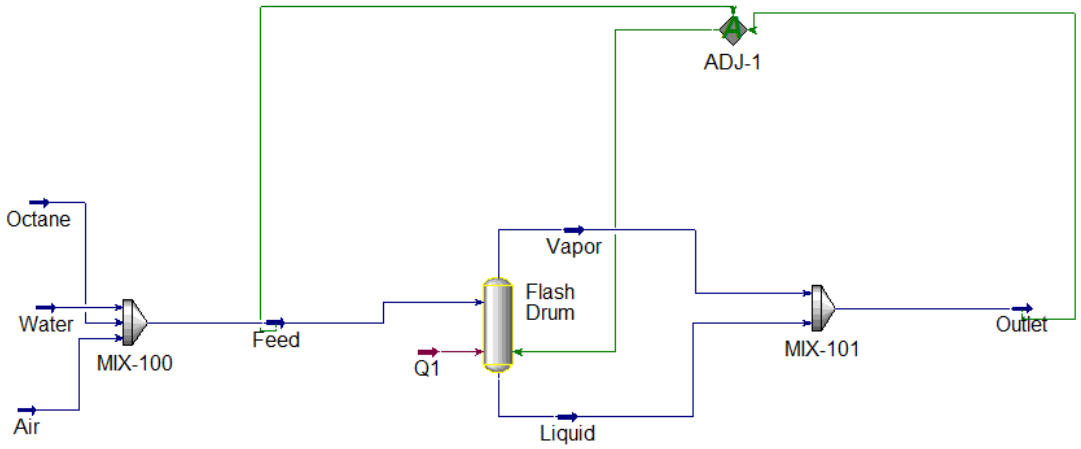


**Figure 38. Air/n-octane/water Process Flow Diagram in Aspen Hysys**

Once this process of calculation completed, iterative total pressure calculation is repeated at a different thermal level, and this until the entire range of temperatures of interest are covered (e.g. 30-110C).

Figure 39 reports a similar Aspen Hysys process simulation for the air/synthetic naphtha/water mixture. In this case, a hydrocarbon blend, designated as synthetic naphtha, which includes paraffinic hydrocarbons, is considered. In the modified PFD of Figure 39, synthetic naphtha is prepared from its constitutive components using a Mole Balance unit, with the rest of the PFD remaining the same as for the n-octane/water systems. The revised PFD thus includes two mixers, a flash drum (2 phase separator), and an Adjust total pressure module.

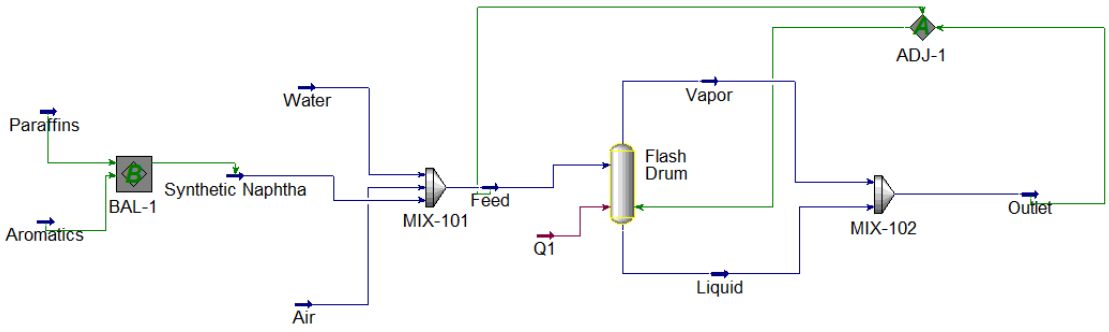


**Figure 39. Air/Synthetic Naphtha/Water Process Flow Diagram in Aspen Hysys**

## 6.2 Thermodynamic Model

Regarding vapor-liquid equilibrium, the thermodynamic package adopted is one of the most important choices in process simulation. Given the high-water content and low-hydrocarbon concentrations in the 30 – 110 °C range to be studied, in one hand, the NRTL and the UNIQUAC activity coefficient models and, on the other the PR-EoS models are package candidates for water/hydrocarbon equilibrium calculations.

However, the activity coefficient models for the n-octane/water system in Aspen Hysys show discrepancy with the saturation vapor pressure of 2 wt% n-octane + 98 wt% water, as shown in Figure 40.

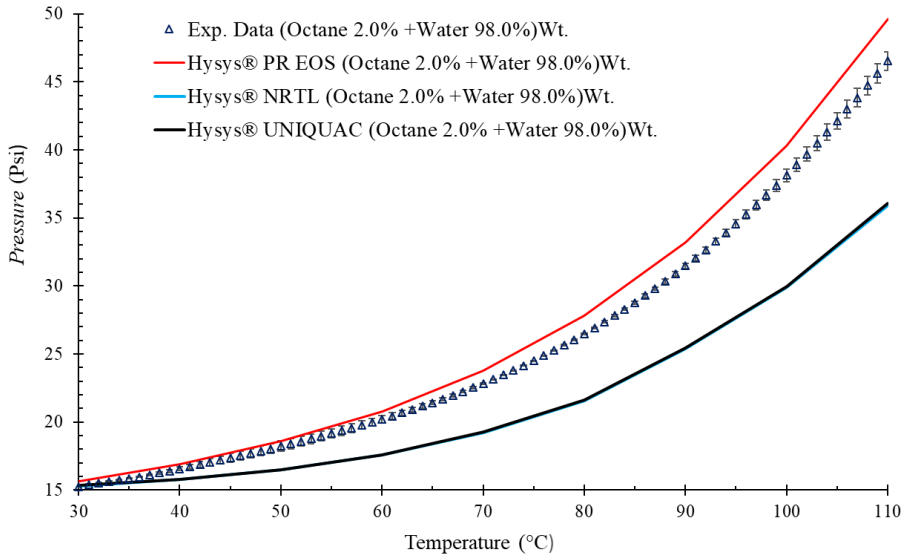


**Figure 40. The saturation vapor pressure estimation with different thermodynamic models in Aspen Hysys. NRTL and UNIQUAC give essentially the same prediction, thus blue and black lines cannot be distinguished. Note: The mixture of *2 wt% n-octane + 98 wt% water + air* is used for all thermodynamic models**

One possible reason for the discrepancy can be traced to the Binary Interaction Parameters (BIPs) of the activity coefficients. One should note that the built-in BIPs are set into zero both for NRTL and UNIQUAC models. Therefore, in our view, the NRTL and UNIQUAC models have to be further reviewed.

However, one can also observe in Figure 40 that the PR-EoS does not show these issues and can be used to simulate n-octane/water and synthetic naphtha/water VL equilibrium blends.

The following from Figure 41 to Figure 43 shows a methodical comparison of experimental data and the PR-EoS simulations for *n-octane/water/air* blends, while Figure 44 and Figure 45 show a systematic *synthetic naphtha/water/air* mixtures. One can see, in all cases, moderate over-prediction provided by PR-EoS model

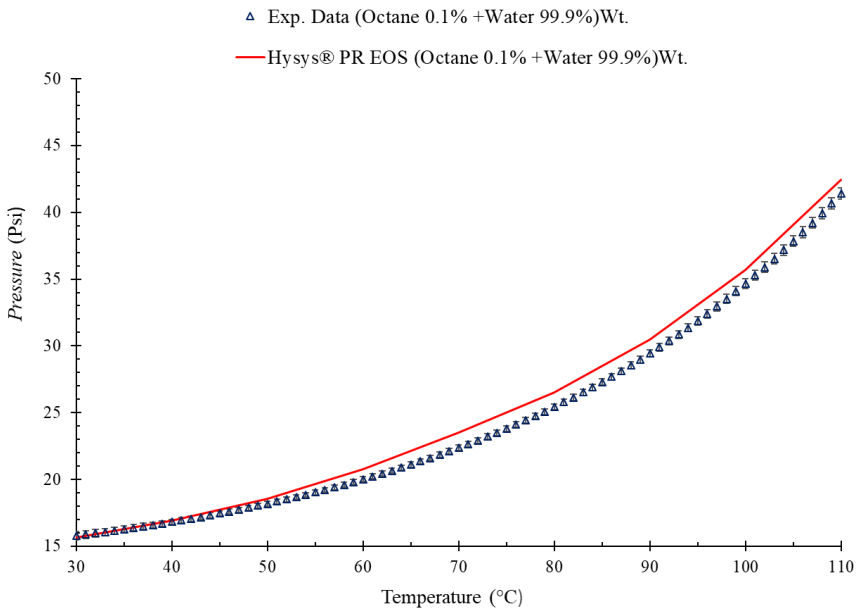


**Figure 41. The saturation vapor pressure estimation with PR-EoS thermodynamic models in Aspen Hysys. Note: The experimental data of *0.1 wt% n-octane + 99.9 wt% water + air* is used to compare with the simulation results**

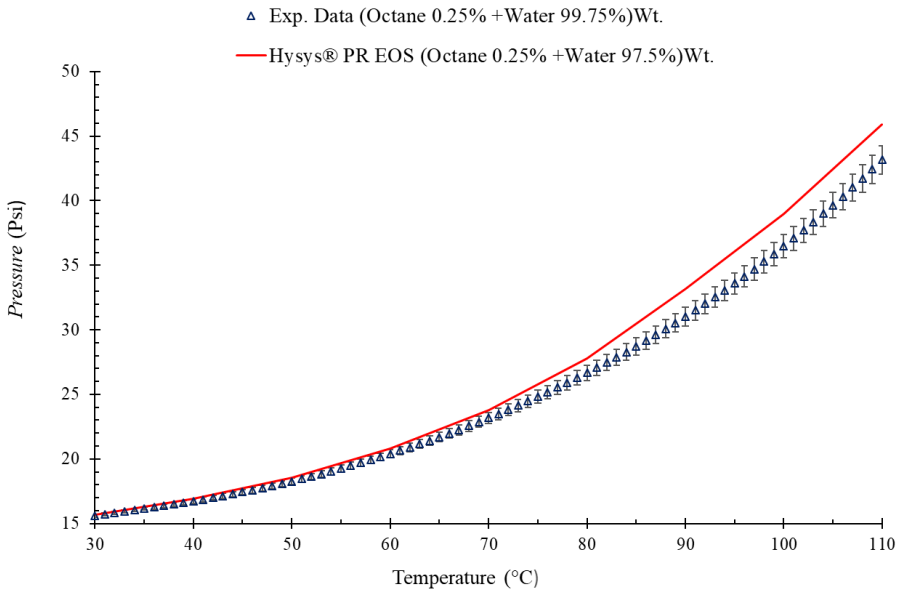


**Figure 42. The saturation vapor pressure estimation with PR-EoS thermodynamic models in Aspen Hysys. Note: The experimental data of *0.25 wt% n-octane + 97.5 wt% water + air* is used to compare with the simulation results**

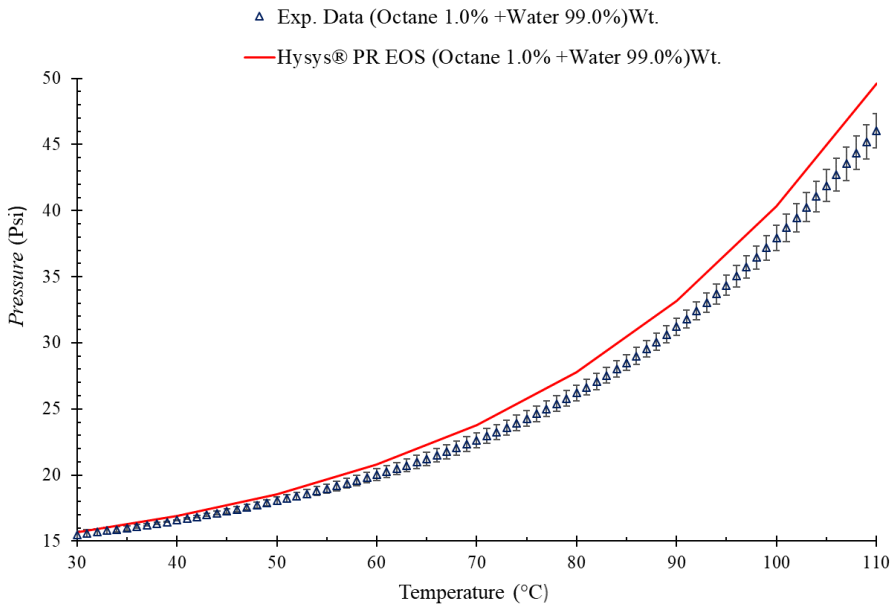


**Figure 43. The saturation vapor pressure estimation with PR-EoS thermodynamic models in Aspen Hysys. Note: The experimental data of *1.0 wt% n-octane + 99.0 wt% water + air* is used to compare with the simulation results**

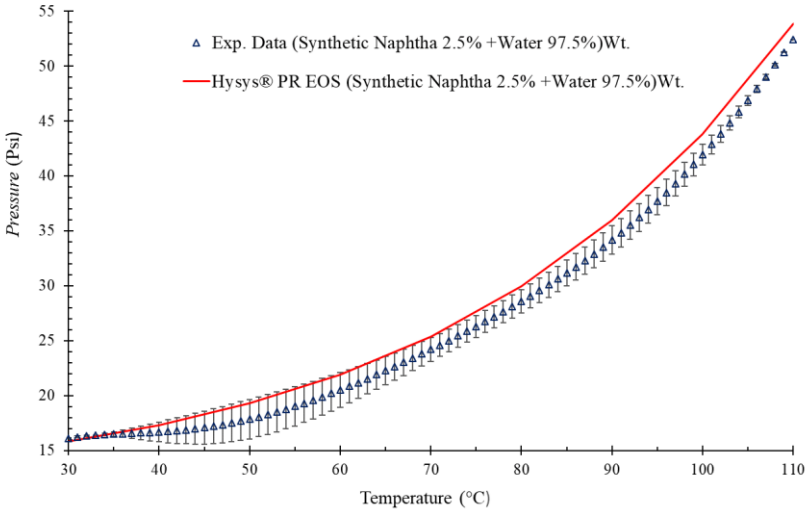


**Figure 44. The saturation vapor pressure estimation with PR-EoS thermodynamic models in Aspen Hysys. Note: The experimental data of *2.5 wt% synthetic naphtha + 97.5 wt% water + air* is used to compare with the simulation results**

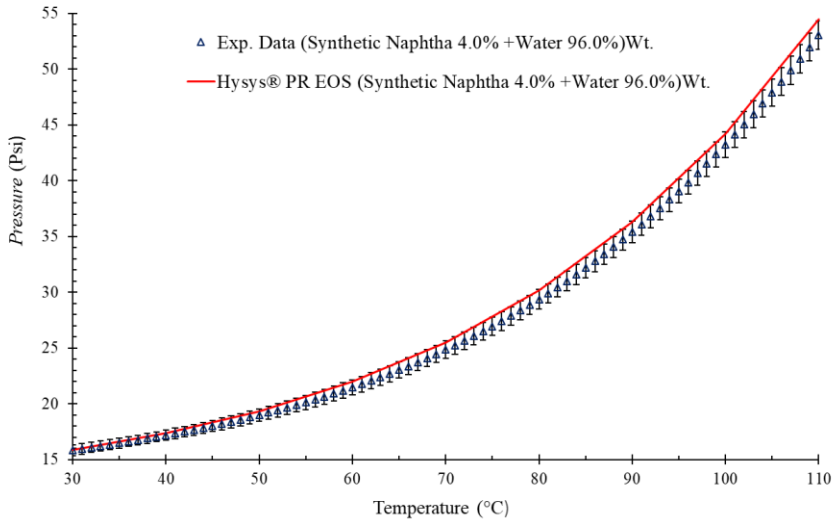


**Figure 45. The saturation vapor pressure estimation with PR-EoS thermodynamic models in Aspen Hysys. Note: The experimental data of *4.0 wt% synthetic naphtha* + *96.0 wt% water* + *air* is used to compare with the simulation results**

As a result, one can conclude that the CREC-VL-Cell data of the present study, obtained with n-octane in water and SN in water blends provide a thorough validation of the PR-EoS model.

## 6.3 Conclusions

(1) A continuous PFD Hysys Aspen model can be used to simulate the "batch" dynamic conditions of the CREC-VL-Cell. This is achieved using an Adjust function which enables to correct the total system pressure until unit incoming and outcoming volumetric flows are identical.

(2) The Peng Robinson Equation of the State (PR-EoS) provides a good first approximation to simulate the total pressure at various thermal levels in hydrocarbon/water blends using Aspen Hysys. The PR-EoS model is validated using T-P data obtained in a CREC-VL-Cell

(3) The alternative activity coefficient models (NRTL and UNIQUAC) do not display the same ability as the PR-EoS with this being assigned to built-in Binary Interaction Parameters set as zero.

# Chapter 7: Experimental Data Results and Discussion

This chapter reports experimental thermodynamic data obtained in a CREC-VL-Cell, using the dynamic method. The CREC-VL-Cell allows the studying of the vapor pressure for water/hydrocarbon samples from the oil sand separation units. Therefore, the complexity of the mixture goes beyond single components. It can include binary mixtures such as n-octane/water and naphtha/water and tertiary blends such as n-octane/solids/water.

Regarding the air contained in the CREC-VL-Cell, our experience shows that it cannot be completely removed from the cell. Thus, a correction is implemented using the gas state equation at close to ideal gas conditions. The adequacy of this correction method is validated with the empty CREC-VL-Cell.

Twelve (12) different n-octane/water compositions are measured with the standard CREC-VL-Cell dynamic method. The measured saturation vapor pressure and temperature are used to calculate the species molar fraction in the mixture.

In this chapter, Pressure and Temperature data are provided for water/synthetic naphtha, with the synthetic naphtha composition determined. Various impeller mixing speeds and their effect on vapor pressure were compared to ensure the adequate environment for the synthetic naphtha/water system. Furthermore, different synthetic naphtha/water compositions are investigated to represent the NRU composition.

Vapor pressures for the n-octane/solids/water mixtures are also considered valuable to provide informative data for the oil sand industry, given the considerable amount of solids contained in various process streams. Hence, silica sand and clay were also blended with n-octane and water to establish the effects of solids vapor pressure.

## 7.1 Air Contained Fraction Correction

Conventional vapor-liquid equilibrium tests consider a degassing process [79]. It is believed, however, that the degassing method alters the total pressure. Thus, an alternative

experimental method is implemented in the CREC-VL-Cell accounting for the air contained, via an air contained factor pressure correction.

In addition, the proposed “Air Contained Fraction Correction” may have the following advantages:

(1) Measurement time

The degassing method takes at least 8 hours to ensure vacuum conditions [75]. Hence, the “Air Contained Fraction Correction” allows measurements saving degassing time.

(2) Research Cost

The degassing process involves a vacuum pump and a sample injector [70]. The “Air Contained Fraction Correction does not require this extra equipment.

(3) Experimental Repeatability

Regarding runs repeatability, one should note that runs involve a multiphase system, with solids, water and hydrocarbons. Feeding liquids and solids can be achieved accurately. However, high mixing is a challenging issue that must be controlled to reduce uncertainty. This is achieved in the CREC-VL-Cell using an air driven mixing device with no mechanical parts, operated slightly above atmospheric pressure. Implemented sealings secure minimum sample loss and adequate total pressure readings.

To proceed to calculate vapor pressure from total pressure, using the “Air Correction Factor”, one can consider the ideal-gas law since air at close to atmospheric pressure behaves as an ideal gas [160].

The “Air Correction Factor” , thus, involves the calculation of moles of air in an empty CREC-VL-Cell operating at room temperature and pressure as follows,

$$n_{Air} = \frac{P_{Air} V_{Total}}{RT} \qquad \text{Equation 29}$$

Where,

$n_{Air}$ = the number of air moles in the CREC-VL-Cell, $P_{Air}$ =1.01 atm, the atmospheric pressure in London, Ontario, $V_{Total}$ = 0.275 L, the total CREC-VL-Cell volume, $R$ = 0.082 $\frac{atm \cdot L}{mole \cdot K}$, universal ideal gas constant, T = 293.15 K, the room temperature.

As a result, the total numbers of moles contained in the CREC-VL-Cell, given Equation 29, can be calculated as $n_{Air}$= 0.0116.

Furthermore, the air in the CREC-VL-Cell affects pressure readings at every temperature, as follows,

$$\Delta P_{Air} = \left(\frac{n_{Air} RT}{V_{\text{Total}}} - P_{Air}\right) \times 14.7 \qquad \text{Equation 30}$$

Where,

$\Delta P_{Air}$= theoretically calculated "Correction Air Factor" in the CREC-VL-Cell in Psia, $n_{Air}$=0.0101 moles, $R$ = 0.082 $\frac{atm \cdot L}{mole \cdot K}$, $T_{exp}$ = experimentally measured temperature in CREC-VL-Cell, $V_{Total}$ = 0.275 L, $P_{Air}$ =1.01 atm. Note: the 14.7 factor converts atm in psia units.

Then $\Delta P_{Air}$ is a correction that can be validated by comparing it to the $\Delta P_{Air,measured}$ in a CREC-VL-Cell filled with air,

$$\Delta P_{Air,measured} = \left(P_{empty\ cell} - P_{Air}\right) \times 14.7 \qquad \text{Equation 31}$$

where,

$\Delta P_{Air,measured}$ = experimental air correction factor in the CREC-VL-Cell in Psia, $P_{empty\ cell}$ = experimental total air pressure in the CREC-VL-Cell filled with air, atm, $P_{Air}$ =1.01 atm, Note: 14.7 factor converts atm into Psia units.

Figure 46 and Table 9 compare both the $\Delta P_{Air}$ experimentally observed and predicted in the CREC-VL-Cell experiment. One can see that both $\Delta P_{Air}$ are in good agreement with each other, as shown in Figure 46, with a standard deviation not exceeding 0.2 psia. Therefore, the "Air Correction Factor" method, including its validation, confirms that: a) pressure measurements are adequate, b) the ideal gas law adopted is suitable.

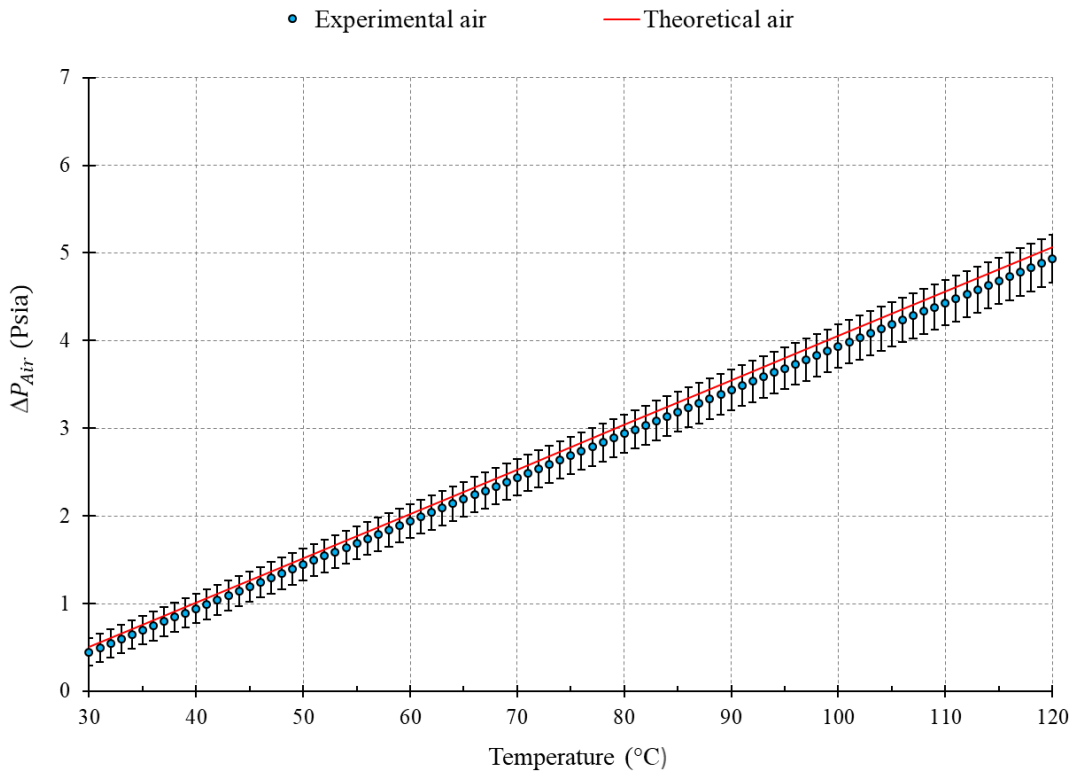


**Figure 46. Comparison of $\Delta P_{Air}$ Experimental (Blue filled circle) and theoretical (Red solid line) in the 30 ℃ to 120 ℃ range. Note: Vertical bars represent standard deviation for experimental repeats.**

**Table 9. Data comparison between theoretical air factor and experimental air factor. Notes: (a) SD indicates Standard deviation, (b) SE indicates Standard Error, (c) LB**

**and UB indicate Lower bound and Upper bound respectively in 95 % Confidence Interval (CI)**

| Theoretical air | | Time | Experimental Corrected Data | | | | 95% CI | |
|---|---|---|---|---|---|---|---|---|
| T (°C) | P vsat (Psia) | (min) | T (°C) | P vsat (Psia) | SD (±) | SE | LB | UB |
| 30 | 0.51 | 0 | 42.0 | 1.0 | 0.2 | 0.1 | 0.8 | 1.2 |
| 40 | 1.01 | 10 | 51.0 | 1.5 | 0.2 | 0.1 | 1.3 | 1.7 |
| 50 | 1.52 | 20 | 59.0 | 1.9 | 0.2 | 0.1 | 1.7 | 2.1 |
| 60 | 2.03 | 30 | 67.0 | 2.3 | 0.2 | 0.1 | 2.1 | 2.5 |
| 70 | 2.53 | 40 | 77.0 | 2.8 | 0.2 | 0.1 | 2.5 | 3.0 |
| 80 | 3.04 | 50 | 85.0 | 3.2 | 0.2 | 0.1 | 2.9 | 3.4 |
| 90 | 3.55 | 60 | 94.0 | 3.6 | 0.2 | 0.1 | 3.4 | 3.9 |
| 100 | 4.05 | 70 | 103.0 | 4.1 | 0.3 | 0.1 | 3.8 | 4.4 |
| 110 | 4.56 | 80 | 112.0 | 4.5 | 0.3 | 0.2 | 4.2 | 4.8 |
| 120 | 5.06 | 90 | 120.0 | 4.9 | 0.3 | 0.2 | 4.6 | 5.2 |

Based on the above, the proposed Air Factor Correction can be applied to various blends studied in this chapter.

One should note that there are assumptions involved in the Air Factor Correction factor other than the ideal gas law: (a) the measuring sample is non-reactive to the air, (b) The humidity level of the air is negligible, (c) the oxygen solubility in water can be neglected.

## 7.2 VLE for Pure Chemical Species

In this chapter, VL equilibrium data for four (4) paraffinic hydrocarbons and water blends are provided. Runs are conducted by using the CREC-VL-Cell method. In these runs, the total vapor pressure and temperature are continuously measured in the range of 30 °C to 110 °C.

The reported experimental data is the average from at least three (3) independent runs. For the statistical analysis, Standard Deviations, Standard Errors and 95 % Confidence Interval are reported. In this respect, the experimental data are compared with data from the open literature.

Regarding the pure hydrocarbon data in the CREC-VL-Cell, they were obtained for the following reasons; (a) Validation of data obtained, (b) Air pressure correction applicability (See 7.1).

### 7.2.1 VLE for Pure Alkane

CREC-VL-Cell measurements were developed with n-hexane, n-octane, n-decane and n-dodecane.

Figure 47, Table 10 and Table 11 report a comparison of n-octane data from the CREC-VL Cell and seven (7) data points from the open-literature as a reference, showing their close agreement.

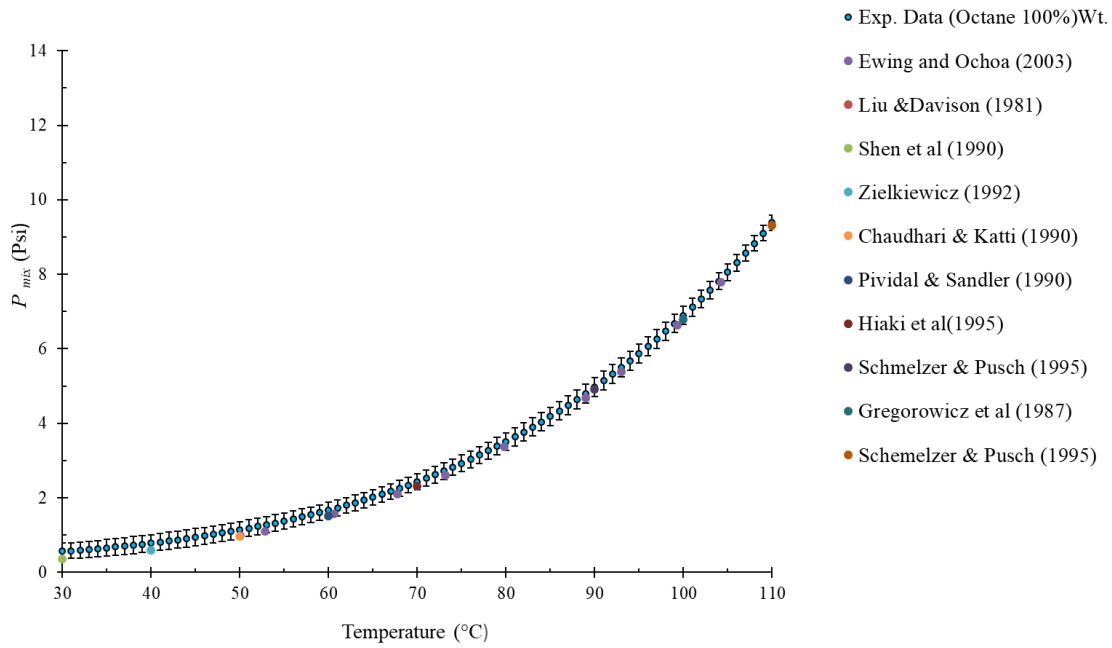


**Figure 47. $P_{mix}$ for n-octane and references data in the range of 30 ℃ to 110 ℃. Note: Vertical bars represent standard deviation**

One can notice in Figure 47, ± 0.25 psia standard deviations for repeat runs. One can observe as well as shown in Appendix A, a systematic uncertainty of 0.08 %, which does not exceed ± 0.26 psia for n-octane, with this being true at various temperature levels.

**Table 10. $P_{mix}$ comparison for n-octane between Literature data and CREC-VL-Cell experimental data**

| | Literature data | | CREC-VL-Cell experimental data |
|---|---|---|---|
| **Temperature (°C)** | **Ref.** | **Vapor pressure (psia)** | **Vapor pressure (psia)** |
| 30 | [161] | 0.36 | 0.8 |
| 40 | [162] | 0.60 | 1.0 |
| 50 | [163] | 0.97 | 1.3 |
| 60 | [164] | 1.52 | 1.9 |
| 70 | [165] | 2.31 | 2.6 |
| 80 | [164] | 3.38 | 3.7 |
| 90 | [166] | 4.85 | 5.2 |
| 100 | [167] | 6.79 | 7.1 |
| 110 | [166] | 9.31 | 9.6 |

**Table 11. n-octane Experimental and Statistical data. Notes: (a) SD = Standard Deviation, (b) SE = Standard Error, (c) CI = Confidence Interval, (d) LB = Lower bound, (e) UB = Upper bound**

| Exp. Data (n-octane 100%) wt. | | | | *95% CI* | |
|---|---|---|---|---|---|
| **Temperature (°C)** | **P mix (psia)** | **SD (±)** | **SE** | **LB** | **UB** |
| 30 | 0.77 | 0.21 | 0.12 | 0.53 | 1.01 |
| 40 | 0.99 | 0.23 | 0.13 | 0.73 | 1.24 |
| 50 | 1.34 | 0.22 | 0.13 | 1.09 | 1.59 |
| 60 | 1.87 | 0.21 | 0.12 | 1.63 | 2.10 |
| 70 | 2.63 | 0.21 | 0.12 | 2.39 | 2.87 |
| 80 | 3.71 | 0.23 | 0.14 | 3.44 | 3.97 |
| 90 | 5.17 | 0.25 | 0.15 | 4.88 | 5.46 |
| 100 | 7.09 | 0.24 | 0.14 | 6.82 | 7.37 |
| 110 | 9.58 | 0.20 | 0.12 | 9.35 | 9.81 |

Furthermore, pure n-hexane experimental data in the CREC-VL-Cell is reported in Figure 48, Table 12 and Table 13. There is also a comparison with six (6) technical literature data points. One can observe, in this case, the close agreement with the literature data, as well as a ± 1.62 psia maximum data uncertainty.

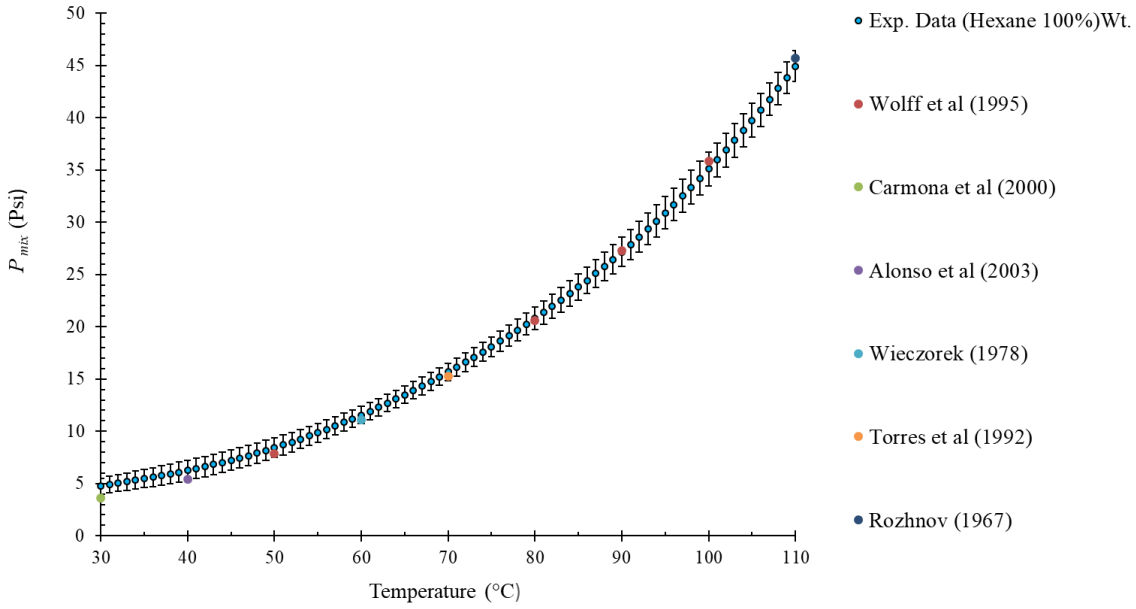


**Figure 48. $P_{mix}$ for n-hexane and references data in the range of 30 ℃ to 110 ℃. Note: Vertical bars represent standard deviation**

**Table 12. $P_{mix}$ comparison for n-hexane between Literature data and CREC-VL-Cell experimental data**

| | Literature data | | Experimental data |
|---|---|---|---|
| **Temperature (℃)** | **Ref.** | **Vapor pressure (psia)** | **Vapor pressure (psia)** |
| 30 | [168] | 3.62 | 4.74 |
| 40 | [169] | 5.41 | 6.26 |
| 50 | [170] | 7.83 | 8.42 |
| 60 | [171] | 11.08 | 11.56 |
| 70 | [172] | 15.30 | 15.67 |

| | | | |
|---|---|---|---|
| 80 | [170] | 20.62 | 20.80 |
| 90 | [170] | 27.27 | 27.16 |
| 100 | [170] | 35.86 | 35.10 |
| 110 | [173] | 45.70 | 44.93 |

**Table 13. n-hexane Experimental and Statistical data. Notes: (a) SD = Standard Deviation, (b) SE = Standard Error, (c) CI = Confidence Interval, (d) LB = Lower bound, (e) UB = Upper bound**

| **Exp. Data (n-hexane 100%) wt.** | | | | ***95% CI*** | |
|---|---|---|---|---|---|
| **Temperature (°C)** | **P mix (psia)** | **SD (±)** | **SE** | **LB** | **UB** |
| 30 | 4.74 | 0.75 | 0.53 | 3.70 | 5.78 |
| 40 | 6.26 | 0.96 | 0.68 | 4.93 | 7.59 |
| 50 | 8.42 | 0.95 | 0.67 | 7.10 | 9.74 |
| 60 | 11.56 | 0.84 | 0.60 | 10.39 | 12.73 |
| 70 | 15.67 | 0.85 | 0.60 | 14.49 | 16.86 |
| 80 | 20.80 | 1.08 | 0.76 | 19.31 | 22.29 |
| 90 | 27.16 | 1.41 | 1.00 | 25.20 | 29.11 |
| 100 | 35.10 | 1.62 | 1.14 | 32.86 | 37.34 |
| 110 | 44.93 | 1.48 | 1.04 | 42.88 | 46.98 |

Furthermore, the pure n-decane data is reported in Figure 49, Table 14 and Table 15. One can see a saturation vapor pressure with less than 3.0 psia standard deviations in the entire experimental range studies. One can also notice that the data uncertainty does not exceed ± 0.45 psia, being in a similar range than those of n-octane and n-hexane. However, one can also note a larger difference with the literature data, with this being assigned to the smaller vapor pressure values measured.

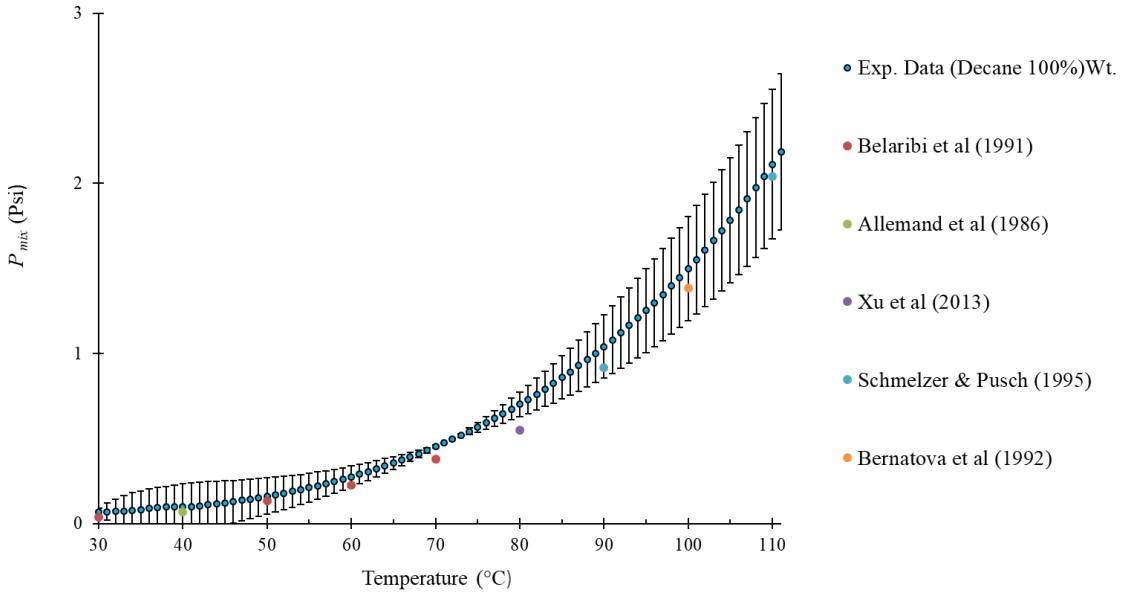


**Figure 49. $P_{mix}$ for n-decane and references data in the range of 30 ℃ to 110 ℃. Note: Vertical bars represent standard deviation**

**Table 14. $P_{mix}$ comparison for n-decane between Literature data and CREC-VL-Cell experimental data**

| | Literature data | | Experimental data |
|---|---|---|---|
| **Temperature (℃)** | **Ref.** | **Vapor pressure (psia)** | **Vapor pressure (psia)** |
| 30 | [174] | 0.04 | 0.07 |
| 40 | [175] | 0.07 | 0.10 |
| 50 | [174] | 0.13 | 0.16 |
| 60 | [174] | 0.23 | 0.28 |
| 70 | [174] | 0.38 | 0.45 |
| 80 | [176] | 0.55 | 0.70 |
| 90 | [77] | 0.92 | 1.04 |
| 100 | [177] | 1.39 | 1.50 |
| 110 | [77] | 2.04 | 2.11 |

**Table 15. n-decane Experimental and Statistical data. Notes: (a) SD = Standard Deviation, (b) SE = Standard Error, (c) CI = Confidence Interval, (d) LB = Lower bound, (e) UB = Upper bound**

| Exp. Data (n-decane 100%) wt. | | | | *95% CI* | |
|---|---|---|---|---|---|
| **Temperature (°C)** | **P mix (psia)** | **SD (±)** | **SE** | **LB** | **UB** |
| 30 | 0.07 | 0.02 | 0.02 | 0.04 | 0.10 |
| 40 | 0.10 | 0.13 | 0.09 | -0.09 | 0.28 |
| 50 | 0.16 | 0.11 | 0.08 | 0.01 | 0.31 |
| 60 | 0.28 | 0.06 | 0.04 | 0.19 | 0.36 |
| 70 | 0.45 | 0.01 | 0.01 | 0.44 | 0.46 |
| 80 | 0.70 | 0.07 | 0.05 | 0.60 | 0.80 |
| 90 | 1.04 | 0.19 | 0.13 | 0.78 | 1.30 |
| 100 | 1.50 | 0.31 | 0.22 | 1.07 | 1.92 |
| 110 | 2.11 | 0.44 | 0.31 | 1.50 | 2.72 |

Finally, the pure n-dodecane vapor pressure data is reported in Figure 50, Table 16 and Table 17, with a maximum saturation pressure of less than 1 psia. One can observe that the experimental data from the CREC-VL-Cell overestimates the vapor pressure of n-dodecane, with a data uncertainty $\leq$ 0.27 psia, comparable to the one with the other hydrocarbons.

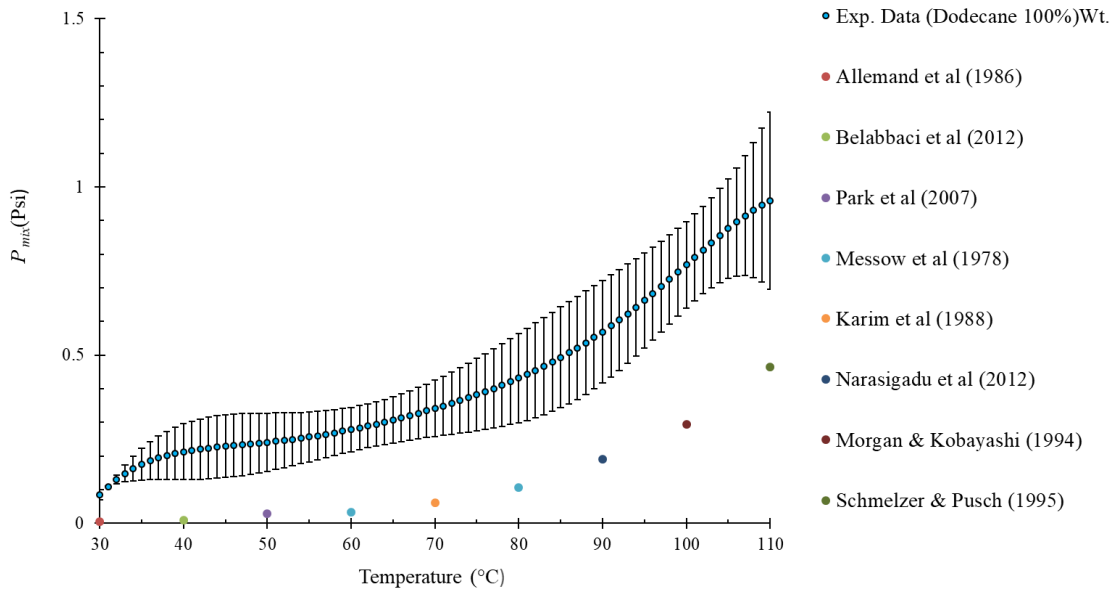


**Figure 50. $P_{mix}$ for n-dodecane and references data in the range of 30 ℃ to 110 ℃.**

**Note: Vertical bars represent standard deviation**

**Table 16. $P_{mix}$ comparison for n-dodecane between Literature data and CREC-VL-Cell experimental data**

| | Literature data | | Experimental data |
|---|---|---|---|
| **Temperature (℃)** | **Ref.** | **Vapor pressure (psia)** | **Vapor pressure (psia)** |
| 30 | [175] | 0.00 | 0.08 |
| 40 | [178] | 0.01 | 0.21 |
| 50 | [179] | 0.03 | 0.24 |
| 60 | [180] | 0.03 | 0.28 |
| 70 | [181] | 0.06 | 0.34 |
| 80 | [180] | 0.11 | 0.43 |
| 90 | [182] | 0.19 | 0.57 |
| 100 | [183] | 0.29 | 0.77 |
| 110 | [166] | 0.46 | 0.96 |

**Table 17. n-dodecane Experimental and Statistical data. Notes: (a) SD = Standard Deviation, (b) SE = Standard Error, (c) CI = Confidence Interval, (d) LB = Lower bound, (e) UB = Upper bound**

| Exp. Data (n-dodecane 100%) wt. | | | | *95% CI* | |
|---|---|---|---|---|---|
| **Temperature (°C)** | **P mix (psia)** | **SD (±)** | **SE** | **LB** | **UB** |
| 30 | 0.08 | 0.01 | 0.01 | 0.06 | 0.10 |
| 40 | 0.21 | 0.08 | 0.06 | 0.10 | 0.33 |
| 50 | 0.24 | 0.09 | 0.06 | 0.12 | 0.36 |
| 60 | 0.28 | 0.07 | 0.05 | 0.19 | 0.37 |
| 70 | 0.34 | 0.08 | 0.06 | 0.23 | 0.46 |
| 80 | 0.43 | 0.13 | 0.09 | 0.25 | 0.62 |
| 90 | 0.57 | 0.15 | 0.11 | 0.36 | 0.78 |
| 100 | 0.77 | 0.13 | 0.09 | 0.59 | 0.95 |
| 110 | 0.96 | 0.26 | 0.19 | 0.59 | 1.32 |

Therefore, one can notice that the vapor pressure obtained in the CREC-VL-Cell shows a good agreement for both n-octane and n-hexane when compared with the data reported in the technical literature. On the other hand, for n-decane and n-dodecane, there is some increased discrepancy, with this being assigned to the higher influence of various measurement errors on the smaller vapor pressure values.

### *7.2.2 VLE for Pure water*

Figure 51, Table 18 and Table 19 reports the vapor pressure for pure water. One can see a good agreement between the experimental data obtained in the CREC-VL-Cell and the literature data, with the data uncertainty being smaller than 0.61 psia for the entire test.

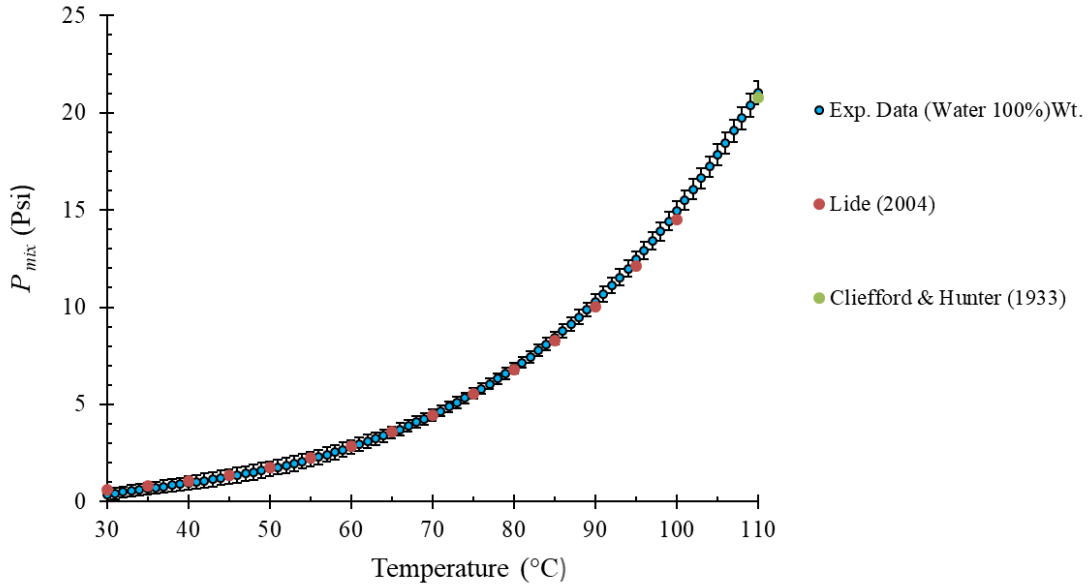


**Figure 51. $P_{mix}$ for single water (Blue filled circle mark), *Lide (2004)* (Red filled circle) and *Cliefford & Hunter (1933)* reference in the range of 30 ℃ to 110 ℃.Note: Vertical bars represent standard deviation.**

Regarding the agreement of $P_{mix}$ with reported saturation pressure values for water, as stated in the technical literature, one can note a close agreement. This agreement also confirms that the air correction method proposed in section 6.1 is adequate in the 275 mL Cell.

**Table 18. $P_{mix}$ comparison for water between Literature data and CREC-VL-Cell experimental data**

| | Literature data | | Experimental data |
|---|---|---|---|
| **Temperature (℃)** | **Ref.** | **Vapor pressure (psia)** | **Vapor pressure (psia)** |
| 30 | | 0.61 | 0.37 |
| 40 | | 1.06 | 0.96 |
| 50 | [184] | 1.77 | 1.69 |
| 60 | | 2.85 | 2.80 |
| 70 | | 4.46 | 4.46 |

| | | | |
|---|---|---|---|
| 80 | | 6.78 | 6.87 |
| 90 | | 10.04 | 10.28 |
| 100 | | 14.51 | 14.96 |
| 110 | [185] | 20.78 | 21.04 |

**Table 19. water Experimental and Statistical data. Notes: (a) SD = Standard Deviation, (b) SE = Standard Error, (c) CI = Confidence Interval, (d) LB = Lower bound, (e) UB = Upper bound**

| **Exp. Data (water 100%) wt.** | | | | ***95% CI*** | |
|---|---|---|---|---|---|
| **Temperature (°C)** | **P mix (psia)** | **SD (±)** | **SE** | **LB** | **UB** |
| 30 | 0.37 | 0.31 | 0.18 | 0.02 | 0.71 |
| 40 | 0.96 | 0.34 | 0.19 | 0.58 | 1.34 |
| 50 | 1.69 | 0.39 | 0.23 | 1.24 | 2.13 |
| 60 | 2.80 | 0.36 | 0.21 | 2.40 | 3.21 |
| 70 | 4.46 | 0.29 | 0.17 | 4.14 | 4.79 |
| 80 | 6.87 | 0.29 | 0.17 | 6.54 | 7.19 |
| 90 | 10.28 | 0.37 | 0.22 | 9.85 | 10.70 |
| 100 | 14.96 | 0.50 | 0.29 | 14.39 | 15.52 |
| 110 | 21.04 | 0.60 | 0.35 | 20.36 | 21.73 |

## 7.3 VLE in n-octane/water Blends

N-octane is one of the main components in naphtha composition, with a boiling point close to the average boiling point for naphtha [186]. Therefore, this research has chosen n-octane and water mixtures to provide a better understanding of the VL equilibrium of the NRU system.

To accomplish this, both Pressure and Temperature are measured in the CREC-VL-Cell using the dynamic technique with the cell temperature augmenting following a set temperature ramp. Twelve (12) different mixtures, including n-octane and water, were studied.

### *7.3.1 P-T data*

Figure 52 reports vapor pressure at various temperatures for twelve (12) n-octane and water blends using the compositions.

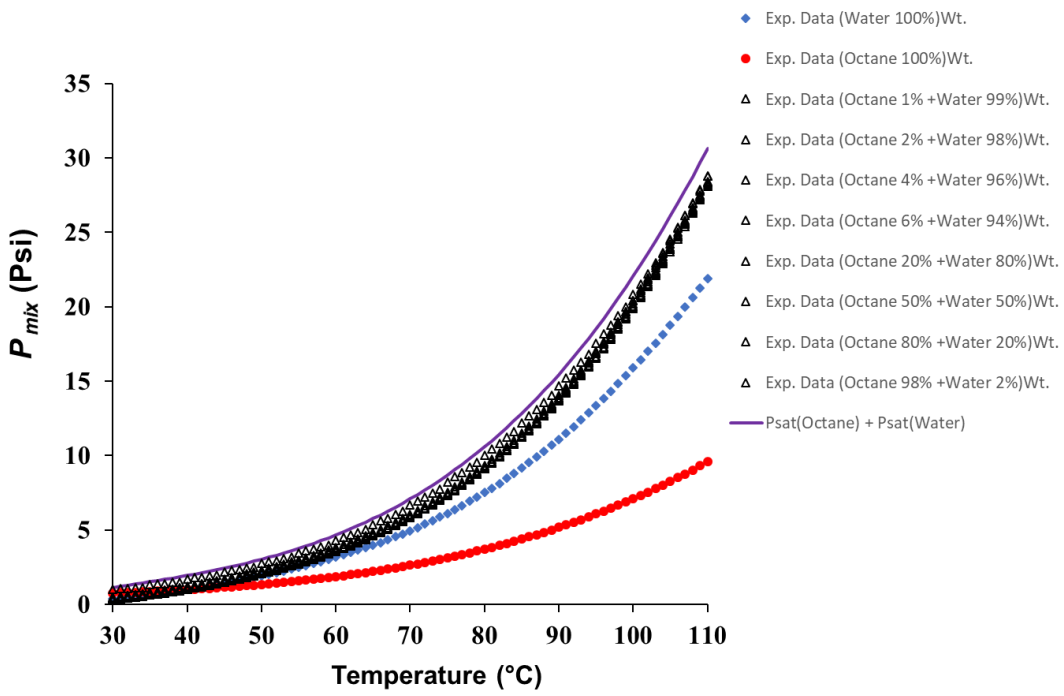


**Figure 52. $P_{mix}$ for VLLE of the n-octane/water mixtures in the range of 30 ℃ to 110 ℃. Notes: (a) Summation of water and n-octane saturation pressures represent a completely immiscible model (purple solid line), (b) 1080 rpm mixing speed is used, (c) Experiment data is the average data of three or more experimental repeats.**

Regarding Figure 52, one can see reviewing the various $P_{mix}$ data points reported that, pure n-octane gave the lowest of all vapor pressures. As well, one can notice that the second lowest data points correspond to pure water (blue dotted diamond line). It is interesting to notice that the observed vapor pressures for all water/n-octane blends surpass all these vapor pressures for pure components.

**Table 20. n-octane 1.0 wt% + water 99.0 wt% Experimental and Statistical data**

| Exp. Data (n-octane 1.0% +water 99.0%) wt. | | | | *95% CI* | |
|---|---|---|---|---|---|
| **Temperature (°C)** | **P mix (psia)** | **SD (±)** | **SE** | **LB** | **UB** |
| 30 | 0.46 | 0.07 | 0.04 | 0.39 | 0.54 |
| 40 | 1.07 | 0.25 | 0.14 | 0.79 | 1.35 |
| 50 | 2.10 | 0.31 | 0.18 | 1.75 | 2.45 |
| 60 | 3.67 | 0.25 | 0.14 | 3.39 | 3.95 |
| 70 | 5.93 | 0.26 | 0.15 | 5.63 | 6.22 |
| 80 | 9.17 | 0.35 | 0.20 | 8.77 | 9.56 |
| 90 | 14.43 | 0.40 | 0.23 | 13.98 | 14.88 |
| 100 | 21.18 | 0.34 | 0.20 | 20.80 | 21.57 |
| 110 | 28.77 | 0.65 | 0.38 | 28.04 | 29.51 |

**Table 21. n-octane 2.0 wt% +water 98.0 wt% Experimental and Statistical data**

| Exp. Data (n-octane 2.0% +water 98.0%) wt. | | | | *95% CI* | |
|---|---|---|---|---|---|
| **Temperature (°C)** | **P mix (psia)** | **SD (±)** | **SE** | **LB** | **UB** |
| 30 | 0.40 | 0.10 | 0.06 | 0.21 | 0.59 |
| 40 | 1.11 | 0.12 | 0.07 | 0.88 | 1.35 |
| 50 | 2.10 | 0.13 | 0.07 | 1.85 | 2.35 |
| 60 | 3.61 | 0.12 | 0.07 | 3.39 | 3.84 |
| 70 | 5.90 | 0.09 | 0.05 | 5.72 | 6.09 |
| 80 | 9.21 | 0.07 | 0.04 | 9.06 | 9.36 |
| 90 | 14.32 | 0.07 | 0.04 | 14.19 | 14.45 |
| 100 | 20.70 | 0.08 | 0.05 | 20.55 | 20.86 |
| 110 | 28.39 | 0.11 | 0.06 | 28.18 | 28.60 |

**Table 22. n-octane 4.0 wt% +water 96.0 wt% Experimental and Statistical data**

| Exp. Data (n-octane 4.0% +water 96.0%) wt. | | | | *95% CI* | |
|---|---|---|---|---|---|
| **Temperature (°C)** | **P mix (psia)** | **SD (±)** | **SE** | **LB** | **UB** |
| 30 | 0.99 | 0.31 | 0.18 | 0.64 | 1.33 |
| 40 | 1.70 | 0.31 | 0.18 | 1.36 | 2.05 |

| | | | | | |
|---|---|---|---|---|---|
| 50 | 2.73 | 0.31 | 0.18 | 2.39 | 3.08 |
| 60 | 4.30 | 0.31 | 0.18 | 3.95 | 4.64 |
| 70 | 6.66 | 0.31 | 0.18 | 6.31 | 7.00 |
| 80 | 10.04 | 0.31 | 0.18 | 9.70 | 10.39 |
| 90 | 15.23 | 0.32 | 0.19 | 14.87 | 15.60 |
| 100 | 21.53 | 0.32 | 0.19 | 21.17 | 21.90 |
| 110 | 28.77 | 0.31 | 0.18 | 28.43 | 29.12 |

**Table 23. n-octane 6.0 wt% +water 94.0 wt% Experimental and Statistical data**

| **Exp. Data (n-octane 6.0% +water 94.0%) wt.** | | | | ***95% CI*** | |
|---|---|---|---|---|---|
| **Temperature (°C)** | **P mix (psia)** | **SD (±)** | **SE** | **LB** | **UB** |
| 30 | 0.27 | 0.16 | 0.09 | 0.09 | 0.45 |
| 40 | 1.01 | 0.13 | 0.07 | 0.86 | 1.16 |
| 50 | 2.04 | 0.16 | 0.09 | 1.86 | 2.23 |
| 60 | 3.56 | 0.20 | 0.11 | 3.34 | 3.78 |
| 70 | 5.84 | 0.21 | 0.12 | 5.61 | 6.07 |
| 80 | 9.18 | 0.22 | 0.13 | 8.93 | 9.43 |
| 90 | 14.44 | 0.28 | 0.16 | 14.12 | 14.76 |
| 100 | 20.93 | 0.32 | 0.18 | 20.57 | 21.29 |
| 110 | 28.31 | 0.09 | 0.05 | 28.21 | 28.40 |

**Table 24. n-octane 20.0 wt% +water 80.0 wt% Experimental and Statistical data**

| **Exp. Data (n-octane 20.0% +water 80.0%) wt.** | | | | ***95% CI*** | |
|---|---|---|---|---|---|
| **Temperature (°C)** | **P mix (psia)** | **SD (±)** | **SE** | **LB** | **UB** |
| 30 | 0.43 | 0.06 | 0.03 | 0.36 | 0.50 |
| 40 | 1.19 | 0.12 | 0.07 | 1.05 | 1.33 |
| 50 | 2.22 | 0.13 | 0.07 | 2.07 | 2.36 |
| 60 | 3.71 | 0.06 | 0.03 | 3.64 | 3.77 |
| 70 | 5.92 | 0.05 | 0.03 | 5.86 | 5.98 |
| 80 | 9.14 | 0.13 | 0.08 | 8.99 | 9.29 |
| 90 | 14.22 | 0.14 | 0.08 | 14.06 | 14.38 |

| | | | | | |
|---|---|---|---|---|---|
| 100 | 20.59 | 0.13 | 0.07 | 20.45 | 20.74 |
| 110 | 28.10 | 0.32 | 0.18 | 27.74 | 28.45 |

**Table 25. n-octane 50.0 wt% +water 50.0 wt% Experimental and Statistical data**

| **Exp. Data (n-octane 50.0% +water 50.0%) wt.** | | | | ***95% CI*** | |
|---|---|---|---|---|---|
| **Temperature (°C)** | **P mix (psia)** | **SD (±)** | **SE** | **LB** | **UB** |
| 30 | 0.44 | 0.04 | 0.02 | 0.39 | 0.49 |
| 40 | 1.20 | 0.09 | 0.05 | 1.10 | 1.31 |
| 50 | 2.29 | 0.07 | 0.04 | 2.21 | 2.37 |
| 60 | 3.82 | 0.10 | 0.06 | 3.71 | 3.94 |
| 70 | 6.06 | 0.19 | 0.11 | 5.84 | 6.27 |
| 80 | 9.34 | 0.31 | 0.18 | 8.99 | 9.68 |
| 90 | 14.59 | 0.46 | 0.26 | 14.07 | 15.10 |
| 100 | 21.11 | 0.59 | 0.34 | 20.45 | 21.77 |
| 110 | 28.39 | 0.61 | 0.35 | 27.70 | 29.09 |

**Table 26. n-octane 80.0 wt% +water 20.0 wt% Experimental and Statistical data**

| **Exp. Data (n-octane 80.0% +water 20.0%) wt.** | | | | ***95% CI*** | |
|---|---|---|---|---|---|
| **Temperature (°C)** | **P mix (psia)** | **SD (±)** | **SE** | **LB** | **UB** |
| 30 | 0.31 | 0.07 | 0.04 | 0.23 | 0.40 |
| 40 | 1.03 | 0.10 | 0.06 | 0.91 | 1.14 |
| 50 | 2.08 | 0.08 | 0.04 | 1.99 | 2.17 |
| 60 | 3.62 | 0.06 | 0.03 | 3.55 | 3.68 |
| 70 | 5.87 | 0.07 | 0.04 | 5.80 | 5.94 |
| 80 | 9.13 | 0.08 | 0.05 | 9.04 | 9.23 |
| 90 | 14.28 | 0.09 | 0.05 | 14.18 | 14.39 |
| 100 | 20.76 | 0.10 | 0.06 | 20.65 | 20.88 |
| 110 | 28.37 | 0.15 | 0.09 | 28.19 | 28.54 |

**Table 27. n-octane 98.0 wt% +water 2.0 wt% Experimental and Statistical data**

| Exp. Data (Octane 98.0% +water 2.0%) wt. | | | | *95% CI* | |
|---|---|---|---|---|---|
| **Temperature (°C)** | **P mix (psia)** | **SD (±)** | **SE** | **LB** | **UB** |
| 30 | 0.37 | 0.05 | 0.03 | 0.31 | 0.44 |
| 40 | 1.08 | 0.09 | 0.05 | 0.98 | 1.18 |
| 50 | 2.12 | 0.13 | 0.07 | 1.97 | 2.26 |
| 60 | 3.63 | 0.17 | 0.10 | 3.44 | 3.82 |
| 70 | 5.85 | 0.23 | 0.13 | 5.59 | 6.11 |
| 80 | 9.10 | 0.31 | 0.18 | 8.76 | 9.45 |
| 90 | 14.28 | 0.38 | 0.22 | 13.86 | 14.71 |
| 100 | 20.76 | 0.39 | 0.23 | 20.32 | 21.21 |
| 110 | 28.18 | 0.31 | 0.18 | 27.83 | 28.52 |

Results reported in Figure 52 point to the essentially immiscible behavior of n-octane and water blends where the blend vapor pressure can be expected to comply with the addition of individual water and n-octane vapor pressure model. As a theoretical reference, the vapor pressure for the fully immiscible model is also provided in Figure 52, with this showing the significant trend of the actual water and n-octane blends to approximate this upper theoretical vapor pressure limit.

Figure 53, Table 28, Table 29 and Table 30, on the other hand, report the vapor pressures for n-octane/water blends with n-octane concentrations smaller than 1.0 wt%. One can thus see that the measured vapor pressures start becoming now smaller than the theoretical limit of the immiscible model suggesting partial miscibility.

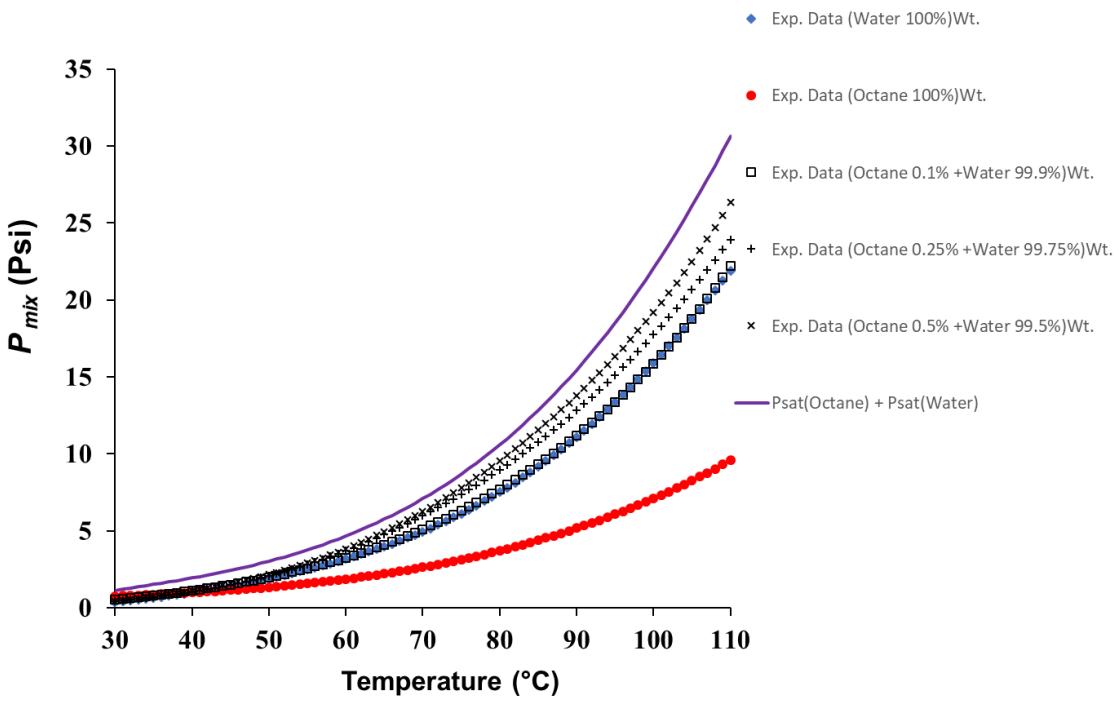


**Figure 53. $P_{mix}$ for VLE of n-octane – water mixture in the range of 30 ℃ to 110 ℃ range. Notes: (a) Summation of water and n-octane saturation pressures represent a completely immiscible model (purple solid line), (b) 1080 rpm mixing speed is used, (c) Experiment data is the average data of three or more experimental repeats.**

**Table 28. n-octane 0.1 wt% +water 99.9 wt% Experimental and Statistical data**

| **Exp. Data (n-octane 0.1% +water 99.9%) wt.** | | | | ***95% CI*** | |
|---|---|---|---|---|---|
| **Temperature (°C)** | **P mix (psia)** | **SD (±)** | **SE** | **LB** | **UB** |
| 30 | 0.51 | 0.14 | 0.08 | 0.35 | 0.67 |
| 40 | 1.12 | 0.11 | 0.06 | 0.99 | 1.24 |
| 50 | 1.98 | 0.06 | 0.04 | 1.90 | 2.05 |
| 60 | 3.25 | 0.05 | 0.03 | 3.20 | 3.30 |
| 70 | 5.10 | 0.07 | 0.04 | 5.03 | 5.18 |
| 80 | 7.69 | 0.11 | 0.06 | 7.57 | 7.81 |

| | | | | | |
|---|---|---|---|---|---|
| 90 | 11.60 | 0.16 | 0.09 | 11.42 | 11.77 |
| 100 | 16.41 | 0.22 | 0.13 | 16.17 | 16.66 |
| 110 | 22.19 | 0.38 | 0.22 | 21.75 | 22.62 |

**Table 29. n-octane 0.25 wt% +water 99.75 wt% Experimental and Statistical data**

| **Exp. Data (n-octane 0.25% +water 99.75%) wt.** | | | | ***95% CI*** | |
|---|---|---|---|---|---|
| **Temperature (°C)** | **P mix (psia)** | **SD (±)** | **SE** | **LB** | **UB** |
| 30 | 0.42 | 0.73 | 0.42 | -0.41 | 1.24 |
| 40 | 1.05 | 0.70 | 0.40 | 0.26 | 1.83 |
| 50 | 2.07 | 0.64 | 0.37 | 1.34 | 2.80 |
| 60 | 3.69 | 0.51 | 0.29 | 3.12 | 4.27 |
| 70 | 5.97 | 0.36 | 0.21 | 5.56 | 6.37 |
| 80 | 8.95 | 0.31 | 0.18 | 8.60 | 9.30 |
| 90 | 13.24 | 0.43 | 0.25 | 12.76 | 13.72 |
| 100 | 18.30 | 0.53 | 0.31 | 17.70 | 18.90 |
| 110 | 23.92 | 0.54 | 0.31 | 23.31 | 24.53 |

**Table 30. n-octane 0.5 wt% +water 99.5 wt% Experimental and Statistical data**

| **Exp. Data (n-octane 0.5% +water 99.5%) wt.** | | | | ***95% CI*** | |
|---|---|---|---|---|---|
| **Temperature (°C)** | **P mix (psia)** | **SD (±)** | **SE** | **LB** | **UB** |
| 30 | 0.43 | 0.03 | 0.02 | 0.39 | 0.46 |
| 40 | 1.11 | 0.03 | 0.02 | 1.08 | 1.15 |
| 50 | 2.17 | 0.06 | 0.04 | 2.10 | 2.24 |
| 60 | 3.82 | 0.08 | 0.04 | 3.74 | 3.91 |
| 70 | 6.25 | 0.10 | 0.06 | 6.14 | 6.37 |
| 80 | 9.55 | 0.16 | 0.10 | 9.37 | 9.74 |
| 90 | 14.27 | 0.29 | 0.16 | 13.95 | 14.60 |
| 100 | 19.81 | 0.40 | 0.23 | 19.35 | 20.27 |
| 110 | 26.34 | 0.44 | 0.25 | 25.84 | 26.83 |

On the other hand, Figure 54 and Table 31 report runs developed in the CREC-VL-Cell using a high n-octane and low water concentration blend: 99.75 wt% n-octane + 0.25 wt%

water. One can notice the significant impact of a small fraction of water on the vapor pressure of the blend, with the vapor pressure surpassing both the pure water vapor pressure and pure n-octane. One could argue in this respect, that at these low water concentrations, this is an indication that no separate water phase exists in the liquid phase, with water being partially solubilized in n-octane.

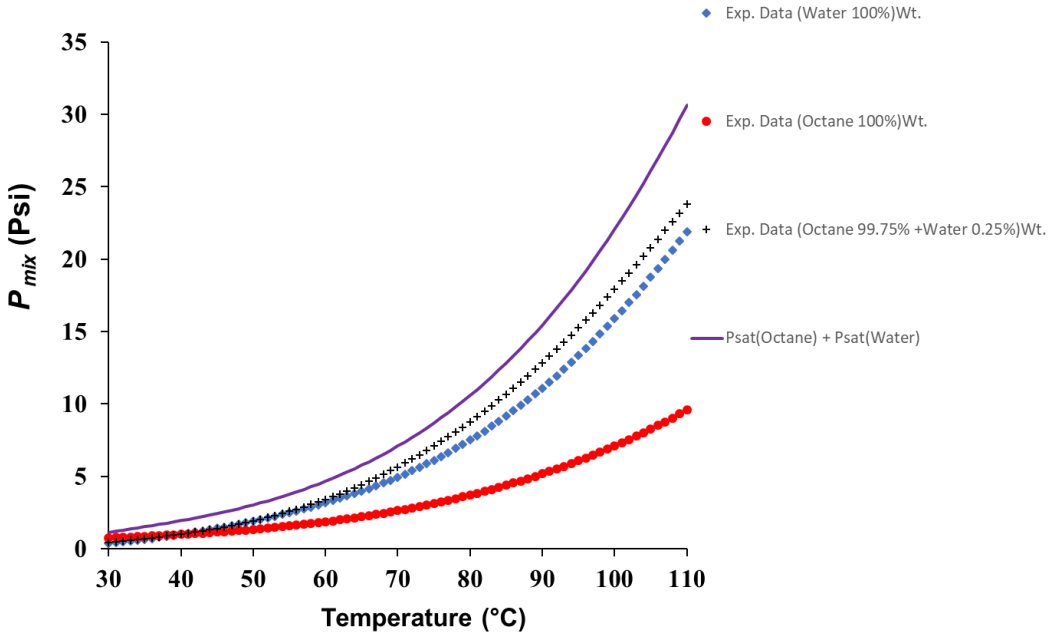


**Figure 54. $P_{mix}$ for 99.75 wt% n-octane + 0.25 wt% water in the range of 30 ℃ to 110 ℃ range. Notes: (a) Summation of water and n-octane saturation pressures represent a completely immiscible model (purple solid line), (b) 1080 rpm mixing speed is used, (c) Experiment data is the average data of three or more experimental repeats.**

**Table 31. n-octane 99.75.0 wt% +water 0.25 wt% Experimental and Statistical data**

| Exp. Data (n-octane 99.75% +water 0.25%) wt. | | | | *95% CI* | |
|---|---|---|---|---|---|
| **Temperature (°C)** | **P mix (psia)** | **SD (±)** | **SE** | **LB** | **UB** |
| 30 | 0.44 | 0.21 | 0.12 | 0.20 | 0.68 |

| | | | | | |
|---|---|---|---|---|---|
| 40 | 1.01 | 0.13 | 0.08 | 0.86 | 1.16 |
| 50 | 1.92 | 0.17 | 0.10 | 1.72 | 2.11 |
| 60 | 3.41 | 0.35 | 0.20 | 3.01 | 3.81 |
| 70 | 5.64 | 0.42 | 0.24 | 5.16 | 6.12 |
| 80 | 8.75 | 0.29 | 0.17 | 8.43 | 9.08 |
| 90 | 13.31 | 0.11 | 0.06 | 13.18 | 13.43 |
| 100 | 18.47 | 0.22 | 0.12 | 18.23 | 18.72 |
| 110 | 23.80 | 0.39 | 0.23 | 23.35 | 24.24 |

## 7.4 **VLE in water/synthetic naphtha (SN) Blends**

### *7.4.1 P-T data on different synthetic naphtha concentration*

In this chapter, results for VLE runs using water/synthetic naphtha (SN) in the CREC-VL-Cell are reported. The SN employed consisted of five (5) paraffinic hydrocarbons. The blend composition was selected to represent typical naphtha, as reported in the technical literature (See 5.1.2). The ratios of SN and water were chosen to represent the naphtha in water in a Naphtha Recovery Unit (NRU) of the oil sand industry. In the NRU, the feed stream contains about 2.0 wt% naphtha and heavier hydrocarbon in smaller amounts [4]. Therefore, 2.5 wt% and 4.0 wt% SN in water were selected for the hydrocarbon blends to be VLE runs of the present study. Furthermore, 97.5 wt% SN in water was also considered for analyzing the VLE of low concentrations of water in SN.

Figure 55 reports the pressure-temperature data for three (3) different water-SN blends. In this series, VLE runs at 1080 rpm in the CREC-VL-Cell were analyzed, in the 30 °C to

110 ℃ range. Statistical data for the three (3) compositions are provided in Table 32**,** Table 33 and Table 34**,** respectively.

Reviewing the data in Figure 55, one can notice that the vapor pressures for 2.5 wt%, 4.0 wt% and 97.5 wt% synthetic naphtha mixture are close in spite of the SN concentrations difference.

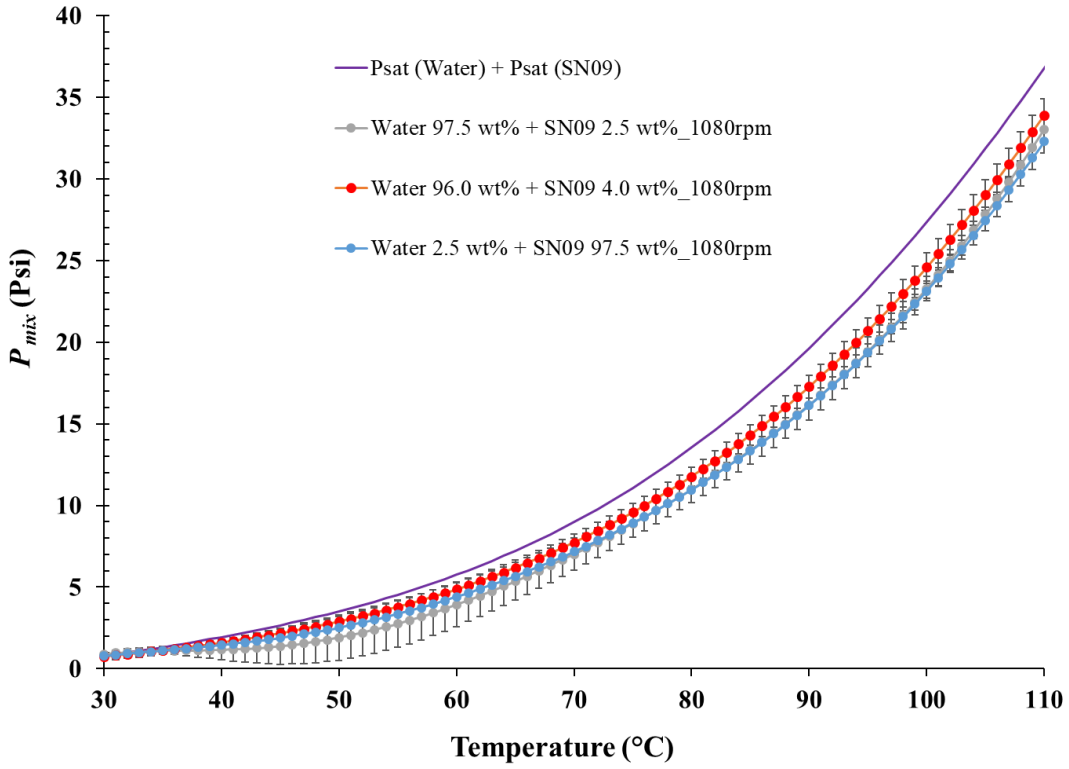


**Figure 55. $P_{mix}$ for water /synthetic naphtha mixtures in the range of 30 ℃ to 110 ℃ . Notes: (a) Summation of water and synthetic naphtha saturation pressures represent a completely immiscible model (purple solid line), (b) 1080 rpm mixing speed is used, (c) Vertical bars indicate the standard deviation of three or more experimental repeats.**

Regarding the results reported in Figure 55, they can be justified given the 2.5wt% and 4wt% SN in water, they form two essentially immiscible liquid phases, with $P_{mix}$ given by the direct addition of the saturation vapour pressures of the SN and water individual

species. A similar result was also obtained at the other extreme of the blends having 2.5wt% water in SN. The closeness of the $\boldsymbol{P_{mix}}$ to the addition of the saturation vapour pressures for SN and water suggests a close to two immiscible phases.

**Table 32. synthetic naphtha 2.5 wt% + water 97.5% Experimental and Statistical data**

| **Exp. Data (synthetic naphtha 2.5 wt% + water 97.5 wt%)** | | | | ***95% CI*** | |
|---|---|---|---|---|---|
| **Temperature (°C)** | **P mix (psia)** | **SD (±)** | **SE** | **LB** | **UB** |
| 30 | 0.89 | 0.10 | 0.07 | 0.76 | 1.03 |
| 40 | 1.16 | 0.62 | 0.44 | 0.29 | 2.02 |
| 50 | 1.90 | 1.38 | 0.98 | -0.01 | 3.82 |
| 60 | 3.93 | 1.34 | 0.95 | 2.07 | 5.79 |
| 70 | 7.02 | 0.97 | 0.69 | 5.67 | 8.37 |
| 80 | 10.99 | 0.82 | 0.58 | 9.85 | 12.12 |
| 90 | 16.15 | 0.91 | 0.64 | 14.90 | 17.41 |
| 100 | 23.28 | 0.76 | 0.54 | 22.23 | 24.33 |
| 110 | 33.03 | 0.05 | 0.04 | 32.96 | 33.10 |

**Table 33. synthetic naphtha 4.0 wt% + water 96.0 wt% Experimental and Statistical data**

| **Exp. Data (synthetic naphtha 4.0 wt% + water 96.0 wt%)** | | | | ***95% CI*** | |
|---|---|---|---|---|---|
| **Temperature (°C)** | **P mix (psia)** | **SD (±)** | **SE** | **LB** | **UB** |
| 30 | 0.74 | 0.21 | 0.15 | 0.45 | 1.03 |
| 40 | 1.61 | 0.19 | 0.13 | 1.34 | 1.87 |
| 50 | 2.89 | 0.30 | 0.21 | 2.48 | 3.31 |
| 60 | 4.87 | 0.42 | 0.30 | 4.28 | 5.46 |
| 70 | 7.74 | 0.51 | 0.36 | 7.03 | 8.45 |
| 80 | 11.76 | 0.59 | 0.42 | 10.95 | 12.58 |
| 90 | 17.27 | 0.71 | 0.50 | 16.30 | 18.25 |
| 100 | 24.60 | 0.88 | 0.62 | 23.39 | 25.82 |
| 110 | 33.91 | 0.99 | 0.70 | 32.55 | 35.28 |

**Table 34. synthetic naphtha 97.5 wt% + water 2.5 wt% Experimental and Statistical data**

| Exp. Data (synthetic naphtha 97.5 wt% + water 2.5 wt%) | | | | *95% CI* | |
|---|---|---|---|---|---|
| **Temperature (°C)** | **P mix (psia)** | **SD (±)** | **SE** | **LB** | **UB** |
| 30 | 0.77 | 0.28 | 0.20 | 0.38 | 1.15 |
| 40 | 1.45 | 0.12 | 0.08 | 1.28 | 1.61 |
| 50 | 2.52 | 0.04 | 0.03 | 2.47 | 2.57 |
| 60 | 4.40 | 0.02 | 0.01 | 4.37 | 4.43 |
| 70 | 7.17 | 0.02 | 0.01 | 7.15 | 7.19 |
| 80 | 10.96 | 0.01 | 0.01 | 10.94 | 10.98 |
| 90 | 16.12 | 0.10 | 0.07 | 15.98 | 16.27 |
| 100 | 23.13 | 0.44 | 0.31 | 22.52 | 23.75 |
| 110 | 32.29 | 0.73 | 0.51 | 31.29 | 33.30 |

### *7.4.2 P-T data at Different Impeller Speeds*

The selection of impellers speed is of critical importance for achieving adequate mixing in the CREC-VL-Cell. Figure 56 reports P-T data for a 97.5 wt% water-2.5 wt% SN blends using five (5) different impeller speeds.

One can see in Figure 56 that $P_{mix}$ increased consistently until 1080 rpm-1200 rpm is reached. At 0 rpm, 550 rpm and 880 rpm mixing speeds, lower $P_{mix}$ values are obtained with these $P_{mix}$, which are justified on the basis of inadequate phase mixing speeds, for phases with different density and limited mass transfer. For instance, the droplet size and its uniform distribution in the bulk of the blend may affect VLE until the mixing condition reaches the desired optimum level.

Furthermore, one noticed that the 1200rpm impeller speed may cause cavitation. As a result, the 1080 rpm condition was chosen for all other experiments without having to be concerned with the cavitation phenomenon [187].

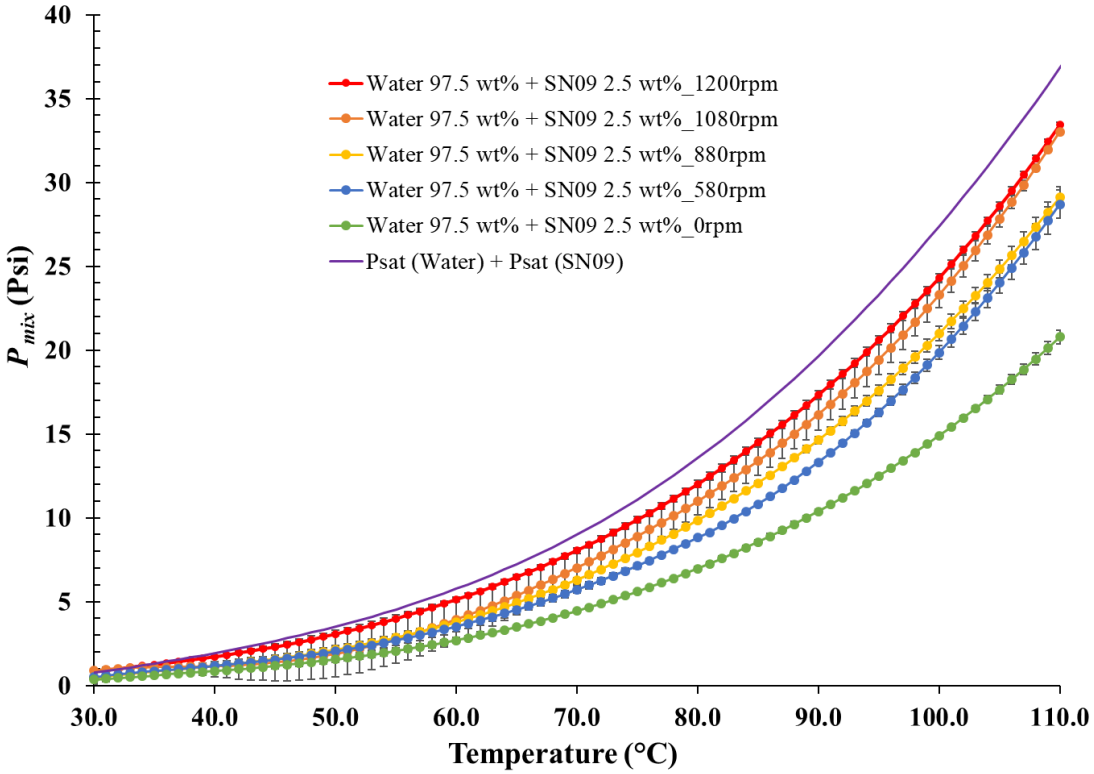


**Figure 56. Mixing-speed effect for 2.5 wt% synthetic naphtha – 97.5 wt% water mixture in the range of 30 ℃ to 110 ℃. Notes: (a) Summation of water and synthetic naphtha saturation pressures represent a completely immiscible model (purple solid line), (b) 1080 rpm mixing speed is used, (c) Vertical bars indicate the standard deviation of three or more experimental repeats.**

Figure 57 reports the mixing speed effect on a 4.0 wt% SN - 96.0 wt% water blend. As well one can notice 580 rpm and 880 rpm mixing speeds are not recommended for accurate $P_{mix}$ measurements. One can also see in the case for 4.0 wt% SN in water blend that 1080rpm and 1200rpm offer conditions for the highest $P_{mix}$, with 1080rpm being preferred to avoid cavitation.

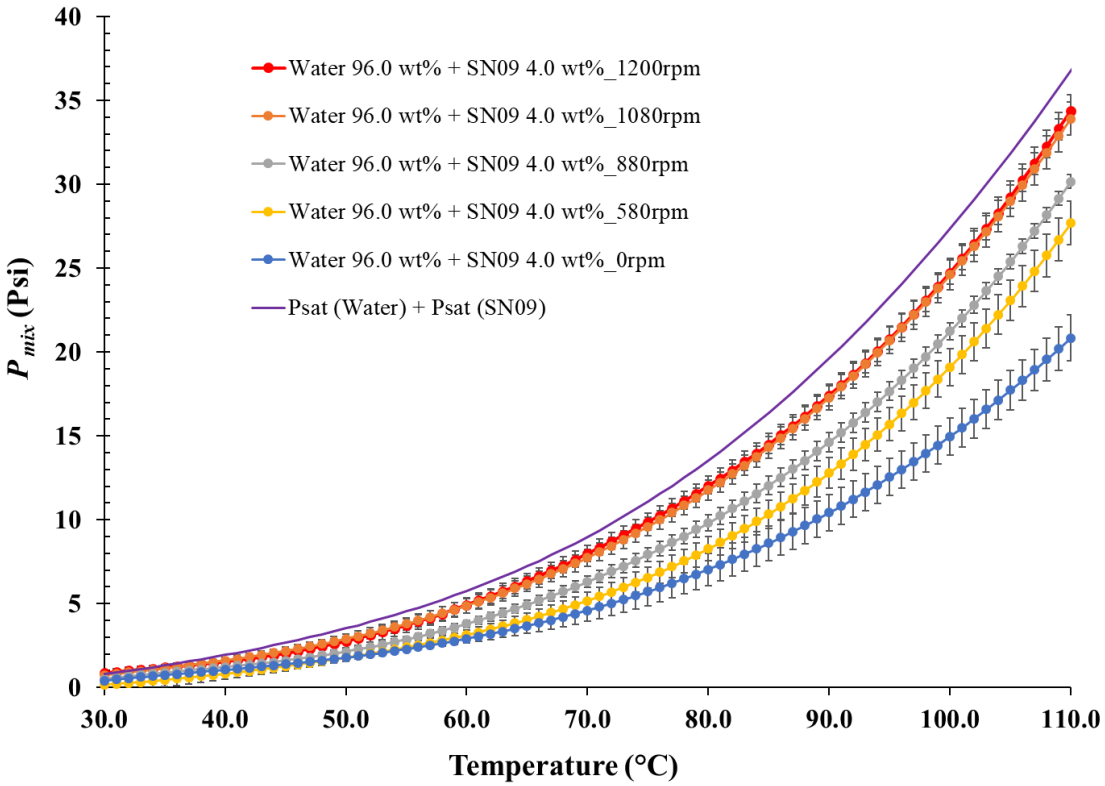


**Figure 57. Mixing-speed effect for 4.0 wt% SN - 96.0 wt% water mixture in the range of 30 ℃ to 110 ℃. Notes: (a) Summation of water and synthetic naphtha saturation pressures represent a completely immiscible model (purple solid line), (b) 1080 rpm mixing speed is used, (c) Vertical bars indicate the standard deviation of three or more experimental repeats.**

Furthermore, Figure 58 reports $P_{mix}$ for 97.5 wt% SN - 2.5 wt% water. Here again, the 1080 rpm is recommended for achieving the highest $P_{mix}$ values.

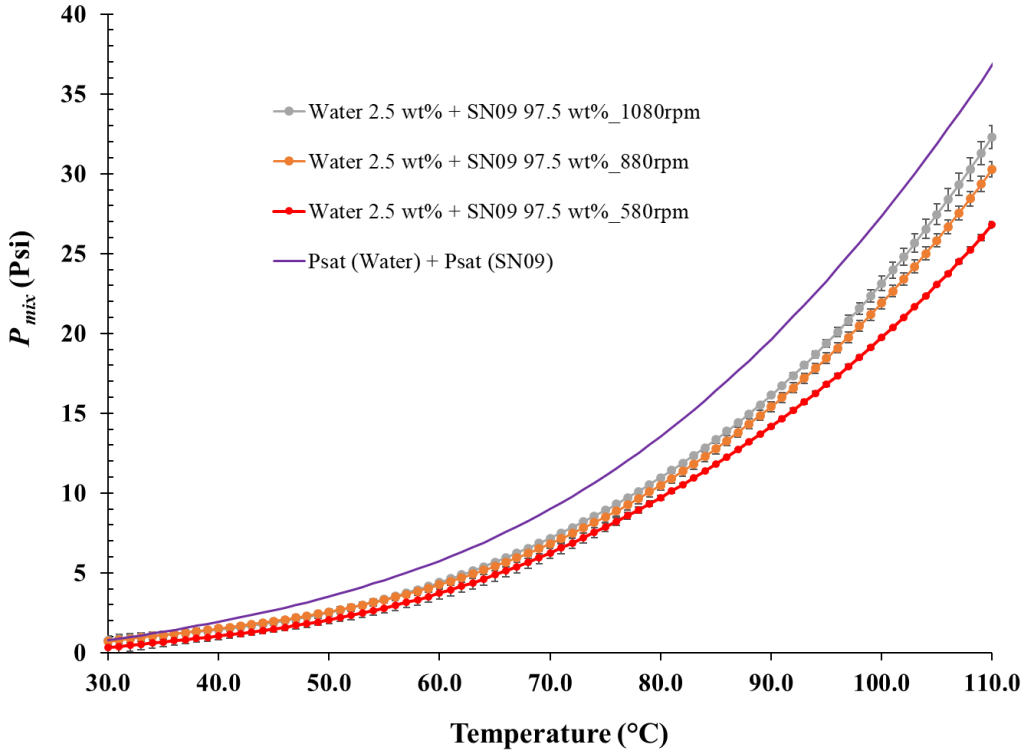


**Figure 58. Mixing-speed effect for 97.5 wt% water – 2.5 wt% synthetic naphtha mixture in the range of 30 ℃ to 110 ℃. Notes: (a) Summation of water and synthetic naphtha saturation pressures represent a completely immiscible model (purple solid line), (b) 1080 rpm mixing speed is used, (c) Vertical bars indicate the standard deviation of three or more experimental repeats.**

## 7.5 VLE in water -solids- n-octane Blends

Both silica sand and kaolin clay are added in the present study into water and n-octane blends mixture, to form a multicomponent mixture. P-T diagrams are investigated to establish the vapor pressure and its change with solids concentrations. Solid particles employed 70 wt % silica sand and 30 wt% kaolin clay. This solid blend is used to closely represent the solids in the NRU (See 5.1.1).

Figure 59 and Table 35 report VLE for 1.0 wt % n-octane mixture in water with 20 wt% of solids. One can, thus, see that the $P_{mix}$ is very close to the vapor pressure for 1.0 wt% n-octane in water without solids, and close as well to the $P_{mix}$ defined with the addition of

the n-octane and water vapour pressure. Thus, the 20 wt% does not have a significant influence on $P_{mix}$ and the n-octane/water blend continues to behave as a quasi-immiscible blend.

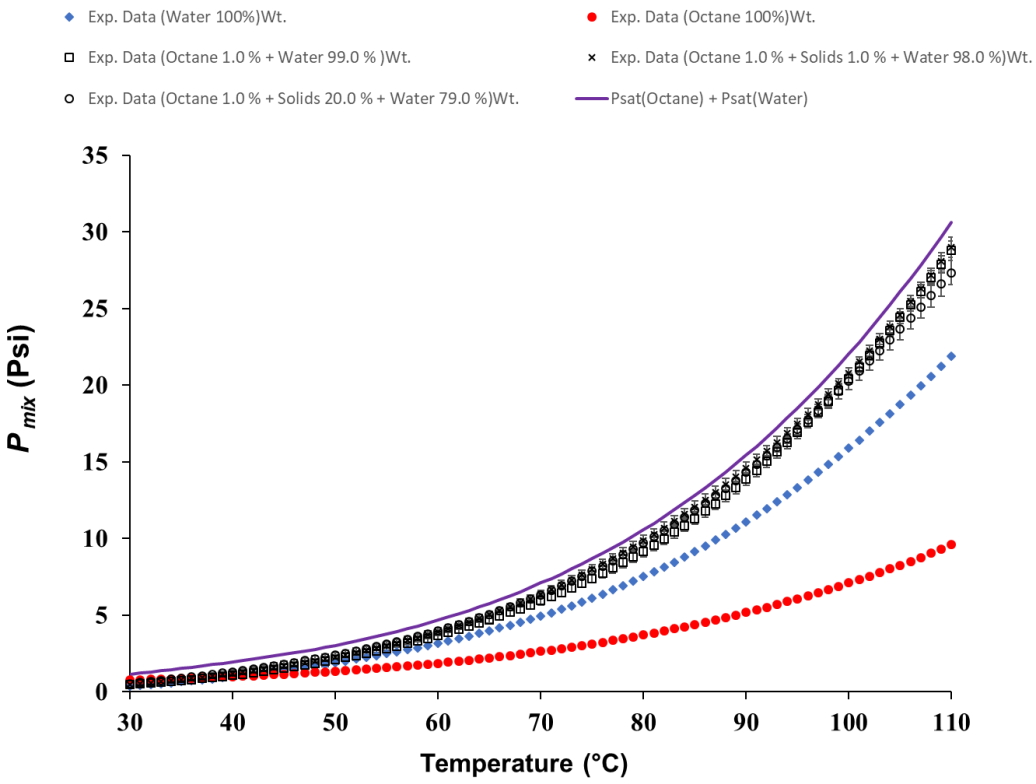


**Figure 59. $P_{mix}$ for 1.0 wt% n-octane and various water-solid compositions in the 30 ℃ to 110 ℃ range. Notes: (a) Summation of water and octane saturation pressures represent a completely immiscible model (purple solid line), (b) 1080 rpm mixing speed is used, (c) Vertical bars indicate the standard deviation of three or more experimental repeats.**

**Table 35. n-octane 1.0 wt% + solids 1.0 wt% + water 98.0 wt% Experimental and Statistical data**

| Exp. Data (n-octane 1.0 % + solids 1.0 % + water 98.0 %) wt. | | | | *95% CI* | |
|---|---|---|---|---|---|
| **Temperature (°C)** | **P mix (psia)** | **SD (±)** | **SE** | **LB** | **UB** |
| 30 | 0.46 | 0.07 | 0.04 | 0.39 | 0.54 |
| 40 | 1.07 | 0.25 | 0.14 | 0.79 | 1.35 |

| | | | | | |
|---|---|---|---|---|---|
| 50 | 2.10 | 0.31 | 0.18 | 1.75 | 2.45 |
| 60 | 3.67 | 0.25 | 0.14 | 3.39 | 3.95 |
| 70 | 5.93 | 0.26 | 0.15 | 5.63 | 6.22 |
| 80 | 9.17 | 0.35 | 0.20 | 8.77 | 9.56 |
| 90 | 14.43 | 0.40 | 0.23 | 13.98 | 14.88 |
| 100 | 21.18 | 0.34 | 0.20 | 20.80 | 21.57 |
| 110 | 28.77 | 0.65 | 0.38 | 28.04 | 29.51 |

**Table 36. n-octane 1.0 wt% + solids 20.0 wt% + water 79.0 wt% Experimental and Statistical data**

| **Exp. Data (n-octane 1.0 % + solids 20.0 % + water 79.0 %) wt.** | | | | ***95% CI*** | |
|---|---|---|---|---|---|
| **Temperature (°C)** | **P mix (psia)** | **SD (±)** | **SE** | **LB** | **UB** |
| 30 | 0.54 | 0.08 | 0.06 | 0.43 | 0.66 |
| 40 | 1.30 | 0.06 | 0.04 | 1.22 | 1.39 |
| 50 | 2.39 | 0.01 | 0.00 | 2.38 | 2.40 |
| 60 | 3.98 | 0.01 | 0.01 | 3.97 | 3.99 |
| 70 | 6.32 | 0.01 | 0.01 | 6.31 | 6.34 |
| 80 | 9.69 | 0.01 | 0.01 | 9.68 | 9.70 |
| 90 | 14.84 | 0.22 | 0.15 | 14.54 | 15.14 |
| 100 | 20.90 | 0.57 | 0.41 | 20.11 | 21.70 |
| 110 | 27.34 | 0.78 | 0.55 | 26.26 | 28.43 |

Figure 60 further report VLE for 2.0 wt % n-octane mixture in water with 20 wt% solids. Here again, there is no difference in the VLE with and without solids, as observed for 1.0 wt% n-octane in water.

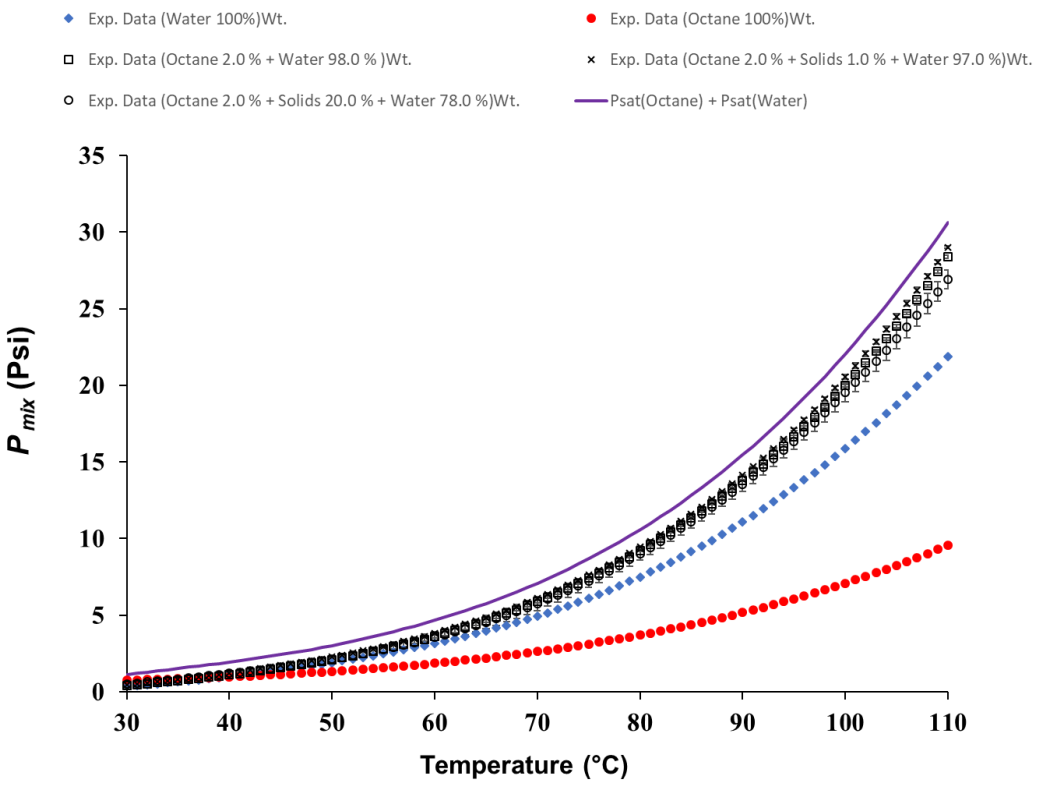


**Figure 60. $P_{mix}$ for 2.0 wt% n-octane and various water-solids compositions in the 30 ℃ to 110 ℃ range. Notes: (a) Summation of water and octane saturation pressures represent a completely immiscible model (purple solid line), (b) 1080 rpm mixing speed is used, (c) Vertical bars indicate the standard deviation of three or more experimental repeats.**

**Table 37. n-octane 2.0 wt% + solids 1.0 wt% + water 97.0 wt% Experimental and Statistical data**

| Exp. Data (n-octane 2.0 % + solids 1.0 % + water 97.0 %) wt. | | | | *95% CI* | |
|---|---|---|---|---|---|
| **Temperature (°C)** | **P mix (psia)** | **SD (±)** | **SE** | **LB** | **UB** |
| 30 | 0.45 | 0.06 | 0.04 | 0.33 | 0.56 |
| 40 | 1.23 | 0.09 | 0.07 | 1.05 | 1.41 |
| 50 | 2.28 | 0.05 | 0.03 | 2.19 | 2.38 |
| 60 | 3.82 | 0.03 | 0.02 | 3.77 | 3.86 |
| 70 | 6.10 | 0.05 | 0.04 | 5.99 | 6.21 |

| | | | | | |
|---|---|---|---|---|---|
| 80 | 9.44 | 0.08 | 0.06 | 9.29 | 9.60 |
| 90 | 14.71 | 0.00 | 0.00 | 14.70 | 14.71 |
| 100 | 21.29 | 0.16 | 0.11 | 20.99 | 21.60 |
| 110 | 29.01 | 0.08 | 0.06 | 28.85 | 29.17 |

**Table 38. n-octane 2.0 wt% + solids 20.0 wt% + water 78.0 wt% Experimental and Statistical data**

| **Exp. Data (n-octane 2.0 % + solids 20.0 % + water 78.0 %) wt.** | | | | ***95% CI*** | |
|---|---|---|---|---|---|
| **Temperature (°C)** | **P mix (psia)** | **SD (±)** | **SE** | **LB** | **UB** |
| 30 | 0.52 | 0.18 | 0.13 | 0.16 | 0.88 |
| 40 | 1.20 | 0.04 | 0.03 | 1.12 | 1.29 |
| 50 | 2.14 | 0.20 | 0.14 | 1.75 | 2.53 |
| 60 | 3.56 | 0.38 | 0.27 | 2.81 | 4.31 |
| 70 | 5.76 | 0.44 | 0.31 | 4.89 | 6.63 |
| 80 | 9.02 | 0.43 | 0.31 | 8.17 | 9.86 |
| 90 | 14.09 | 0.48 | 0.34 | 13.15 | 15.03 |
| 100 | 20.19 | 0.63 | 0.44 | 18.96 | 21.42 |
| 110 | 26.92 | 0.62 | 0.44 | 25.70 | 28.15 |

Figure 61 and Figure 62 further show 4.0 wt% and 6.0 wt% n-octane in water blends with added 20 wt% solids. Here as well, there is a negligible difference on $\boldsymbol{P_{mix}}$ recorded values, without and with 20 wt% solids.

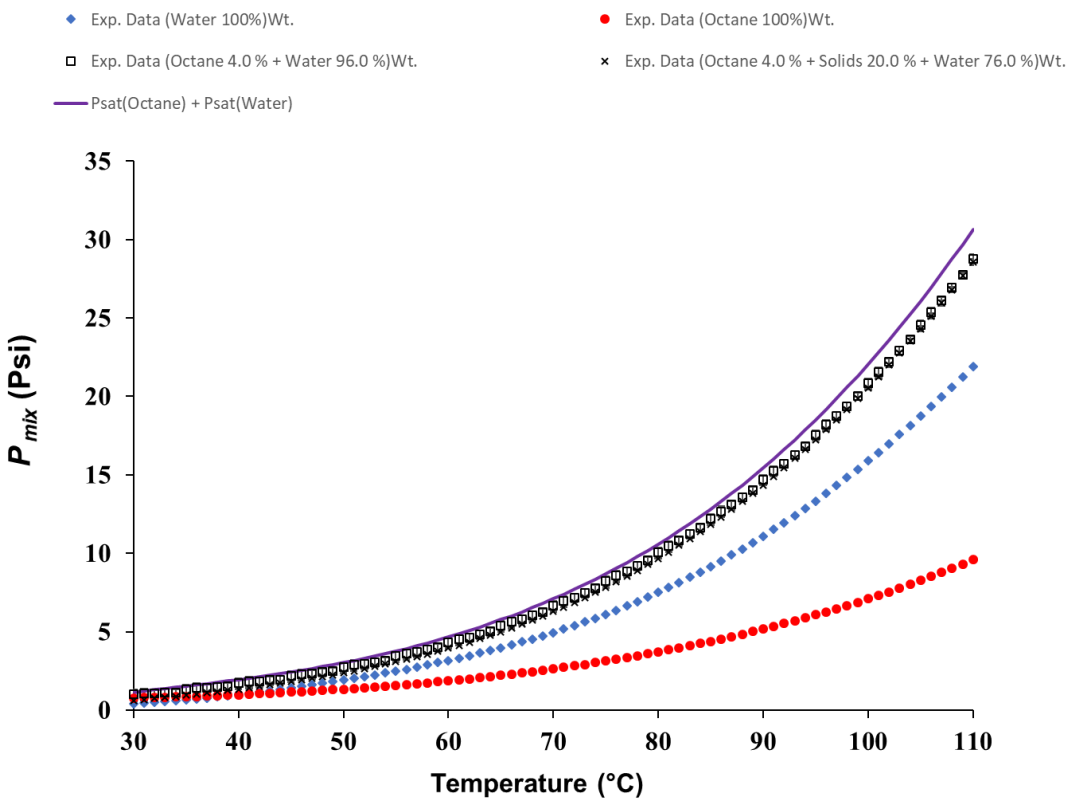


**Figure 61. $P_{mix}$ for 4.0 wt% n-octane and various water-solid compositions in the 30 ℃ to 110 ℃ range. Notes: (a) Summation of water and octane saturation pressures represent a completely immiscible model (purple solid line), (b) 1080 rpm mixing speed is used, (c) Vertical bars indicate the standard deviation of three or more experimental repeats.**

**Table 39. n-octane 4.0 wt% + solids 20.0 wt% + water 76.0 wt% Experimental and Statistical data**

| Exp. Data (n-octane 4.0 % + solids 20.0 % + water 76.0 %) wt. | | | | *95% CI* | |
|---|---|---|---|---|---|
| **Temperature (°C)** | **P mix (psia)** | **SD (±)** | **SE** | **LB** | **UB** |
| 30 | 0.61 | 0.06 | 0.04 | 0.52 | 0.69 |
| 40 | 1.34 | 0.03 | 0.02 | 1.29 | 1.38 |
| 50 | 2.38 | 0.02 | 0.02 | 2.35 | 2.41 |
| 60 | 3.94 | 0.03 | 0.02 | 3.90 | 3.98 |
| 70 | 6.29 | 0.04 | 0.03 | 6.23 | 6.34 |

| | | | | | |
|---|---|---|---|---|---|
| 80 | 9.68 | 0.03 | 0.02 | 9.63 | 9.72 |
| 90 | 14.90 | 0.02 | 0.01 | 14.87 | 14.93 |
| 100 | 21.26 | 0.12 | 0.08 | 21.10 | 21.43 |
| 110 | 28.58 | 0.21 | 0.15 | 28.29 | 28.87 |

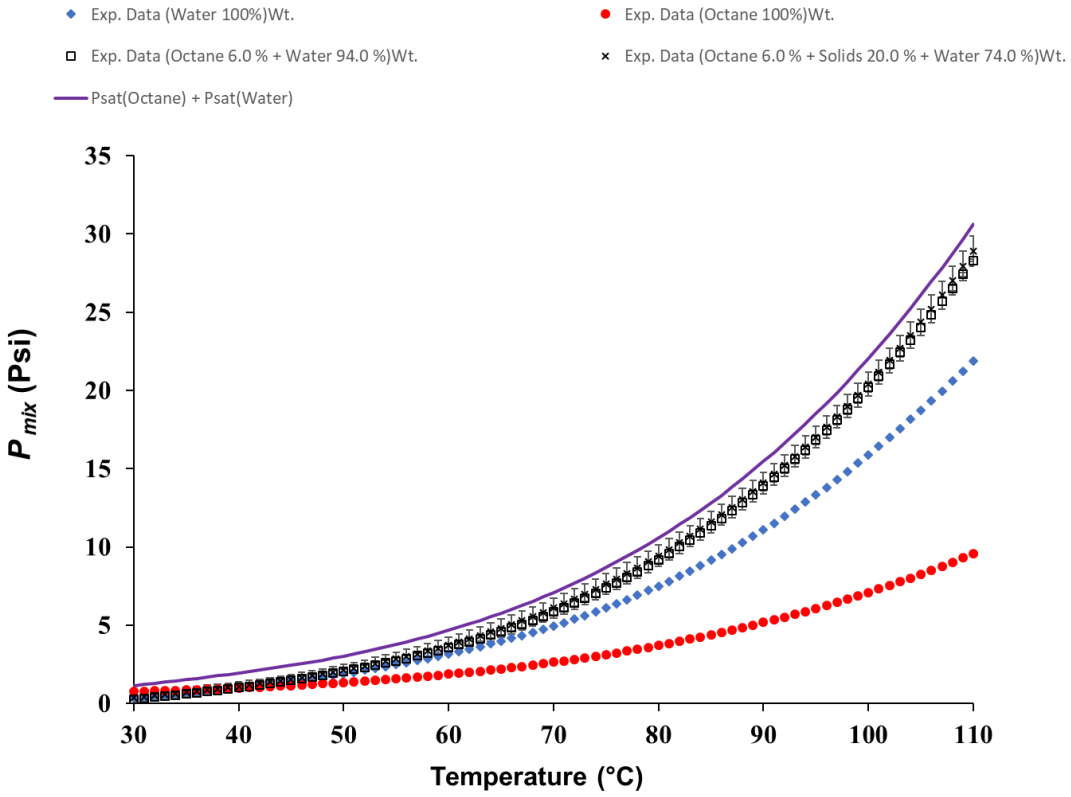


**Figure 62. $P_{mix}$ for 6.0 wt% n-octane and various water-solid compositions in the 30 ℃ to 110 ℃ range. Notes: (a) Summation of water and octane saturation pressures represent a completely immiscible model (purple solid line), (b) 1080 rpm mixing speed is used, (c) Vertical bars indicate the standard deviation of three or more experimental repeats.**

**Table 40. n-octane 6.0 wt% + solids 20.0 wt% + water 74.0 wt% Experimental and Statistical data**

| **Exp. Data (n-octane 6.0 % + solids 20.0 % + water 74.0 %) wt.** | | | | ***95% CI*** | |
|---|---|---|---|---|---|
| **Temperature (°C)** | **P mix (psia)** | **SD (±)** | **SE** | **LB** | **UB** |

| | | | | | |
|---|---|---|---|---|---|
| 30 | 0.36 | 0.35 | 0.25 | -0.13 | 0.85 |
| 40 | 1.09 | 0.29 | 0.21 | 0.68 | 1.49 |
| 50 | 2.13 | 0.35 | 0.25 | 1.64 | 2.62 |
| 60 | 3.73 | 0.51 | 0.36 | 3.02 | 4.43 |
| 70 | 6.09 | 0.64 | 0.45 | 5.20 | 6.97 |
| 80 | 9.44 | 0.68 | 0.48 | 8.50 | 10.38 |
| 90 | 14.64 | 0.68 | 0.48 | 13.70 | 15.59 |
| 100 | 21.16 | 0.77 | 0.55 | 20.09 | 22.23 |
| 110 | 28.90 | 0.97 | 0.68 | 27.56 | 30.24 |

Finally, Figure 63 and Table 41 reports 0.25 wt% n-octane in water with 20 wt% of solids. One can notice that $P_{mix}$ decreases in all cases with and without solids displaying a difference with the $P_{mix}$ for the fully insoluble phases, with this being the result as explained in 7.2.2 of partial hydrocarbon miscibility at the lower hydrocarbon concentrations studied.

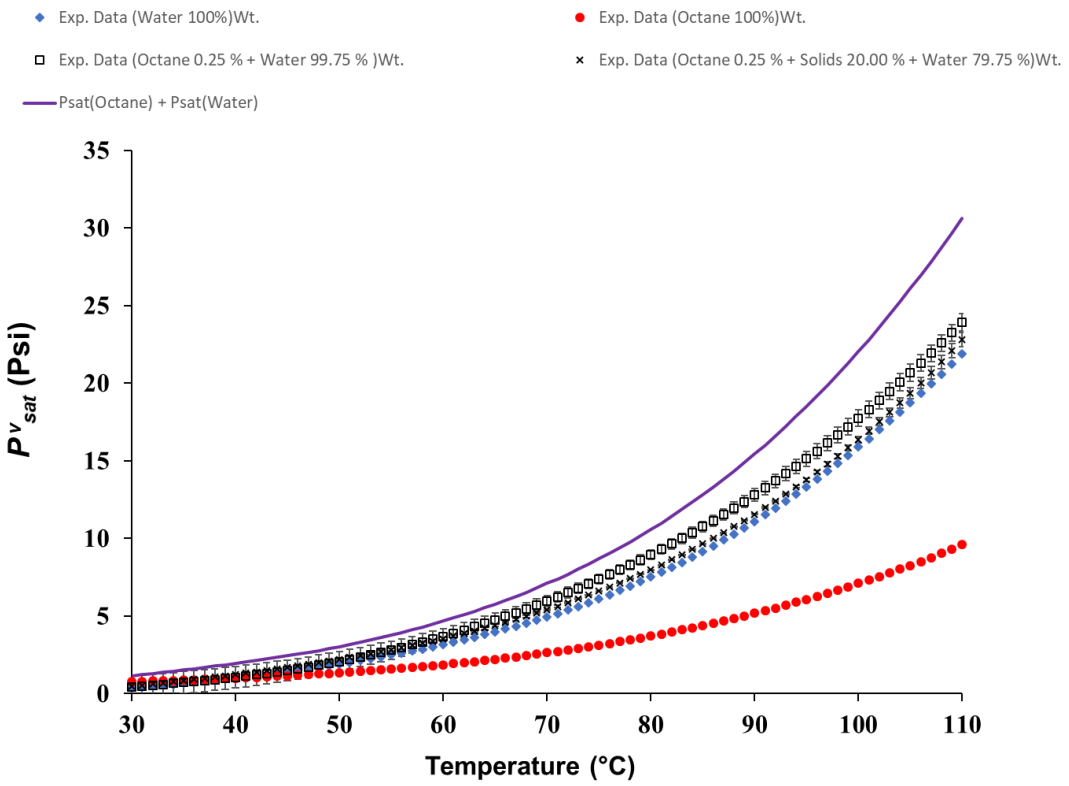


**Figure 63. $P_{mix}$ for 0.25 wt% n-octane and various water-solid compositions in the 30 ℃ to 110 ℃ range. Notes: (a) Summation of water and octane saturation pressures represent a completely immiscible model (purple solid line), (b) 1080 rpm mixing speed is used, (c) Vertical bars indicate the standard deviation of three or more experimental repeats.**

**Table 41. n-octane 0.25 wt% + solids 20.00 wt% + water 79.75 wt% Experimental and Statistical data**

| Exp. Data (n-octane 0.25 % + solids 20.00 % + water 79.75 %) wt. | | | | *95% CI* | |
|---|---|---|---|---|---|
| **Temperature (°C)** | **P mix (psia)** | **SD (±)** | **SE** | **LB** | **UB** |
| 30 | 0.47 | 0.04 | 0.03 | 0.42 | 0.52 |
| 40 | 1.23 | 0.01 | 0.00 | 1.22 | 1.24 |
| 50 | 2.21 | 0.05 | 0.04 | 2.14 | 2.28 |
| 60 | 3.54 | 0.09 | 0.06 | 3.42 | 3.66 |
| 70 | 5.40 | 0.06 | 0.04 | 5.32 | 5.48 |

| | | | | | |
|---|---|---|---|---|---|
| 80 | 7.99 | 0.01 | 0.01 | 7.98 | 8.01 |
| 90 | 11.98 | 0.04 | 0.03 | 11.92 | 12.04 |
| 100 | 16.94 | 0.23 | 0.16 | 16.61 | 17.26 |
| 110 | 22.81 | 0.47 | 0.33 | 22.15 | 23.46 |

Therefore, one can conclude that for all n-octane/water blends studied, kaolin clay and silica sand blend at 20 wt% does not influence the $\boldsymbol{P_{mix}}$. While sand particles are massive, kaolin clay particles display a BET specific internal surface area and, in principle, could adsorb hydrocarbon species, affecting the vapor pressure measured (See 5.1.1). However, despite this, it appears hydrocarbon adsorption on kaolin clay while present is not significant enough to affect $\boldsymbol{P_{mix}}$.

## 7.6 Conclusions

(1) Pressure data from runs in the CREC-VL-Cell can be corrected using an "Air contained fraction correction" factor.

(2) VLE measurements in the CREC-VL-Cell were successfully validated using pure n-octane, pure n-hexane and pure water. This was the case, given the good agreement of measurements with data reported in the technical literature

(3) VLE measurements in the CREC-VL-Cell for n-octane/water blends showed consistency with the insoluble phase model, with this being true for all n-octane concentrations, except for the 0.5 wt% lowest n-octane concentration.

(4) VLE measurements in the CREC-VL-Cell using SN and water blends were investigated using 2.5 wt% SN in water, in the 0 - 1200 rpm impeller speed range. It was proven that the 1080rpm impeller speed provides adequate mixing, preventing cavitation.

(5) VLE measurements using 0.5 wt to 97.5 wt% SN in water blends displayed a $\boldsymbol{P_{mix}}$ consistently in agreement, with the insoluble two liquid phase model.

(6) VLE measurements employing n-octane in water, with a 20 wt% added silica sand-kaolin clay solids, showed no influence of solids on $P_{mix}$ measurements.

# Chapter 8: Bounding Equilibrium Molar Fraction in the CREC-VL-Cell

Runs in CREC-VL-Cell involve a dynamic method with both total pressure and temperature changing with run time. On this basis and as shown in Chapter 6, the PR-EoS model is able to represent well the P-T pairs in the CREC-VL-Cell, and this is for the various blends studied both with n-octane in water as well as SN in water.

However, one is also looking for a model that in addition of being able to represent the P-T pairs should be able to provide additional data such as the molar fractions in the liquid phase and vapor phases.

## 8.1 Conservation Molar Fractions Based Model in the CREC-VL-Cell.

The CREC-VL-Cell experiments are targeted to measure the vapor pressure and temperature for a diversity of initial feed compositions. Vapor pressure data is essential to determine plant designs, operational costs and product recovery in the petroleum industry [188].

In this regard, a mass fraction analysis is a critical one for establishing conditions that the mass fraction of n-octane/water binary mixtures in equilibrium should comply.

Mass fractions can be established from blends using analytical methods such as Gas Chromatography (GC) [189]. However, the GC technique is not adequate to analyze chemical blends involving high water concentrations, given water (steam) can damage the GC column [190]. Since our mixture contained significant amounts of water in the context of a Naphtha Recovery Unit process, the GC method could not be used.

As an alternative, n-octane/water mass fractions can be “bound” by using mass and mole balances in the CREC-VL Cell. One should emphasize that results obtained from this analysis provide an “upper limit” to n-octane mass fractions in the liquid phase. There is no constraint in this analysis to a specific n-octane and water concentration range, with this approach being very valuable to screen possible VL equilibrium models.

Regarding mole balances in the CREC-VL-Cell, they can be established accounting for water and n-octane in the liquid and vapor phases, as shown in Equation 32 and Equation 33

$$n_{oct}^{l} + n_{w}^{l} = n^{l} \qquad \text{Equation 32}$$

$$n_{oct}^{v} + n_{w}^{v} = n^{v} \qquad \text{Equation 33}$$

And adding Equation 32 and Equation 33, it gives,

$$n^{l} + n^{v} = n \qquad \text{Equation 34}$$

Furthermore, mass balance of species can be also written as in Equation 35 and Equation 36

$$m_{oct}^{l} + m_{oct}^{v} = m_{oct} \qquad \text{Equation 35}$$

$$m_{w}^{l} + m_{w}^{v} = m_{w} \qquad \text{Equation 36}$$

And adding Equation 35 and Equation 36, it gives,

$$m^{l} + m^{v} = m \qquad \text{Equation 37}$$

One should note that the mole balances from Equation 32 and Equation 33 in both vapor and liquid phases, can be expressed as well using molecular weight and chemical species mass as in Equation 38 and Equation 39

$$\frac{m_{oct}^{l}}{MW_{oct}} + \frac{m_{w}^{l}}{MW_{w}} = n^{l} \qquad \text{Equation 38}$$

$$\frac{m_{oct}^{v}}{MW_{oct}} + \frac{m_{w}^{v}}{MW_{w}} = n^{v} \qquad \text{Equation 39}$$

Or alternatively adding Equations from Equation 38 and Equation 39, it results,

$$\frac{m_{oct}}{MW_{oct}} + \frac{m_{w}}{MW_{w}} = n \qquad \text{Equation 40}$$

As well considering the ideal gas model applies, one can obtain,

$$PV^v = n^v RT \qquad \text{Equation 41}$$

Furthermore, and given that the CREC-VL cell is a "batch" unit of constant volume without chemical reaction taking place, both the total unit volume and the water/n-octane blends total moles can be described at any time during the dynamic experiment via Equation 42 and Equation 43.

$$V = V^l + V^v \qquad \text{Equation 42}$$

$$n = n^l + n^v \qquad \text{Equation 43}$$

Regarding $n^v$ the total moles in the vapor phase, they can be calculated using Equation 41 and Equation 43 as follows,

$$n_v = n - \frac{m^l}{MW^l} \qquad \text{Equation 44}$$

$$n_v = \frac{PV^v}{RT} \qquad \text{Equation 45}$$

$$n - \frac{m^l}{MW^l} = \frac{PV^v}{RT} \qquad \text{Equation 46}$$

Furthermore, Equation 46 can be rearranged using Equation 42 so that the liquid mass becomes expressed in terms of all the other variables:

$$n - \frac{m^l}{MW^l} = \frac{P(V - V^l)}{RT} \qquad \text{Equation 47}$$

$$n - \frac{m^l}{MW^l} = \frac{P\left(V - \frac{m^l}{\rho^l}\right)}{RT} \qquad \text{Equation 48}$$

$$n - \frac{m^l}{MW^l} = \frac{PV}{RT} - \frac{P}{RT}\frac{m^l}{\rho^l} \qquad \text{Equation 49}$$

$$n - \frac{PV}{RT} = m^l \left( \frac{1}{MW^l} - \frac{P}{RT\rho^l} \right) \quad \text{Equation 50}$$

$$m^l = \frac{n - \frac{PV}{RT}}{\left( \frac{1}{MW^l} - \frac{P}{RT\rho^l} \right)} \quad \text{Equation 51}$$

Given that P, V, T and $n$ in Equation 51 are known parameters, $m^l$ can be determined, provided $MW^l$ and $\rho^l$ are given. Thus, using Equation 37, $m^v$ can be calculated as well.

One should note that one can define a range of the average density variation in the liquid phase is as follows:

$$\rho^l_{min} < \rho^l < \rho^l_{max} \quad \text{Equation 52}$$

Where, $\rho^l_{max}$ is the liquid density with no n-octane present, so it represents the water density and the $\rho^l_{min}$ the liquid density at initial n-octane/water composition conditions.

One can thus see that both minimum and maximum density value change with temperature conditions differing in the worst situation, for 2.0 wt% n-octane + 98.0 wt% water mixture by 0.02 % error. Thus, it can be considered that the effect of composition and compositions changes on the liquid density in Equation 52 can be neglected.

Regarding the molecular weight of liquid ($MW^l$) it can be calculated via Equation 53 and Equation 55.

$$MW^l = \frac{m^l}{n^l} \quad \text{Equation 53}$$

Its variation can, however, be bound between the minimum and the maximum values,

$$MW_w < MW^l < MW^l_{max} \quad \text{Equation 54}$$

$$MW_{max}^{l} = \frac{m^{l}}{\frac{m_{oct}^{l}}{MW_{oct}} + \frac{m_{w}^{l}}{MW_{w}}} = \frac{1}{\frac{x_{oct}^{l}}{MW_{oct}} + \frac{x_{w}^{l}}{MW_{w}}} \qquad \text{Equation 55}$$

It is important to note that when $MW$ reaches $MW_w$, it represents a liquid phase free of n-octane. Regarding $MW_{max}^{l}$ it can, in principle, be calculated with the feed composition. However, one should check if under these conditions, $m^l < m$. If the m value exceeds *"m"* one should limit the $MW_{max}^{l}$, until this condition is met.

On this basis knowing, one can establish $n_w^l = \frac{m_w^l}{MW_w}$, $n_{oct}^l = \frac{m_{oct}^l}{MW_{oct}}$ and calculate for every condition, such as the upper bound for the molar fractions of n-octane in the CREC-VL-Cell runs.

$$y_w > \frac{n_w^v}{n^v} \qquad \text{Equation 56}$$

$$y_{oct} < \frac{n_{oct}^v}{n^v} \qquad \text{Equation 57}$$

$$x_w > \frac{n_w^l}{n^l} \qquad \text{Equation 58}$$

$$x_{oct} < \frac{n_{oct}^l}{n^l} = x_{oct,upper\ limit} \qquad \text{Equation 59}$$

Thus, the calculated mass fractions provide for every condition of upper molar fraction boundary. The upper boundary requires to be satisfied by the thermodynamic model under consideration.

To illustrate the value of the proposed bounding model, the molar fraction obtained via the PR-EoS and experimental data from the CREC-VL-Cell, are compared with the requirement that $x_{oct,PR\ EoS} < x_{oct,upper\ limit}$

Figure 64 shows that $x_{oct}$ molar fractions in the 0.1 ~ 2 wt% n-octane in water initial concentration range, using Aspen Hysys and PR-EoS model (continuous lines) surpasses in all cases of $x_{oct,upper\ limit}$ from Equation 59 as follows,

$$x_{oct,PR\ EoS} > x_{oct,upper\ limit}$$

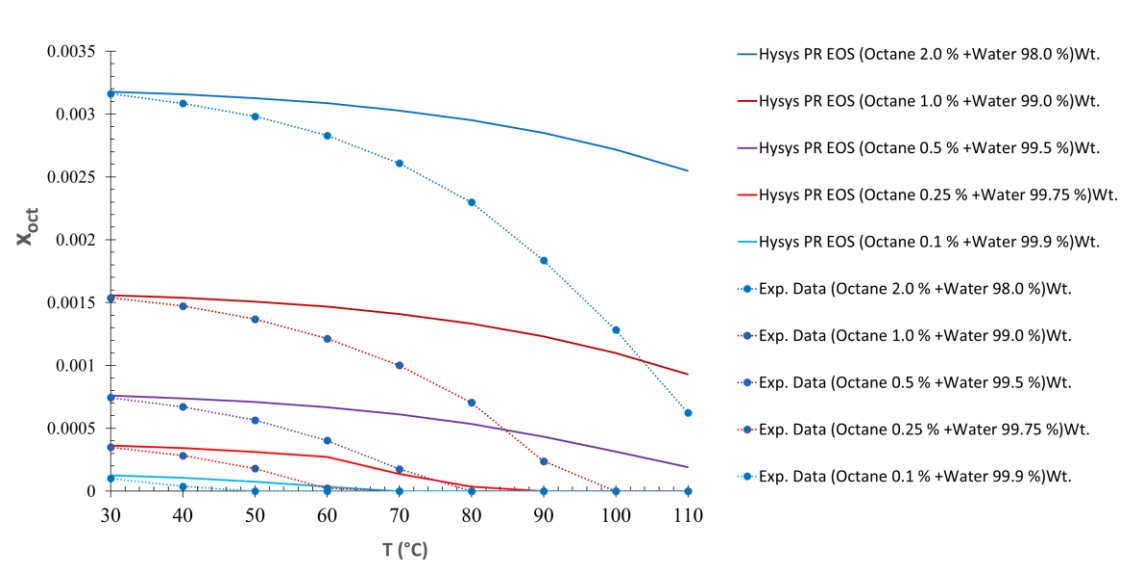


**Figure 64. Molar fraction upper boundaries in n-octane/water mixtures and estimated molar fractions by PR-EOS**

As a result, even if the PR-EoS could be considered adequate for predicting the total pressure of n-octane in water blends in the 30 – 110 °C range as shown in Chapter 6:, this model shows to be inadequate, for assessing the molar fraction of n-octane molar fraction in the liquid phase.

In summary, it can be concluded that the proposed PR-EoS model and any other alternative thermodynamic models have to closely predict the total pressure of the system, providing n-octane in water complying with $x_{oct,PR\ EoS} < x_{oct,upper\ limit}$ test condition.

## 8.2 Conclusions

(1) The mass balance-based method is developed to set the anticipated upper bound for n-octane fractions in the liquid phase.

(2) The derived upper bound represents a general constraint which is independent of the model selected.

(3) The proposed model allows to show that the PR-EoS, in spite of being adequate (first approximation) for predicting the total system pressure at various thermal levels, does not comply consistently with the condition of $x_{oct,PR\ EoS} < x_{oct,upper\ limit}$.

(4) The proposed methodology of establishing an upper bound for the n-octane molar fraction provides additional and valuable constraints to any thermodynamic model being considered for n-octane in water blends.

# Chapter 9: Conclusions and Recommendations

## 9.1 Conclusions

(1) It is demonstrated that CREC-VL-Cell displayed optimum operation under the following operating conditions: (a) 100mL sample volume, (b) 1.5 cm clearance with marine impeller, (c) interface baffle, (d) 1080 mixing speed,

(2) It is shown that high impeller speeds (e.g. 1080 rpm) are essential to provide adequate mixing in the batch CREC-VL-Cell, with impeller mixing speed in excess to 1080 rpm not having beneficial effects on vapor pressure measurements and promoting cavitation.

(3) It is proven that the CREC-VL-Cell operates close to thermal equilibrium with less than 1.6 % temperature difference between phases, and vapor pressures obtained with the dynamic technique, differing in less than 1.0 % from the vapor pressure employing conventional static methods

(4) It is shown that the SN (synthetic naphtha) using five alkanes can be used to emulate the vapor pressure of the industrial naphtha.

(5) It is proven that air contained CREC-VL-Cell fraction can be discounted from vapor pressure measurements, allowing hydrocarbon-water measurements without the need of degassing the cell with vacuum.

(6) It is shown that CREC-VL-Cell can be used to measure the vapor pressures of different n-octane/water blends (0.1 ~ 99.75 wt% n-Octane). The $P_{mix}$ data shows three equilibrium behaviors such as (a) the VLLE conditions, (b)the VLE under high octane dilutions in water, (c) the VLE under high water dilution in n-octane

(7) It is proven that CREC-VL-Cell can be employed to measure the vapor pressures of different SN/water compositions (2.5 ~ 97.5 wt% synthetic naphtha) with the close to the insoluble two liquid phase model being a dominant observed trend.

(8) It is shown that CREC-VL-Cell can be used to measure the vapor pressures of different solids/n-octane/water compositions, with no significant pressure difference observed when 20 wt% solid was added to the multiphase system.

(9) It is proven that the vapour pressure in the CREC-VL-Cell system can be simulated (first approximation) by adjusting the total phase volumetric flow of a continuous separator module in Aspen HYSYS with PR-EoS

(10) It is demonstrated that Aspen HYSYS with the PR-EoS package is unable to predict n-octane/water fraction below limiting trends, as resulting from mass analysis data from the CREC-VL-Cell.

## 9.2 Recommendations

(1) An analytical experimental method should be developed to sample liquid and vapor phases simultaneously in the CREC-VL-Cell.

(2) The range of experimental measurements should be extended to a higher temperature and pressure controlling tightly pressure leakages.

(3) The application of CREC-VL-Cell method should be further applied with different hydrocarbon-water blends, such as naphtha-bitumen mixtures and various process additives.

(4) An advanced thermodynamic model should be developed to ensure both enhanced prediction of vapor pressure and n-octane molar fractions falling in the boundaries anticipated with the mass balances developed with the CREC-VL-Cell data.

# Bibliography


[1] G. of Canada, “Oil Resources,” 2015. [Online]. Available: https://www.nrcan.gc.ca/energy/energy-sources-distribution/crude-oil/oil-resources/18085?wbdisable=true.

[2] Canada National Energy Board, “Canada’s Oil Sands Opportunities and challenges 2015,” 2006.

[3] “Naphtha Recovery Units,” *OIL SAND MAGAZINE*, 2018. [Online]. Available: https://www.oilsandsmagazine.com/technical/mining/froth-treatment/naphthenic/nru-naphtha-recovery-unit.

[4] J. Du and W. R. Cluett, “Modelling of a Naphtha Recovery Unit ( NRU ) with Implications for Process Optimization,” 2018, doi: 10.3390/pr6070074.

[5] E. J. Henley and J. D. Seader, “Equilibrium-stage separation operations in chemical engineering.,” 1981, doi: 10.1016/0300-9467(82)85033-8.

[6] M. L. Huber, A. Laesecke, and D. G. Friend, “Correlation for the vapor pressure of mercury,” *Ind. Eng. Chem. Res.*, 2006, doi: 10.1021/ie060560s.

[7] O. C. DÍAZ, “Measurement and modelling methodology for heavy oil and bitumen vapor pressure,” 2012.

[8] S. F. Ali and N. Yusoff, “Determination of Optimal Cut Point Temperatures at Crude Distillation Unit using the Taguchi Method,” *Int. J. Eng. Technol.*, vol. 12, no. 06, pp. 36–46, 2012.

[9] C. R. Feed, “Naphtha ( Petroleum ), Hydrotreated Heavy Icsc : 1380,” vol. 3, pp. 1–27, 2001.

[10] J. Tamim and W. L. H. Hallett, “A continuous thermodynamics model for multicomponent droplet vaporization,” *Chem. Eng. Sci.*, 1995, doi: 10.1016/0009-2509(95)00131-N.

[11] G. D. Holder and J. H. Hand, “Multiple-phase equilibria in hydrates from methane, ethane, propane and water mixtures,” *AIChE J.*, 1982, doi: 10.1002/aic.690280312.

[12] B. Nestler, H. Garcke, and B. Stinner, “Multicomponent alloy solidification: Phase-field modeling and simulations,” *Phys. Rev. E - Stat. Nonlinear, Soft Matter Phys.*, 2005, doi: 10.1103/PhysRevE.71.041609.

[13] B. Lotfollahi, Mohammad Nader, Modarress, Hamid; Khodakarami, “VLE Predictions of Strongly Non-Ideal Binary Mixtures by Modifying Van Der Waals and Orbey-Sandler Mixing Rules,” vol. 26, no. 3, pp. 73–80, 2007.

[14] A. Aasen, M. Hammer, G. Skaugen, J. P. Jakobsen, and Wilhelmsen, “Thermodynamic models to accurately describe the PVTxy-behavior of water / carbon dioxide mixtures,” *Fluid Phase Equilib.*, vol. 442, no. March, pp. 125–139, 2017, doi: 10.1016/j.fluid.2017.02.006.

[15] A. K. Coker, *Fortran Programs for Chemical Process Design, Analysis, and Simulation*. 1995.

[16] T. M. Zygula and E. Roy, “The Importance of Thermodynamics on Process Simulation Modeling,” vol. 1024, pp. 1–30, 2001.

[17] B. Falkenhainer and K. D. Forbus, “Cmpositional modeling: finding the right model for the job,” *Artif. Intell.*, 1991, doi: 10.1016/0004-3702(91)90109-W.

[18] W. W. Graessley *et al.*, “Thermodynamics of Mixing for Blends of Model Ethylene-Butene Copolymers,” *Macromolecules*, 1994, doi: 10.1021/ma00092a033.

[19] M. E. Boudh-Hir and G. A. Mansoori, “Theory for interfacial tension of partially miscible liquids,” *Phys. A Stat. Mech. its Appl.*, 1991, doi: 10.1016/0378-4371(91)90060-P.

[20] T. P. Silverstein, “Polarity, miscibility, and surface tension of liquids,” *J. Chem. Educ.*, vol. 70, no. 3, p. 253, 1993, doi: 10.1021/ed070p253.

[21] SILBERBERG., *Chemistry: The Molecular Nature of Matter and Change with Advanced Topics*, 8th, illustr ed. McGraw-Hill Education, 2001, 2011.

[22] W. Guo, P. Bali, and J. R. Errington, “Calculation of the Saturation Properties of a Model Octane-Water System Using Monte Carlo Simulation,” *J. Phys. Chem. B*, vol. 122, no. 23, pp. 6260–6271, 2018, doi: 10.1021/acs.jpcb.8b01411.

[23] C. T. Chiou, *Hazard Assessment of Chemicals: Current Departments Volume 1*, no. 0404. Academic Press, 1981.

[24] J. Bibette, D. C. Morse, T. A. Witten, and D. A. Weitz, “Stability criteria for emulsions,” *Phys. Rev. Lett.*, 1992, doi: 10.1103/PhysRevLett.69.2439.

[25] T. F. Tadros, “Emulsion Formation, Stability, and Rheology,” in *Emulsion Formation and Stability*, 2013.

[26] H. Holthoff, S. U. Egelhaaf, M. Borkovec, P. Schurtenberger, and H. Sticher, “Coagulation rate measurements of colloidal particles by simultaneous static and dynamic light scattering,” *Langmuir*, 1996, doi: 10.1021/la960326e.

[27] K. S. Saladin, “The brain and cranial nerves,” in *Anatomy and Physiology: the Unity of Form and Function*, 2007.

[28] H. Rabinowitz and S. Vogel, “The Manual of Scientific Style: A Guide for Authors, Editors, and Researchers,” p. 968, 2009.

[29] R. J. Ouellette and J. D. Rawn, *Robert J. Ouellette, J. David Rawn, in Principles of Org*. Academic Press, 2015.

[30] I. Montes, C. Lai, and D. Sanabria, “Like dissolves like: A classroom demonstration and a guided-inquiry experiment for organic chemistry,” *J. Chem. Educ.*, 2003, doi: 10.1021/ed080p447.

[31] J. Clayden, N. Greeves, S. Warren, and P. Wothers, “Organic Chemistry,” *Am. Nat.*, 2001, doi: 10.1086/278635.

[32] E. Brunner, “Fluid mixtures at high pressures IX. Phase separation and critical

phenomena in 23 (n-alkane + water) mixtures," *J. Chem. Thermodyn.*, 1990, doi: 10.1016/0021-9614(90)90120-F.

[33] A. L. Ferguson, P. G. Debenedetti, and A. Z. Panagiotopoulos, "Solubility and molecular conformations of n-Alkane chains in water," *J. Phys. Chem. B*, 2009, doi: 10.1021/jp811229q.

[34] C. Tsonopoulos, "Thermodynamic analysis of the mutual solubilities of normal alkanes and water," in *Fluid Phase Equilibria*, 1999, doi: 10.1016/S0378-3812(99)00021-7.

[35] A. N. Lukyanov and V. P. Torchilin, "Micelles from lipid derivatives of water-soluble polymers as delivery systems for poorly soluble drugs," *Adv. Drug Deliv. Rev.*, 2004, doi: 10.1016/j.addr.2003.12.004.

[36] E. Peake and G. W. Hodgson, "Alkanes in aqueous systems. I. Exploratory investigations on the accommodation of C20−C33 n-alkanes in distilled water and occurrence in natural water systems," *J. Am. Oil Chem. Soc.*, vol. 43, no. 4, pp. 215–222, 1966, doi: 10.1007/BF02641090.

[37] D. G. Shaw, *Hydrocarbons With Water and Seawater, Part I: Hydrocarbons C5 to C7*. Pergamon Pr, 1989.

[38] A. Mączyński, B. Wiśniewska-Gocłowska, and M. Góral, "Recommended liquid-liquid equilibrium data. Part 1. Binary alkane-water systems," *J. Phys. Chem. Ref. Data*, vol. 33, no. 2, pp. 549–577, 2004, doi: 10.1063/1.1643922.

[39] W. A. Fouad, D. Ballal, K. R. Cox, and W. G. Chapman, "Examining the consistency of water content data in alkanes using the perturbed-chain form of the statistical associating fluid theory equation of state," *J. Chem. Eng. Data*, 2014, doi: 10.1021/je400749e.

[40] M. L. Corazza, W. A. Fouad, and W. G. Chapman, "PC-SAFT predictions of VLE and LLE of systems related to biodiesel production," *Fluid Phase Equilib.*, 2016, doi: 10.1016/j.fluid.2015.09.044.

[41] N. Haarmann, S. Enders, and G. Sadowski, "Modeling binary mixtures of n-alkanes and water using PC-SAFT," *Fluid Phase Equilib.*, 2018, doi: 10.1016/j.fluid.2017.11.015.

[42] P. Gateau, I. Hénaut, L. Barré, and J. F. Argillier, "Heavy oil dilution," *Oil Gas Sci. Technol.*, 2004, doi: 10.2516/ogst:2004035.

[43] R. Prestvik, K. Moljord, K. Grande, and A. Holmen, "Compositional Analysis of Naphtha and Reformate," 2004.

[44] R. P. Philp, "Petroleum Formation and Occurrence," *Eos, Trans. Am. Geophys. Union*, 1985, doi: 10.1029/eo066i037p00643.

[45] K. Kamegawa, K. Nishikubo, M. Kodama, Y. Adachi, and H. Yoshida, "Oxidative degradation of carbon blacks with nitric acid - II. Formation of water-soluble polynuclear aromatic compounds," *Carbon N. Y.*, 2002, doi: 10.1016/S0008-6223(01)00310-4.

[46] T. A. Al-Sahhaf and E. Kapetanovic, “Measurement and prediction of phase equilibria in the extraction of aromatics from naphtha reformate by tetraethylene glycol,” *Fluid Phase Equilib.*, vol. 118, no. 2, pp. 271–285, 1996, doi: 10.1016/0378-3812(95)02849-8.

[47] H. Chen and Q. Xu, “Experimental study of fibers in stabilizing and reinforcing asphalt binder,” *Fuel*, 2010, doi: 10.1016/j.fuel.2009.08.020.

[48] D. Jones, *Cambridge University Press*, no. 2011. Cambridge University Press, 2011.

[49] B. Sellers, S. Store, B. Again, and B. B. Ones, “Ullmann ’ s Encyclopedia of Industrial Chemistry,” pp. 4–6, 2003.

[50] H. La and S. E. Guigard, “Extraction of hydrocarbons from Athabasca oil sand slurry using supercritical carbon dioxide,” *J. Supercrit. Fluids*, 2015, doi: 10.1016/j.supflu.2015.01.020.

[51] M. Porto, P. Caputo, V. Loise, S. Eskandarsefat, B. Teltayev, and C. O. Rossi, “Bitumen and bitumen modification: A review on latest advances,” *Applied Sciences (Switzerland)*. 2019, doi: 10.3390/app9040742.

[52] A. Bazyleva, M. Fulem, M. Becerra, B. Zhao, and J. M. Shaw, “Phase behavior of athabasca bitumen,” *J. Chem. Eng. Data*, vol. 56, no. 7, pp. 3242–3253, 2011, doi: 10.1021/je200355f.

[53] K. Takamura and R. S. Chow, “The electric properties of the bitumen/water interface Part II. Application of the ionizable surface-group model,” *Colloids and Surfaces*, vol. 15, no. C, pp. 35–48, 1985, doi: 10.1016/0166-6622(85)80053-6.

[54] J. Masliyah, Z. J. Zhou, Z. Xu, J. Czarnecki, and H. Hamza, “Understanding Water-Based Bitumen Extraction,” *Can. J. Chem. Eng.*, vol. 82, no. August, pp. 628–654, 2004.

[55] M. J. Amani, M. R. Gray, and J. M. Shaw, “Phase behavior of Athabasca bitumen + water mixtures at high temperature and pressure,” *J. Supercrit. Fluids*, vol. 77, pp. 142–152, 2013, doi: 10.1016/j.supflu.2013.03.007.

[56] A. Hart, “A review of technologies for transporting heavy crude oil and bitumen via pipelines,” *Journal of Petroleum Exploration and Production Technology*. 2014, doi: 10.1007/s13202-013-0086-6.

[57] X. Yang and J. Czarnecki, “The effect of naphtha to bitumen ratio on properties of water in diluted bitumen emulsions,” *Colloids Surfaces A Physicochem. Eng. Asp.*, vol. 211, no. 2–3, pp. 213–222, 2002, doi: 10.1016/S0927-7757(02)00279-0.

[58] K. H. Baek, F. J. Argüelles-Vivas, R. Okuno, K. Sheng, H. Sharma, and U. P. Weerasooriya, “An experimental study of emulsion phase behavior and viscosity for athabasca bitumen/diethylamine/brine mixtures,” in *SPE Reservoir Evaluation and Engineering*, 2019, doi: 10.2118/189768-PA.

[59] J. S. Smith, *Food Additive User’s Handbook*. 1991.

[60] D. Langevin, S. Poteau, I. Hénaut, and J. F. Argillier, “Crude oil emulsion properties and their application to heavy oil transportation,” *Oil Gas Sci. Technol.*, 2004, doi:

10.2516/ogst:2004036.

[61] A. A. Umar, I. B. M. Saaid, and A. A. Sulaimon, “Rheological and stability study of water-in-crude oil emulsions,” *AIP Conf. Proc.*, vol. 1774, no. October 2016, 2016, doi: 10.1063/1.4965086.

[62] P. Haimi, *Vapour liquid equilibrium three methods: static measurements with circulation still and total pressure, inert gas stripping*. 2012.

[63] J. D. Seader, E. J. Henley, and D. K. Roper, *Separation Process Principles 3rd Edition*. 2006.

[64] P. Uusi-Kyyny, *VAPOUR LIQUID EQUILIBRIUM MEASUREMENTS FOR PROCESS DESIGN*, no. May. 2014.

[65] S. Bruin, “Phase equilibria for food product and process design 1,” *Fluid Phase Equilib.*, 1999, doi: 10.1016/s0378-3812(99)00130-2.

[66] “Physical and Chemical Data,” in *Handbook of Biochemistry and Molecular Biology, Fourth Edition*, 2010.

[67] J. D. Raal and A. L. Mühlbauer, “The Measurement of High Pressure Vapour-Liquid-Equilibria: Part I: Dynamic Methods,” *Dev. Chem. Eng. Miner. Process.*, vol. 2, no. 2–3, pp. 69–87, 1994, doi: 10.1002/apj.5500020201.

[68] F. Zhang, E. El Ahmar, A. Valtz, E. Boonaert, C. Coquelet, and A. Chapoy, “Phase Equilibrium of Three Binary Mixtures Containing NO and Components Present in Ambient Air,” *J. Chem. Eng. Data*, 2018, doi: 10.1021/acs.jced.7b00782.

[69] P. Uusi-Kyyny, *Vapour Liquid Equilibrium Measurements Vapour Liquid Equilibrium Measurements*, no. 45. 2004.

[70] P. N. Bengesai, “High Pressure Vapour-Liquid Equilibrium Measurements For R116 and Ethane with Perfluorohexane and Perfluorooctane. MSc,” no. January, 2015.

[71] M. M. Abbott, “Low-pressure phase equilibria: Measurement of VLE,” *Fluid Phase Equilib.*, vol. 29, no. C, pp. 193–207, 1986, doi: 10.1016/0378-3812(86)85021-X.

[72] P. Luis, C. Wouters, N. Sweygers, C. Creemers, and B. Van Der Bruggen, “The potential of head-space gas chromatography for VLE measurements,” *J. Chem. Thermodyn.*, 2012, doi: 10.1016/j.jct.2012.01.020.

[73] F. Zhang, P. Théveneau, E. El Ahmar, X. Canet, C. Bin Soo, and C. Coquelet, “An improved static-analytic apparatus for vapor-liquid equilibrium (PTxy) measurement using modified in-situ samplers,” *Fluid Phase Equilib.*, 2016, doi: 10.1016/j.fluid.2015.10.041.

[74] B. Kolbe and J. Gmehling, “Thermodynamic properties of ethanol + water. I. Vapour-liquid equilibria measurements from 90 to 150°C by the static method,” *Fluid Phase Equilib.*, 1985, doi: 10.1016/0378-3812(85)90007-X.

[75] A. M. M. Motchelaho, “Vapour-Liquid Equilibrium Measurements Using a Static Total Pressure Apparatus,” 2006.

[76] P. Reddy, “Development of Novel Apparatus for Vapour-liquid Equilibrium

Measurements at Moderate Pressures. PhD Thesis.," 2006.

[77] J. Freitag, H. Kosuge, J. P. Schmelzer, and S. Kato, "VLE measurements using a static cell vapor phase manual sampling method accompanied with an empirical data consistency test," *J. Chem. Thermodyn.*, 2015, doi: 10.1016/j.jct.2014.08.024.

[78] A. Bertucco and G. V. Elsevier, *High Pressure Process Technology: Fundamentals and Applications*, vol. 9. 2001.

[79] P. Naidoo, D. Ramjugernath, and J. D. Raal, "A new high-pressure vapour-liquid equilibrium apparatus," *Fluid Phase Equilib.*, vol. 269, no. 1–2, pp. 104–112, 2008, doi: 10.1016/j.fluid.2008.05.002.

[80] "Measurement of the Thermodynamic Properties of Multiple Phases," *Chem. Int. -- Newsmag. IUPAC*, 2014, doi: 10.1515/ci.2005.27.6.26b.

[81] "Measurement of the Thermodynamic Properties of Single Phases, Vol. VI," *Chem. Int. -- Newsmag. IUPAC*, 2014, doi: 10.1515/ci.2003.25.6.25a.

[82] J. Gmehling, M. Kleiber, B. Kolbe, and J. Rarey, *Chemical Thermodynamics for Process Simulation*. 2019.

[83] J. P. M. Trusler, *Measurement of the Thermodynamic Properties of Single Phases*. 2003.

[84] P. Reddy, J. D. Raal, and D. Ramjugernath, "A novel dynamic recirculating apparatus for vapour-liquid equilibrium measurements at moderate pressures and temperatures," *Fluid Phase Equilib.*, 2013, doi: 10.1016/j.fluid.2013.07.044.

[85] A. W. Islam and M. H. Rahman, "A review of Barker's activity coefficient method and VLE data reduction," *J. Chem. Thermodyn.*, vol. 44, no. 1, pp. 31–37, 2012, doi: 10.1016/j.jct.2011.08.013.

[86] P. Uusi-Kyyny, J. P. Pokki, M. Laakkonen, J. Aittamaa, and S. Liukkonen, "Vapor liquid equilibrium for the binary systems 2-methylpentane + 2-butanol at 329.2 K and n-hexane + 2-butanol at 329.2 and 363.2 K with a static apparatus," *Fluid Phase Equilib.*, vol. 201, no. 2, pp. 343–358, 2002, doi: 10.1016/S0378-3812(02)00080-8.

[87] R. Dohrn, J. M. S. Fonseca, and S. Peper, "Experimental Methods for Phase Equilibria at High Pressures," *Annu. Rev. Chem. Biomol. Eng.*, vol. 3, no. 1, pp. 343–367, 2012, doi: 10.1146/annurev-chembioeng-062011-081008.

[88] M. A. Joseph, D. Ramjugernath, and J. D. Raal, "Computer-aided measurement of vapour-liquid equilibria in a dynamic still at sub-atmospheric pressures," *Dev. Chem. Eng. Miner. Process.*, 2002, doi: 10.1002/apj.5500100612.

[89] N. Juntarachat, A. Valtz, C. Coquelet, R. Privat, and J. N. Jaubert, "Experimental measurements and correlation of vapor-liquid equilibrium and critical data for the CO2 + R1234yf and CO2 + R1234ze(E) binary mixtures," *Int. J. Refrig.*, 2014, doi: 10.1016/j.ijrefrig.2014.09.001.

[90] P. ATKINS and J. DE PAULA, *ATKINS' PHYSICAL CHEMISTRY*. 2006.

[91] Y. T. Paul E. Laibinis, William H. Dalzell, "Vapor Liquid Equilibrium (VLE) A Guide," 2002. [Online]. Available:

http://web.mit.edu/10.213/www/handouts/vle.pdf.

[92] J. M. Smith, *INTRODUCTION TO CHEMICAL ENGINEERING THERMODYNAMICS EIGHTH EDITION*. 2005.

[93] R. J. Silbey, R. A. Alberty, and M. G. Bawendi, "Physical Chemistry 4th Edition," p. 960, 2004.

[94] F. -X Ball, H. Planche, W. Fürst, and H. Renon, "Representation of deviation from ideality in concentrated aqueous solutions of electrolytes using a mean spherical approximation molecular model," *AIChE J.*, 1985, doi: 10.1002/aic.690310802.

[95] B. J. Schwarz, J. A. Wilhelm, and J. M. Prausnitz, "Vapor Pressures and Saturated-Liquid Densities of Heavy Fossil-Fuel Fractions," 1987.

[96] E. Haskin, "The Principles of Chemical Equilibrium," *Nucl. Technol.*, 1972, doi: 10.13182/nt72-a31106.

[97] P. E. Liley, "Thermophysical Properties of Fluids," in *Mechanical Engineers' Handbook: Energy and Power: Third Edition*, 2006.

[98] A. Ilia, "VAPOR – LIQUID EQUILIBRIUM MEASUREMENTS IN BINARY POLAR SYSTEMS," 2016.

[99] A. N. Campbell and B. G. Oliver, "Activities from vapor pressure measurements of lithium and of sodium chlorates in water and water–dioxane solvents," *Can. J. Chem.*, 1969, doi: 10.1139/v69-439.

[100] E. Neau, J. Escandell, and C. Nicolas, "Modeling of highly nonideal systems: 1. A generalized version of the NRTL equation for the description of low-pressure equilibria," *Ind. Eng. Chem. Res.*, 2010, doi: 10.1021/ie100121c.

[101] R. C. Reid, T. K. Sherwood, and R. E. Street, "The Properties of Gases and Liquids," *Phys. Today*, 1959, doi: 10.1063/1.3060771.

[102] C. Puentes, X. Joulia, V. Athès, and M. Esteban-Decloux, "Review and Thermodynamic Modeling with NRTL Model of Vapor-Liquid Equilibria (VLE) of Aroma Compounds Highly Diluted in Ethanol-Water Mixtures at 101.3 kPa," *Industrial and Engineering Chemistry Research*. 2018, doi: 10.1021/acs.iecr.7b03857.

[103] J. . Rowlinson, "Molecular thermodynamics of fluid-phase equilibria," *J. Chem. Thermodyn.*, 1970, doi: 10.1016/0021-9614(70)90078-9.

[104] Ø. Wilhelmsen *et al.*, "Thermodynamic Modeling with Equations of State: Present Challenges with Established Methods," *Industrial and Engineering Chemistry Research*. 2017, doi: 10.1021/acs.iecr.7b00317.

[105] I. Ashour, N. Al-Rawahi, A. Fatemi, and G. Vakili-Nezh, "Applications of Equations of State in the Oil and Gas Industry," in *Thermodynamics - Kinetics of Dynamic Systems*, 2011.

[106] J. S. Lopez-Echeverry, S. Reif-Acherman, and E. Araujo-Lopez, "Peng-Robinson equation of state: 40 years through cubics," *Fluid Phase Equilib.*, 2017, doi: 10.1016/j.fluid.2017.05.007.

[107] A. M. Abudour, S. A. Mohammad, R. L. Robinson, and K. A. M. Gasem, “Volume-translated Peng-Robinson equation of state for liquid densities of diverse binary mixtures,” *Fluid Phase Equilib.*, 2013, doi: 10.1016/j.fluid.2013.04.002.

[108] R. Stryjek and J. H. Vera, “PRSV: An improved peng—Robinson equation of state for pure compounds and mixtures,” *Can. J. Chem. Eng.*, 1986, doi: 10.1002/cjce.5450640224.

[109] C. H. Twu, J. E. Coon, and D. Bluck, “Comparison of the Peng-Robinson and Soave-Redlich-Kwong equations of state using a new zero-pressure-based mixing rule for the prediction of high-pressure and high-temperature phase equilibria,” *Ind. Eng. Chem. Res.*, 1998, doi: 10.1021/ie9706424.

[110] A. Faghri and Y. Zhang, *Transport Phenomena in Multiphase Systems*. 2006.

[111] C. E. Brennen, *Fundamentals of multiphase flow*. 2013.

[112] J. Du and W. Cluett, “Modelling of a Naphtha Recovery Unit (NRU) with Implications for Process Optimization,” 2018.

[113] A. K. Coker, *Ludwig’s Applied Process Design for Chemical and Petrochemical Plants*. 2007.

[114] Z. Gropşian, R. Minea, E. Brînzei, and A. Tămaş, “Separation Processes,” *Rev. Chim.*, 2004, doi: 10.1201/b14397-6.

[115] N. Harnby, M. F. Edwards, and A. W. Nienow, “Mixing in the process industries.,” 1985, doi: 10.1016/b978-0-7506-3760-2.x5020-3.

[116] V. G. Pangarkar, *Design of Multiphase Reactors*. 2014.

[117] P. Zhang, G. Chen, J. Duan, and W. Wang, “Mixing characteristics in a vessel equipped with cylindrical stirrer,” *Results Phys.*, 2018, doi: 10.1016/j.rinp.2018.07.024.

[118] F. Goodarzi and S. Zendehboudi, “A Comprehensive Review on Emulsions and Emulsion Stability in Chemical and Energy Industries,” *Can. J. Chem. Eng.*, 2019, doi: 10.1002/cjce.23336.

[119] J.-L. Salaguer, “FIRP BOOKLET # E120-N in English INTERFACIAL PHENOMENA in LABORATORY OF FORMULATION , INTERFACES,” *Rheology*, vol. 1, 1994.

[120] L. Abu-farah, F. Al-qaessi, and A. Schönbucher, “Cyclohexane / water dispersion behaviour in a stirred batch vessel experimentally and with CFD simulation,” *Procedia Comput. Sci.*, vol. 1, no. 1, pp. 655–664, 2012, doi: 10.1016/j.procs.2010.04.070.

[121] D. V. Gradov, G. González, M. Vauhkonen, A. Laari, and T. Koiranen, “Experimental and Numerical Study of Multiphase Mixing Hydrodynamics in Batch Stirred Tank Applied to Ammoniacal Thiosulphate Leaching of Gold,” vol. 8, no. 3, pp. 1–17, 2017, doi: 10.4172/2157-7048.1000348.

[122] F. E. Selamat, “Design and Analysis of Centrifugal Pump Impeller for Performance Design and Analysis of Centrifugal Pump Impeller for Performance Enhancement,”

no. April, 2018.

[123] A. K. Coker, *Ludwig's applied process design for chemical and petrochemical plants: Fourth edition*. 2010.

[124] X. Han, Y. Kang, D. Li, and W. Zhao, "Impeller optimized design of the centrifugal pump: A numerical and experimental investigation," *Energies*, vol. 11, no. 6, 2018, doi: 10.3390/en11061444.

[125] S. D. Vlaev and I. Tsibranska, "Shear stress generated by radial flow impellers at bioreactor integrated membranes," *Theor. Found. Chem. Eng.*, 2016, doi: 10.1134/S004057951606018X.

[126] R. Sardeing, J. Aubin, and C. Xuereb, "Gas-liquid mass transfer: A comparison of down- And up-pumping axial flow impellers with radial impellers," *Chem. Eng. Res. Des.*, 2004, doi: 10.1205/cerd.82.12.1589.58030.

[127] A. Ochieng, M. S. Onyango, A. Kumar, K. Kiriamiti, and P. Musonge, "Mixing in a tank stirred by a Rushton turbine at a low clearance," *Chem. Eng. Process. Process Intensif.*, 2008, doi: 10.1016/j.cep.2007.01.034.

[128] R. P. Chhabra and J. F. Richardson, "Non-Newtonian flow in the process industries : fundamentals and engineering applications," *Non-Newtonian Flow Process Ind. Butterworth-Heinemann*, 1999, doi: 10.1016/B978-0-7506-3770-1.X5000-3.

[129] Z. Li, Y. Bao, and Z. Gao, "PIV experiments and large eddy simulations of single-loop flow fields in Rushton turbine stirred tanks," *Chem. Eng. Sci.*, vol. 66, no. 6, pp. 1219–1231, 2011, doi: 10.1016/j.ces.2010.12.024.

[130] N. K. Nere, A. W. Patwardhan, and J. B. Joshi, "Liquid-phase mixing in stirred vessels: Turbulent flow regime," *Industrial and Engineering Chemistry Research*. 2003, doi: 10.1021/ie0206397.

[131] M. Jaszczur, A. Młynarczykowska, and L. Demurtas, "Effect of impeller design on power characteristics and Newtonian fluids mixing efficiency in a mechanically agitated vessel at low reynolds numbers," *Energies*, 2020, doi: 10.3390/en13030640.

[132] D. Chapple, S. M. Kresta, A. Wall, and A. Afacan, "The effect of impeller and tank geometry on power number for a pitched blade turbine," *Chem. Eng. Res. Des.*, vol. 80, no. 4, pp. 364–372, 2002, doi: 10.1205/026387602317446407.

[133] Z. Trad, J. Fontaine, C. Larroche, and C. Vial, "Experimental and numerical investigation of hydrodynamics and mixing in a dual-impeller mechanically-stirred digester," *Chem. Eng. J.*, vol. 329, pp. 142–155, 2017, doi: 10.1016/j.cej.2017.07.038.

[134] A. Škerlavaj, L. Škerget, J. Ravnik, and A. Lipej, "Predicting free-surface vortices with single-phase simulations," *Eng. Appl. Comput. Fluid Mech.*, 2014, doi: 10.1080/19942060.2014.11015507.

[135] A. Busciglio, F. Grisafi, F. Scargiali, M. L. Daví, and A. Brucato, "Vortex shape in unbaffled stirred vessels: Experimental study via digital image analysis," in *Chemical Engineering Transactions*, 2011, doi: 10.3303/CET1124232.

[136] V. da S. Rosa and D. de M. Junior, “Design of Heat Transfer Surfaces in Agitated Vessels,” 2017.

[137] A. K. Pukkella, R. Vysyaraju, V. Tammishetti, and B. Rai, “Improved mixing of solid suspensions in stirred tanks with interface ba ffl es : CFD simulation and experimental validation,” *Chem. Eng. J.*, vol. 358, no. February 2018, pp. 621–633, 2019, doi: 10.1016/j.cej.2018.10.020.

[138] R. Lecuna, F. Delgado, A. Ortiz, P. B. Castro, I. Fernandez, and C. J. Renedo, “Thermal-fluid characterization of alternative liquids of power transformers: A numerical approach,” *IEEE Trans. Dielectr. Electr. Insul.*, vol. 22, no. 5, pp. 2522–2529, 2015, doi: 10.1109/TDEI.2015.004793.

[139] M. Nazari, S. Rashidi, and J. A. Esfahani, “Mixing process and mass transfer in a novel design of induced-charge electrokinetic micromixer with a conductive mixing-chamber,” *Int. Commun. Heat Mass Transf.*, vol. 108, no. August, p. 104293, 2019, doi: 10.1016/j.icheatmasstransfer.2019.104293.

[140] H. Nouanegue, A. Muftuoglu, and E. Bilgen, “Conjugate heat transfer by natural convection, conduction and radiation in open cavities,” *Int. J. Heat Mass Transf.*, vol. 51, no. 25–26, pp. 6054–6062, 2008, doi: 10.1016/j.ijheatmasstransfer.2008.05.009.

[141] M. Dular *et al.*, “Use of hydrodynamic cavitation in (waste)water treatment,” *Ultrason. Sonochem.*, vol. 29, pp. 577–588, 2016, doi: 10.1016/j.ultsonch.2015.10.010.

[142] T. Yamamoto, M. Kato, T. Kato, and K. Saito, “Heat transport via a local two-state system near thermal equilibrium,” *New J. Phys.*, vol. 20, no. 9, 2018, doi: 10.1088/1367-2630/aadf09.

[143] V. C. Smith and R. L. Robinson, “Vapor-Liquid Equilibria at 25° C in the Binary Mixtures Formed by Hexane, Benzene, and Ethanol,” *J. Chem. Eng. Data*, vol. 15, no. 3, pp. 391–395, 1970, doi: 10.1021/je60046a005.

[144] G. T. Coyle, T. C. Harmon, and I. H. Suffet, “Aqueous solubility depression for hydrophobic organic chemicals in the presence of partially miscible organic solvents,” *Environ. Sci. Technol.*, vol. 31, no. 2, pp. 384–389, 1997, doi: 10.1021/es960184a.

[145] D. K. Banerjee, *Oil Sands, Heavy Oil and Bitumen - From Recovery to Refinery*. 2012.

[146] C. Haligva, P. Linga, J. A. Ripmeester, and P. Englezos, “Recovery of methane from a variable-volume bed of silica sand/hydrate by depressurization,” *Energy and Fuels*, vol. 24, no. 5, pp. 2947–2955, 2010, doi: 10.1021/ef901220m.

[147] J. M. Gautier, E. H. Oelkers, and J. Schott, “Are quartz dissolution rates proportional to B.E.T. surface areas?,” *Geochim. Cosmochim. Acta*, vol. 65, no. 7, pp. 1059–1070, 2001, doi: 10.1016/S0016-7037(00)00570-6.

[148] A. M. SOYDAN, A. SARI, B. Duymaz, R. AKDENİZ, and B. TUNABOYLU, “Characterization of Fiber-Cement Composites Reinforced with Alternate

Cellulosic Fibers," *Anadolu Univ. J. Sci. Technol. Appl. Sci. Eng.*, no. September, pp. 1–1, 2018, doi: 10.18038/aubtda.338380.

[149] Z. A. Zhou, H. Li, R. Chow, O. B. Adeyinka, Z. Xu, and J. Masliyah, "Impact of fine solids on mined athabasca oil sands extraction II. Effect of fine solids with different surface wettability on bitumen recovery," *Can. J. Chem. Eng.*, vol. 95, no. 1, pp. 120–126, 2017, doi: 10.1002/cjce.22564.

[150] I. V. Babich and J. A. Moulijn, *Science and technology of novel processes for deep desulfurization of oil refinery streams: A review*, vol. 82, no. 6. 2003.

[151] G. J.Antos and Abdulla M. Aitani, *Catalytic naphtha reforming*. 2017.

[152] G. W. Meindersma, *Extraction of Aromatics from Naphtha with Ionic Liquids*, no. May. 2005.

[153] B. L. Smith and T. J. Bruno, "Advanced distillation curve measurement with a model predictive temperature controller," *Int. J. Thermophys.*, vol. 27, no. 5, pp. 1419–1434, 2006, doi: 10.1007/s10765-006-0113-7.

[154] M. Espinosa-Peña, Y. Figueroa-Gómez, and F. Jiménez-Cruz, "Simulated distillation yield curves in heavy crude oils: A comparison of precision between ASTM D-5307 and ASTM D-2892 physical distillation," *Energy and Fuels*, vol. 18, no. 6, pp. 1832–1840, 2004, doi: 10.1021/ef049919k.

[155] A. J. Austrich, E. Buenrostro-Gonzalez, and C. Lira-Galeana, "ASTM D-5307 and ASTM D-7169 SIMDIS standards: A comparison and correlation of methods," *Pet. Sci. Technol.*, vol. 33, no. 6, pp. 657–663, 2015, doi: 10.1080/10916466.2015.1004345.

[156] D. L. Katz and G. G. Brown, "Vapor Pressure and Vaporization of Petroleum Fractions," *Ind. Eng. Chem.*, vol. 25, no. 12, pp. 1373–1384, 1933, doi: 10.1021/ie50288a018.

[157] L. Liu, S. Hou, and N. Zhang, "Incorporating numerical molecular characterization into pseudo-component representation of light to middle petroleum distillates," *Chem. Eng. Sci. X*, vol. 3, p. 100029, 2019, doi: 10.1016/j.cesx.2019.100029.

[158] Omega®, *Omega i-series user's guide*. 2012.

[159] ASTM, "StandardTest Method for Vapor Pressure of Petroleum Products ( Mini Method ) 1," 2018.

[160] Y. Park and R. E. Sonntag, "Thermodynamic properties of ideal gas air," *Int. J. Energy Res.*, vol. 20, no. 9, pp. 771–785, 1996, doi: 10.1002/(SICI)1099-114X(199609)20:9<771::AID-ER192>3.0.CO;2-C.

[161] S. Weiguo, A. X. Qin, P. J. McElroy, and A. G. Williamson, "(Vapour + liquid) equilibria of (n-hexane + n-hexadecane), (n-hexane + n-octane), and (n-octane + n-hexadecane)," *J. Chem. Thermodyn.*, vol. 22, no. 9, pp. 905–914, 1990, doi: 10.1016/0021-9614(90)90179-T.

[162] J. A. N. Zielkiewicz, "( V a p o u r + l i q u i d ) equilibria in at the temperature 313 . 15 K," vol. 462, pp. 455–462, 1992.

[163] E. S. P. B. V, S. K. Chaudhari, S. S. Katti, and P. C. Division, “VAPOUR-LIQUID EQUILIBRIA OF BINARY MIXTURES OF n-HEXANE, n-HEPTANE AND n-OCTANE WITH 1,2-DICHLOROETHANE AT 323.15 K *,” vol. 57, no. 4696, pp. 297–306, 1990.

[164] K. A. Pivldal and S. I. Sandler, “Neighbor Effects on the Group Contribution Method: Infinite Dilution Activity Coefficients of Binary Systems Containing Primary Amines and Alcohols,” *J. Chem. Eng. Data*, vol. 35, no. 1, pp. 53–60, 1990, doi: 10.1021/je00059a018.

[165] T. Hiaki, K. Takahashi, T. Tsuji, M. Hongo, and K. Kojima, “Vapor-Liquid Equilibria of Ethanol + Octane at 343.15 K and 1-Propanol + Octane at 358.15 K,” *J. Chem. Eng. Data*, 1995, doi: 10.1021/je00017a059.

[166] J. Schmelzer and J. Pusch, “Phase equilibria in binary systems containing N-monosubstituted amides and hydrocarbons,” *Fluid Phase Equilib.*, vol. 110, no. 1–2, pp. 183–196, 1995, doi: 10.1016/0378-3812(95)02753-2.

[167] J. Gregorowicz, K. Kiciak, and S. Malanowski, “Vapour pressure data for 1-butanol, cumene, n-octane and n-decane and their statistically consistent reduction with the antoine equation,” *Fluid Phase Equilib.*, 1987, doi: 10.1016/0378-3812(87)90006-9.

[168] F. J. Carmona, J. A. González, I. García De La Fuente, J. C. Cobos, V. R. Bhethanabotla, and S. W. Campbell, “Thermodynamic properties of n-alkoxyethanols + organic solvent mixtures. XI. Total vapor pressure measurements for n-hexane, cyclohexane or n-heptane + 2-ethoxyethanol at 303.15 and 323.15 K,” *J. Chem. Eng. Data*, 2000, doi: 10.1021/je990292n.

[169] C. Alonso, E. A. Montero, C. R. Chamorro, J. J. Segovia, M. C. Martín, and M. A. Villamañán, “Vapor-liquid equilibrium of octane-enhancing additives in gasolines: 5. Total pressure data and GE for binary and ternary mixtures containing 1,1-dimethylpropyl methyl ether (TAME), 1-propanol and n-hexane at 313.15 K,” *Fluid Phase Equilib.*, 2003, doi: 10.1016/S0378-3812(03)00268-1.

[170] H. Wolff, H. Landeck, H. P. Frerichs, and E. Wolff, “The association of normal and tertiary butylamine in mixtures with n-hexane according to isothermal vapour pressure measurements,” *Fluid Phase Equilib.*, 1995, doi: 10.1016/0378-3812(95)02725-T.

[171] S. A. Wieczorek and J. Stecki, “Vapour pressures and thermodynamic properties of hexan-1-ol + n-hexane between 298.230 and 342.824 K,” *J. Chem. Thermodyn.*, 1978, doi: 10.1016/0021-9614(78)90123-4.

[172] M. A. Y. Torres, S. B. Bottini, E. A. Brignole, V. Sanhueza, and R. Reich, “Vapor-liquid equilibria for binary mixtures with anisole,” *Fluid Phase Equilib.*, vol. 71, no. 1–2, pp. 85–98, 1992, doi: 10.1016/0378-3812(92)85006-T.

[173] M. S. K. Rozhnov, “Phase and volume relationships in the butadiene plus hydrocarbon systems Prom-st. (Moscow),” 1967.

[174] B. F. Belaribi, A. Ait-Kaci, and J. Jose, “Liquid vapor equilibrium. Decane-1-hexyne system,” *Int. DATA Ser., Sel. Data Mix.*, 1991, doi: 10.1021/je60019a024.

[175] N. Allemand, J. Jose, and J. C. Merlin, “Mesure des pressions de vapeur d’hydrocarbures C10 A C18 n-alcanes etn-alkylbenzenes dans le domaine 3-1000 pascal,” *Thermochim. Acta*, 1986, doi: 10.1016/0040-6031(86)85225-X.

[176] D. Xu, H. Li, and Z. Li, “Determination and modeling of isobaric vapor-liquid equilibria for the methylcarbamate + Methyl-N-phenyl carbamate system at different pressures,” *J. Chem. Eng. Data*, 2013, doi: 10.1021/je400551d.

[177] S. Bernatová, J. Linek, and I. Wichterle, “Vapour-liquid equilibrium in the butyl alcohol -n-decane system at 85, 100 and 115°C,” vol. 74, pp. 1133–1138, 1992, doi: 10.1016/B978-0-444-88677-4.50008-8.

[178] A. Belabbaci, R. M. Villamañán, L. Negadi, and M. C. Martín, “Vapor-liquid equilibria of binary mixtures containing 2-butanol and hydrocarbons at 313.15 K,” *J. Chem. Eng. Data*, vol. 57, no. 3, pp. 982–987, 2012, doi: 10.1021/je201284y.

[179] S. J. Park, K. J. Han, and J. Gmehling, “Isothermal phase equilibria and excess molar enthalpies for binary systems with dimethyl ether at 323.15 K,” *J. Chem. Eng. Data*, 2007, doi: 10.1021/je700174h.

[180] U. Messow, U. Doye, and Kuchenbecker, “Thermodynamische untersuchungen an lösungsmittel/n-paraffin systemen. V. Die systeme aceton/n-decan, aceton/n-dodecan, aceton/n-tetradecan und aceton/n-hexadecan,” *D. Z. Phys. Chem.*, vol. 5, pp. 159–189, 1978.

[181] K. Sasse, J. Jose, and J. C. Merlin, “A static apparatus for measurement of low vapor pressures. Experimental results on high molecular-weight hydrocarbons,” *Fluid Phase Equilib.*, 1988, doi: 10.1016/0378-3812(88)80065-7.

[182] C. Narasigadu, S. C. Subramoney, P. Naidoo, C. Coquelet, D. Richon, and D. Ramjugernath, “Isothermal vapor-liquid equilibrium data for the propan-1-ol + dodecane system at (323.0, 343.4, 353.2, 363.1, and 369.2) K,” *J. Chem. Eng. Data*, 2012, doi: 10.1021/je201032t.

[183] D. L. Morgan and R. Kobayashi, “Direct vapor pressure measurements of ten n-alkanes m the 10-C28 range,” *Fluid Phase Equilib.*, 1994, doi: 10.1016/0378-3812(94)85017-8.

[184] *CRC Handbook of Chemistry and Physics, 95th Edition*. 2014.

[185] I. L. Clifford and E. Hunter, “The system ammonia-water at temperatures up to 150°C. And at pressures up to twenty atmospheres,” *J. Phys. Chem.*, 1933, doi: 10.1021/j150343a014.

[186] M. R. Rahimpour, M. Jafari, and D. Iranshahi, “Progress in catalytic naphtha reforming process: A review,” *Applied Energy*. 2013, doi: 10.1016/j.apenergy.2013.03.080.

[187] I. Tzanakis, G. S. B. Lebon, D. G. Eskin, and K. Pericleous, “Investigation of the factors influencing cavitation intensity during the ultrasonic treatment of molten aluminium,” *Mater. Des.*, 2016, doi: 10.1016/j.matdes.2015.11.010.

[188] G. J, M. Kleiber, B. Kolbe, and J. Rarey, “Chemical Thermodynamics for Process Simulation.” Wiley, 2019.

[189] G. R. Van Der Hoff and P. Van Zoonen, “Trace analysis of pesticides by gas chromatography,” *J. Chromatogr. A*, vol. 843, no. 1–2, pp. 301–322, 1999, doi: 10.1016/S0021-9673(99)00511-7.

[190] K. Hartonen, A. Helin, J. Parshintsev, and M. L. Riekkola, “Problems Caused by Moisture in Gas Chromatographic Analysis of Headspace SPME Samples of Short-Chain Amines,” *Chromatographia*, vol. 82, no. 1, pp. 307–316, 2019, doi: 10.1007/s10337-018-3641-y.

[191] I. Farrance and R. Frenkel, “Uncertainty of measurement: A review of the rules for calculating Uncertainty components through functional relationships,” *Clinical Biochemist Reviews*. 2012.

[192] E. M. Scott, G. T. Cook, and P. Naysmith, “Error and Uncertainty in Radiocarbon Measurements,” *Radiocarbon*, 2007, doi: 10.1017/s0033822200042351.

[193] R. Willink and R. Willink, “Guide to the Expression of Uncertainty in Measurement,” in *Measurement Uncertainty and Probability*, 2013.

[194] K. K. Movassaghi, “Project management — A managerial approach,” *Eur. J. Oper. Res.*, 1990, doi: 10.1016/0377-2217(90)90203-n.

[195] A. H. S. Dehaghani and M. H. Badizad, “Experimental study of Iranian heavy crude oil viscosity reduction by diluting with heptane, methanol, toluene, gas condensate and naphtha,” *Petroleum*, 2016, doi: 10.1016/j.petlm.2016.08.012.

# Appendices

## Appendix A: Uncertainty

Uncertainty can be defined as any type of error containing multiple causes in the measurement, whereas error merely demonstrates the numerical deviation between the measurement and true value [191]. Hence, uncertainty has better data reliability than error [192]. International Organization for Standardization (ISO) also guides researchers to provide uncertainty to show the credibility of experiment data [193].

The uncertainty must involve a statistical point of view, showing how far the reality is situated from the experimental measurement. Several statistical methods can be selected to determine the experimental uncertainty. Therefore, the experimentalist should address the viability of the selected analytical method.

In this thesis, possible uncertainties from the experiment environment may involve systematic and human factors. Systematic and human uncertainties are interpreted by a calibration parameter and an experimental repeatability value. The following is a possible expression:

$$u_c(T) = \pm\sqrt{u_{calib}(T)^2 + u_{rep}(T)^2}$$

For the calibration uncertainty, one has to consider that a calibrated K-type thermocouple, with a $\pm$ 2.2 ℃ uncertainty, was used in the experiments. The value is provided from $OMEGA^{TM}$ and the method is in accordance with ASTM E230.

Repeatability tests were also conducted for every experiment with at least 3 (three) repeats per experiment. One can also refer to the uncertainty of repeatability as the standard error.

The following is the equation to find the repeatability uncertainty:

$$u_{rep}(T) = \frac{\sigma}{\sqrt{n}}$$

Thus, uncertainty is a statistical based, single value parameter. However, uncertainty can also be considered using a more elaborated assessment with uncertainty multiplied by a k-factor, which rescales the value as a confidence level. In this respect, 1.96 was used in the present study for k-factor, which gives a 95 % confidence interval assuming a normal Gaussian distribution.

As a result, the following expression can be considered for the experimentally measured temperature including a calculated uncertainty with a 95 % confidence interval:

$$T_{final} = T_{measured} + ku_c(T)$$

A similar approach can be employed to determine the uncertainty for pressure measurement. One should note, however, that the pressure transducer used in the experiments has shown different uncertainty levels with this being dependent on the pressure measured.

$OMEGA^{TM}$ provides a 0.08 % systematic uncertainty for the measured pressure. While VL-Cell pressure transducer measures up to 50 psi, the maximum calibration uncertainty does not exceed $\pm$ 0.04 psi. Furthermore, the largest standard error in the experiment is $\pm$ 1.01 psi. Therefore, the combined possible uncertainty is less than $\pm$ 1.09 psi for the pressure data.

## Appendix B: Risk Analysis

Risk Analysis is a systematic technique to identify the source of harm, minimizing the risk to achieve a target [194]. CREC-VL-Cell operation has several potential hazards to cause severe potential harm to the researcher. Furthermore, risk analysis facilitates the understanding of the experimental method. It can lead to preventing repetitive human error and reducing research costs.

The following steps are required to execute the risk analysis

1. Hazard identification
2. Numerical Risk estimation on each hazard
3. Risk Priority Number (RPN) determination with a detection level
4. Determining the remedial measures

Preliminary Hazard Analysis (PHA) and Fault Tree Analysis (FTA) are complementary analysis techniques to have different advantages in safety engineering. PHA is an inductive method to identify the hazard in the project development step. On the other hand, FTA is a graphical analysis tool to start from the top event to the undesired consequences.

Table 1 shows the PHA tool for the overall VL-Cell operation. P and S stand for the Probability and severity, respectively. The factor of risk is determined by multiplying the Probability and Severity. Remedial measures indicate the required action to prevent and recover operational risks.

**Table 42. Preliminary Hazard Analysis for VL-Cell operation**

| Hazard | P | S | Risk | Remedial measures |
|---|---|---|---|---|
| Exposure to residues | 3 | 3 | 9 | • Use clean 100 mL bottle to subdivide the chemical |
| Contaminates | 3 | 3 | 9 | • Change the syringe or Pipette each time used |
| Inhalation from chemicals | 3 | 3 | 9 | • Use certified respiratory mask |

| Hazard | P | S | Risk | Remedial measures |
|---|---|---|---|---|
| Chemical Exposure to skin | 3 | 3 | 9 | • Use certified/right-size latex gloves and change it every time to use |
| Inhalation from solids | 3 | 3 | 9 | • Use adequate mask that filter the fine-size solids |
| Pressure leakage | 3 | 3 | 9 | • Check Pressure leakage every time before running an experiment and add a alarm system sensor when ramp-pressure has unusual behavior |
| Injury from Hot-plate | 3 | 3 | 9 | • Put the 'Hot' warning sign on the hotplate with large font size |
| Impeller rotation and hand stuck | 3 | 3 | 9 | • Train the operator to inform the procedure not to manipulate impeller in the middle of the operation |
| High temperature parts | 3 | 2 | 6 | • Put the 'Hot' warning sign on the hotplate with large font size |
| Exposure to skin from solids | 3 | 2 | 6 | • Measure the solids inside of Lab hood |
| Thermocouple overshoot | 2 | 3 | 6 | • Check cold junction of the thermocouple on the open space |
| Temperature controller error | 2 | 3 | 6 | • Add the alarm sound on the controller option and stay in the area when experiment is operating |
| parts contamination from Bitumen | 3 | 2 | 6 | • Clean the part as soon as the experiment terminates and use naphtha to clean Bitumen sample |
| Smoke point from heat transfer fluid | 2 | 3 | 6 | • Check the smoke point of the heat transfer fluid and limit the heat transfer fluid temperature |
| Impeller breakage from wrong placement | 2 | 2 | 4 | • Use a adjustable bolt to prevent the impeller breakage |
| Worn Parts | 2 | 2 | 4 | • Regularly test the pressure leakage and check parts where high frictions are applied |
| Heat transfer fluid leakage | 2 | 2 | 4 | • Regularly check the magnetic stirrer region to check the abrasion and limit the heat transfer volume considering the density change |
| Lost Parts | 2 | 2 | 4 | • Sort the parts and place the designated area |

| Hazard | P | S | Risk | Remedial measures |
|---|---|---|---|---|
| Fire due to the flash point | 1 | 3 | 3 | • Check the flammability condition from using chemicals and adjust the measurement limits<br>• Place a fire extinguisher around the apparatus |
| Electric shock | 1 | 3 | 3 | • Place Warning sign where electronic shock could occur from the apparatus |
| Exposure to surface currents | 1 | 3 | 3 | • Cover the current area with rubber tape to protect |
| Electrostatic discharge | 1 | 3 | 3 | • Receive a electrician review for the present electronic device arrangement to prevent the electrostatic discharge |
| Pressure transducer error | 1 | 3 | 3 | • Receive a regular calibration |
| Liquid overflow from the VL-Cell | 1 | 3 | 3 | • Check the density change of the measurement sample and limit the sample volume |
| Temperature Data acquisition error | 1 | 3 | 3 | • Add the alarm sound and error message for the issue |
| Pressure Data acquisition error | 1 | 3 | 3 | • Add the alarm sound and error message for the issue |
| Impeller vibration | 3 | 1 | 3 | • Use a adjustable bolt to prevent the impeller vibration, Stay in the area during the experiment run, Test pre-running before normal condition is applied |
| Impeller breakage from cavitation | 1 | 2 | 2 | • Check the condition of forming cavitation and limit the experimental condition |
| Baffle breakage | 1 | 2 | 2 | • Check the distance between baffle and impeller every time before running experiment |
| Heat exchanger water leakage | 1 | 2 | 2 | • Regularly check the pipe and (specially) fitting region, Use Teflon tape the reduce the small gap between the pipe and screw |
| Electronic part breakage (Fuse) | 1 | 2 | 2 | • Check the fuse specification if it is standard for the electronic parts, Retain spare fuse |
| Heat transfer fluid acidification | 1 | 2 | 2 | • Regularly check the odor and color condition, regularly replace the heat transfer fluid |
| Parts with low temperature | 1 | 1 | 1 | • Maintain standard temperature condition in the laboratory |

Figure 65 and Figure 66 describe the FTA methodology for chemical inhalation and pressure leakage events, all events possible whole operating the CREC-VL-Cell. The reported schematics describe the logical steps used to interpret event and consequences. Basic events (circles) connect to an AND gate. Intermediate events join with the OR gate. Consequently, the Top event appears due to various sub-events occurring during the operation.

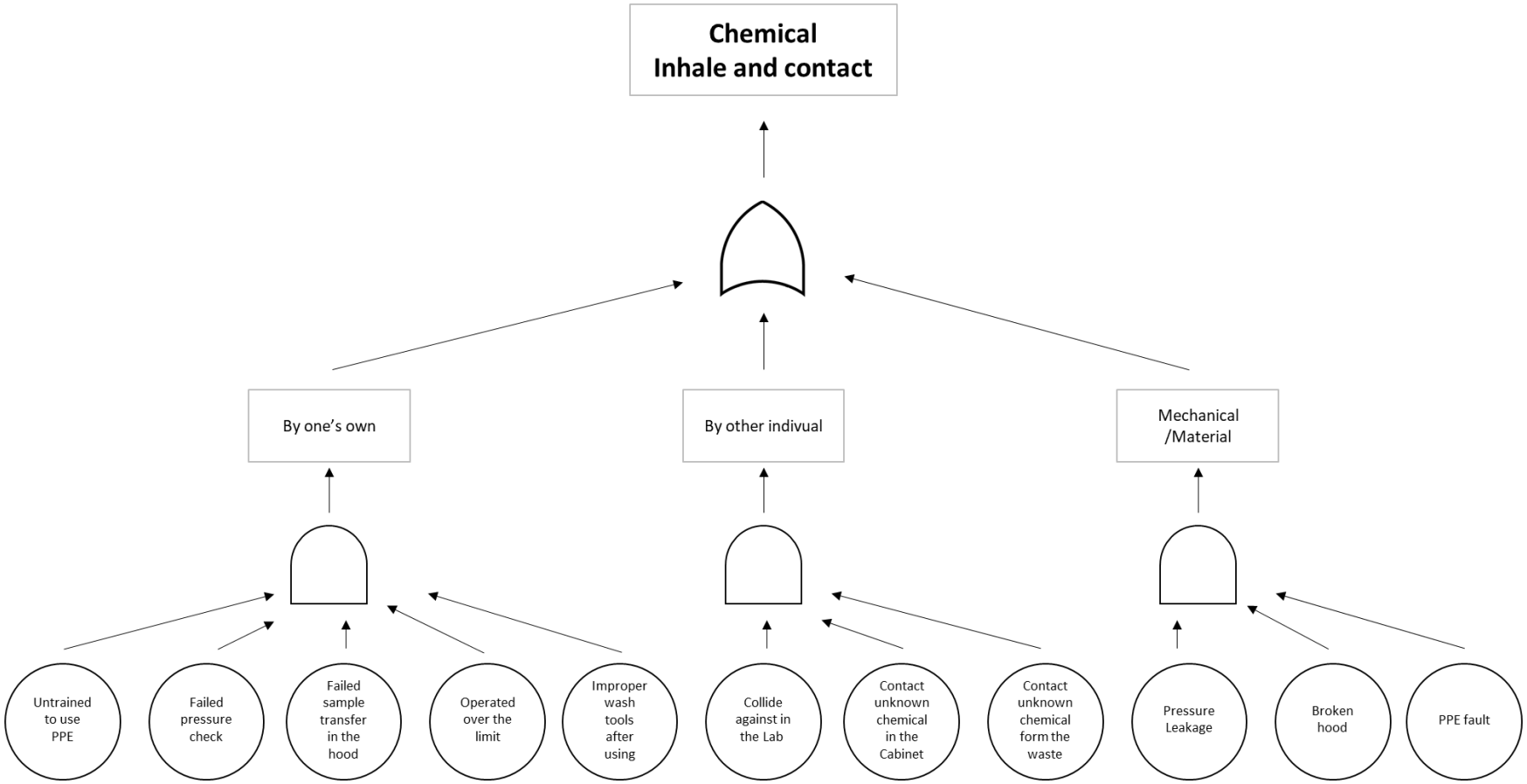


**Figure 65. Fault Tree Analysis for Chemical inhale and contact event**

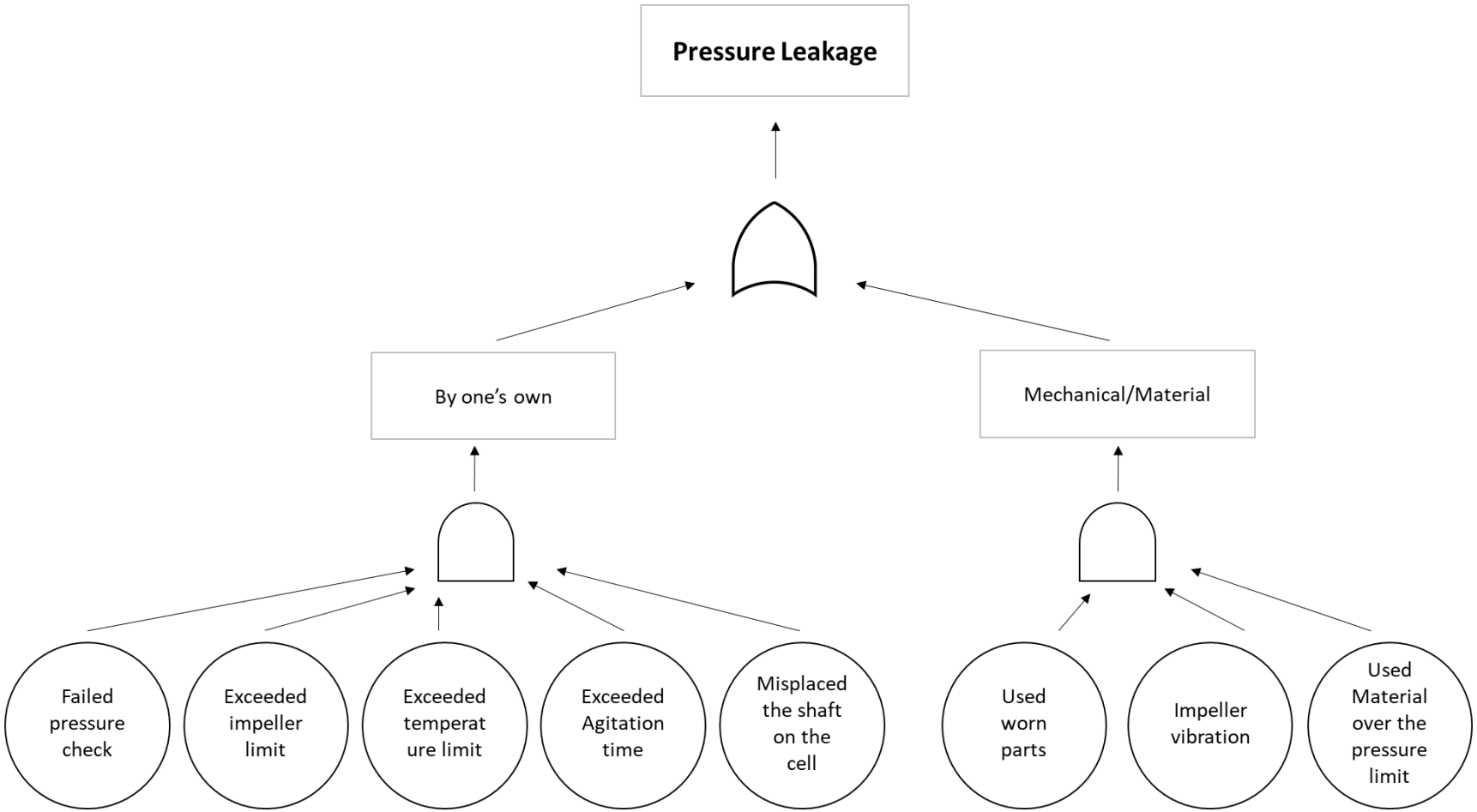


**Figure 66. Fault Tree Analysis for Pressure leak**

## Appendix C. Aromatic Synthetic Naphtha

Synthetic Naphtha (SN) is prepared using five paraffinic components. However, one may argue that the paraffins are insufficient to emulate naphtha. Dehaghani and Baizad (2016) addressed that 12.1 vol.% aromatic components may contain in the industrial naphtha [195]. Therefore, this appendix introduces the aromatic synthetic naphtha and compares its PR EoS simulation result with the results of paraffinic synthetic naphtha.

Table 43 reports the compositions of the n-paraffin group and aromatic groups to create synthetic naphtha. The aromatic group includes five (5) aromatic compounds ranging C6 to C12, and the compositions are set to be same as paraffinic group.

**Table 43. Compositions of n-paraffin group and aromatic group for Synthetic Naphtha**

**n-paraffin**

| | Hexane | Heptane | Octane | Decane | Dodecane |
|---|---|---|---|---|---|
| Formula | C6H14 | C7H16 | C8H18 | C10H22 | C12H26 |
| wt % | 10 | 22 | 60 | 6 | 2 |
| Boiling Point (℃) | 68.7 | 98.4 | 125.6 | 174.1 | 216.2 |

**Aromatics**

| | Benzene | Toluene | Xylene | Durene | Hexamethylbenzene |
|---|---|---|---|---|---|
| Formula | C6H6 | C7H9 | C8H10 | C10H14 | C12H18 |
| wt % | 10 | 22 | 60 | 6 | 2 |
| Boiling Point (℃) | 80.1 | 110.6 | 138.4 | 196.8 | 263.4 |

Table 44 describes the compositions between n-paraffins and aromatic seen in Table 43. The CREC SN_Aroma15 was generated based on the open literature reference, which claims that aromatic contains 12.1 vol% in naphtha [195]. Furthermore, the CREC SN_Aroma10 was prepared with low aromatic, and this given low aromatic contents in naphtha is a frequently desired formulation.

**Table 44. Synthetic Naphtha compositions**

| CREC SN_Aroma0 | | |
|---|---|---|
| Contents | wt.% | vol.% |
| n-paraffin | 100 | 100 |

| CREC SN_Aroma15 | | |
|---|---|---|
| Contents | wt.% | vol.% |
| n-paraffin | 85 | 87.6 |
| Aromatics | 15 | 12.5 |

| CREC SN_Aroma10 | | |
|---|---|---|
| Contents | wt.% | vol.% |
| n-paraffin | 90 | 91.8 |
| Aromatics | 10 | 8.2 |

Figure 67 reports True Boiling Point (TBP) data for typical naphtha and two (2) Synthetic Naphtha by using Hysys PR-EoS. The CREC SN_Aroma 10 is not reported here because it has an essentially TBP essentially identical to CREC SN_Aroma 15. One can observe that aromatic content has no significant effect on TNP distillation up to 65 wt%.

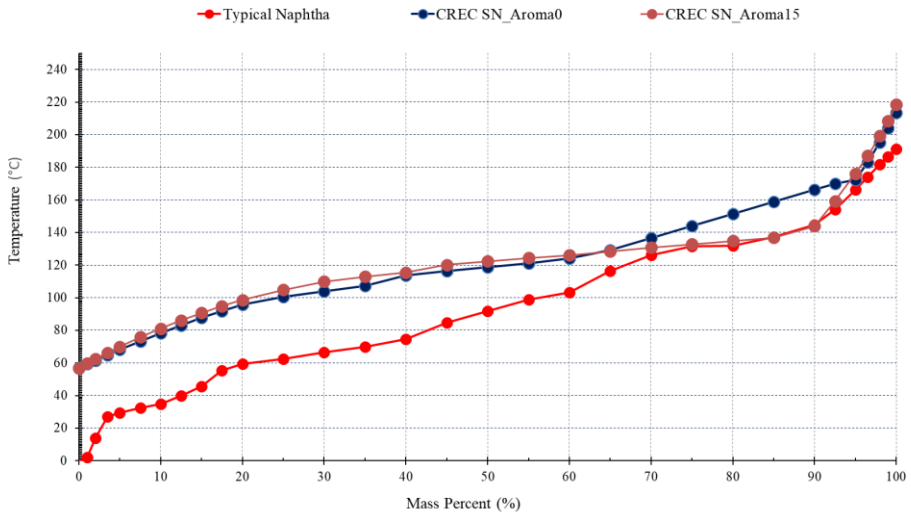


**Figure 67. TBP analysis of Typical Naphtha and Synthetic Naphtha by using Hysys PR-EOS.**

Figure 68 describes the pressure change using as a reference, the CREC SN_Aroma0 synthetic naphtha without aromatics. One can see that The CREC SN_Aroma15 has less than 1.37 % pressure difference compared to the pressure of the CREC SN_Aroma0. As well one can observe that The CREC SN_Aroma10 has less than 2.2 %.

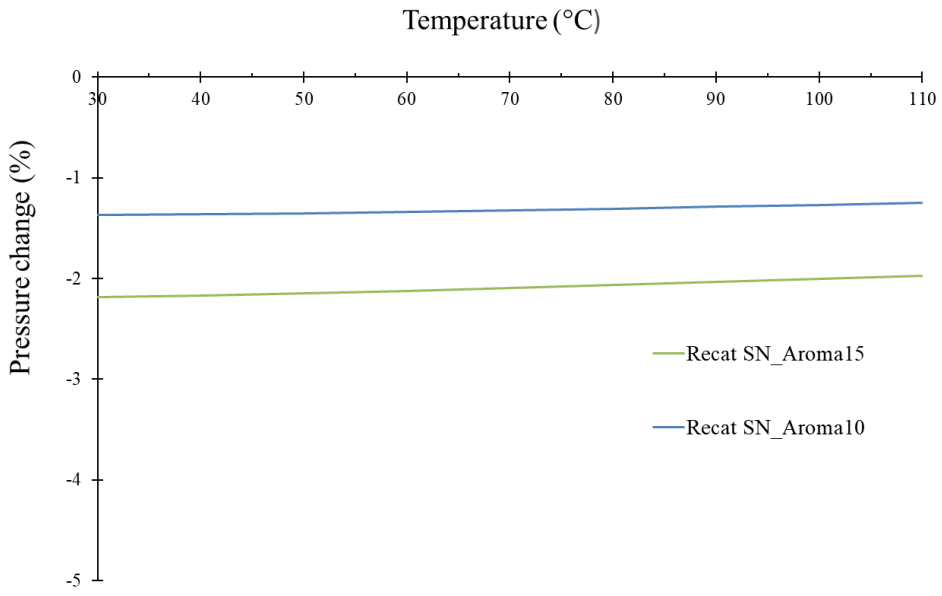


**Figure 68. Pressure changes of synthetic aromatic naphtha while compared to the CREC SN_Aroma0.**

A similar analysis was developed to investigate the influence of the excess of water in synthetic naphtha-water blends. Figure 69 and Figure 70 report the pressure change when 97.5 wt% water-2.5wt% Synthetic Aromatic Naphtha and 96.0 wt% water- 4wt% Synthetic Aromatic Naphtha are compared with CREC SN_Aroma0. One can observe that the aromatic compounds reduce the vapor pressure in the simulation of Hysys PR EoS, for less than 1 % in the range of 30 – 110 ℃.

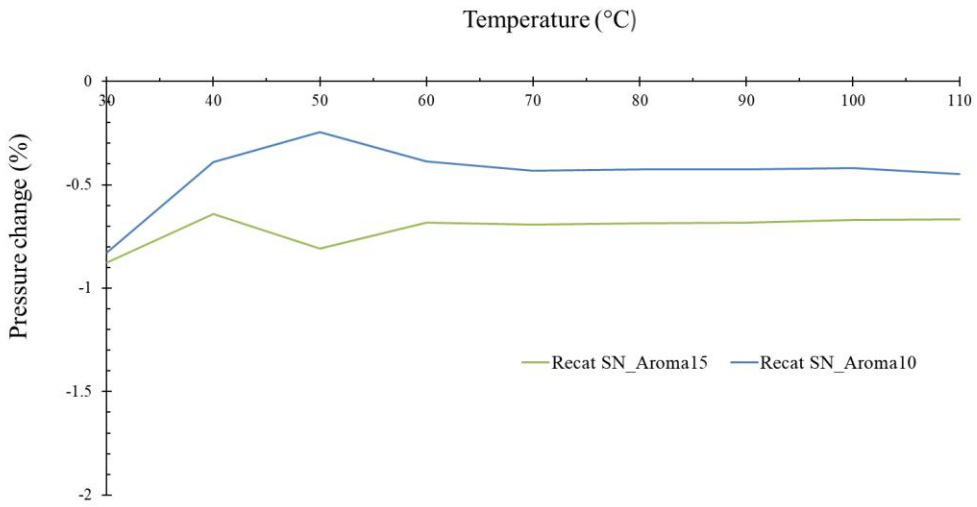


**Figure 69. Pressure changes of 97.5 wt% water + 2.5 wt% synthetic aromatic naphtha compared to the CREC SN_Aroma0**

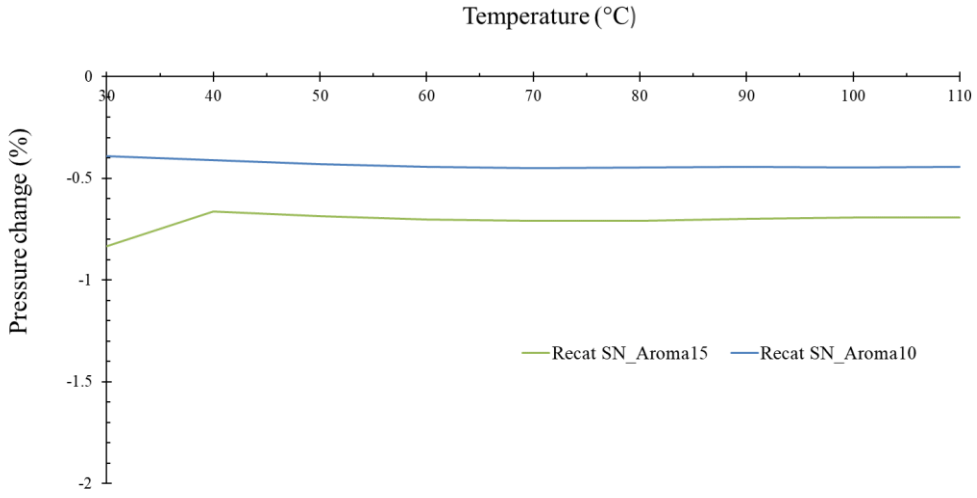


**Figure 70. Pressure changes of 96.0 wt% water + 4.0 wt% synthetic aromatic naphtha compared to the CREC SN_Aroma0**

## Appendix D. CREC-VL-Cell Photos

The following are photos for the experimental set up and auxiliary equipment as presently available in CREC laboratories

**Figure 71. CREC-VL-Cell setup image**

**Figure 72. 275mL Equilibrium cell image**


**Figure 73. Water-cooled heat exchanger in CREC-VL-cell**

# Appendix E. Copyright Permission

# Curriculum Vitae

**Name:** Jeonghoon Kong

**Post-secondary Education and Degrees:**

Western University
London, Ontario, Canada
2018-2020 MESc. Chemical Engineering

Kwangwoon University
Seoul, South Korea
2009-2016 B.Eng Chemical Engineering

**Related Work Experience**

Research Assistant
Western University
2018-2020

Teaching Assistant
Western University
2019-2019

Manufacturing Engineer
LT Material Ltd.
2016-2017

Research Intern
Seoul Broadcasting System
2015-2015